

## INFORMATION TO USERS

This manuscript has been reproduced from the microfilm master. UMI films the text directly from the original or copy submitted. Thus, some thesis and dissertation copies are in typewriter face, while others may be from any type of computer printer.

**The quality of this reproduction is dependent upon the quality of the copy submitted.** Broken or indistinct print, colored or poor quality illustrations and photographs, print bleedthrough, substandard margins, and improper alignment can adversely affect reproduction.

In the unlikely event that the author did not send UMI a complete manuscript and there are missing pages, these will be noted. Also, if unauthorized copyright material had to be removed, a note will indicate the deletion.

Oversize materials (e.g., maps, drawings, charts) are reproduced by sectioning the original, beginning at the upper left-hand corner and continuing from left to right in equal sections with small overlaps.

Photographs included in the original manuscript have been reproduced xerographically in this copy. Higher quality 6" x 9" black and white photographic prints are available for any photographs or illustrations appearing in this copy for an additional charge. Contact UMI directly to order.

ProQuest Information and Learning  
300 North Zeeb Road, Ann Arbor, MI 48106-1346 USA  
800-521-0600

**UMI<sup>®</sup>**



**University of Alberta**

**Developing Microfluidic Devices for Genetic and Biochemical Analyses**

**by**

**Guifeng Jiang** ©

A thesis submitted to the Faculty of Graduate Studies and Research in partial fulfillment  
of the requirements for the degree of Doctor of Philosophy

Department of Chemistry

Edmonton, Alberta

Spring 2001



**National Library  
of Canada**

**Acquisitions and  
Bibliographic Services**

395 Wellington Street  
Ottawa ON K1A 0N4  
Canada

**Bibliothèque nationale  
du Canada**

**Acquisitions et  
services bibliographiques**

395, rue Wellington  
Ottawa ON K1A 0N4  
Canada

*Your file Votre référence*

*Our file Notre référence*

**The author has granted a non-exclusive licence allowing the National Library of Canada to reproduce, loan, distribute or sell copies of this thesis in microform, paper or electronic formats.**

**The author retains ownership of the copyright in this thesis. Neither the thesis nor substantial extracts from it may be printed or otherwise reproduced without the author's permission.**

**L'auteur a accordé une licence non exclusive permettant à la Bibliothèque nationale du Canada de reproduire, prêter, distribuer ou vendre des copies de cette thèse sous la forme de microfiche/film, de reproduction sur papier ou sur format électronique.**

**L'auteur conserve la propriété du droit d'auteur qui protège cette thèse. Ni la thèse ni des extraits substantiels de celle-ci ne doivent être imprimés ou autrement reproduits sans son autorisation.**

0-612-60304-0

**Canada**

# University of Alberta

## Library Release Form

**Name of Author:** Guifeng Jiang

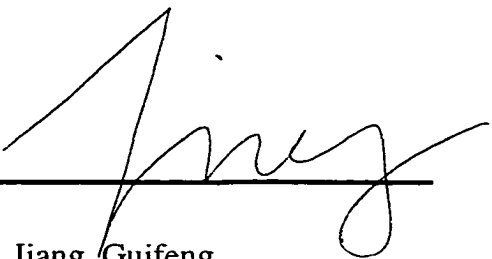
**Title of Thesis:** Developing Microfluidic Devices for Genetic and Biochemical Analyses

**Degree:** Doctor of Philosophy

**Year this Degree Granted:** 2001

Permission is hereby granted to the University of Alberta Library to reproduce single copies of this thesis and to lend or sell such copies for private, scholarly or scientific research purpose only.

The author reserves all other publication and other rights in association with the copyright in the thesis, and except as herein before provided, neither the thesis nor any substantial portion thereof may be printed or otherwise reproduced in any material form whatever without the author's prior written permission.



---

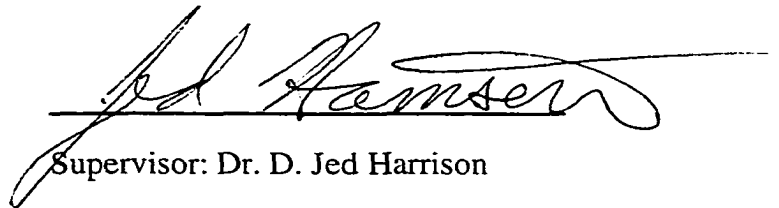
Jiang, Guifeng  
RH 407, Michener Park  
Edmonton, Alberta T6H 4M5  
CANADA

Date: April 2001

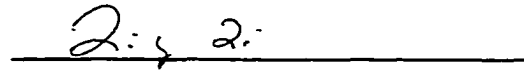
University of Alberta

Faculty of Graduate Studies and Research

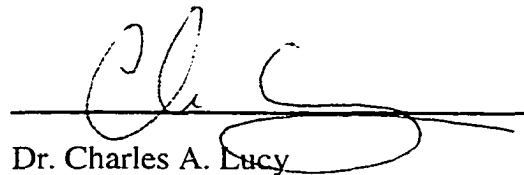
The undersigned certify that they have read, and recommend to the Faculty of Graduate Studies and Research for acceptance, a thesis entitled "**Developing Microfluidic Devices for Genetic and Biochemical Analyses**" submitted by **Guifeng Jiang** in partial fulfillment of the requirements for the degree of **Doctor of Philosophy**.



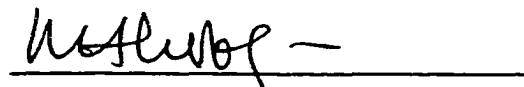
Supervisor: Dr. D. Jed Harrison



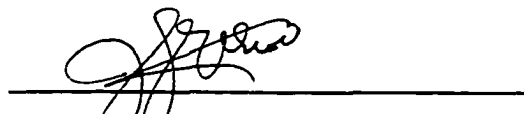
Dr. Liang Li



Dr. Charles A. Lucy

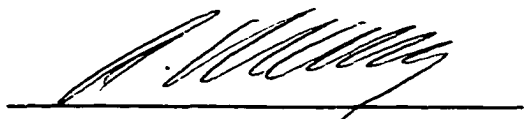


Dr. Mariusz Klobukowski



Dr. John F. Elliott

April 2nd, 2001



External Examiner: Dr. Andreas Manz

## *DEDICATION*

*To my parents, my brothers for their guidance, love and support, and my husband and my son for their continuous encouragement and boundless love.*

## Thesis Abstract

The application of microfluidic device in genetic and bioanalytical analysis is explored in this thesis. The first integration of mRNA isolation and cDNA synthesis on microfluidic device was demonstrated. In addition, in order to detect protein biological threat agent simulant, ovalbumin (Ov), by performing an immunoassay separation in the field, the laser induced fluorescence detection of Cy-5 using diode laser was also tested.

We develop some of the individual components required to ultimately create an integrated microfluidic device for complementary DNA (cDNA) library construction. The first two steps required include the isolation and purification of messenger RNA (mRNA), followed by first strand synthesis of cDNA using reverse transcription (RT). We describe the use of paramagnetic oligo-dT beads for mRNA capture within microfluidic channels. A simple Y-intersection flow design mixes beads and total RNA (TRNA) on-chip to allow capture of the mRNA, and uses a magnetic field to trap the beads. Initial designs show a capture efficiency of about 26 % compared to conventional methods, which is assigned to poor flow dynamics. The capillary gel electrophoresis (CGE) detection of the total unamplified mRNA isolated on chip, and of a reverse transcription-polymerase chain reaction (RT-PCR) amplified rare gene indicated that mRNA could be captured by oligo-dT beads on-chip. The isolated mRNA was suitable for constructing a cDNA library. The limit of detection for the rare bicoid gene of *Drosophila Melanogaster* corresponded to the capture of approximately 1-5 ng of mRNA from 0.85  $\mu$ g of total RNA within the microchip. The subsequent RT reaction was performed for 2 hours from 30 °C to 45 °C on mRNA bound to the bead bed within the channel and 35 °C gave the best result. The bead-cDNA complex was then released from the chip and polymerase chain reaction was employed to amplify the cDNA bound to the beads. Capillary gel electrophoresis detection of the PCR product indicated that mRNA isolation and cDNA synthesis could be integrated on microfluidic device, representing the first two steps towards cDNA library construction using microfluidic device.

A highly sensitive laser induced fluorescence (LIF) detection system based on a 635 nm laser diode and cyanine-5 (Cy-5) dye, is described for use with a planar, microfluidic, capillary electrophoresis (CE) chip. The CE-chip is able to detect a protein biological threat agent simulant, ovalbumin (Ov), by performing an immunoassay. The Cy-5 labeled



anti-ovalbumin is separated from its complex with Ov by CE, in under 30 s. A confocal, epiluminescent detection system utilizing a photomultiplier tube gave optimum results with a 400  $\mu\text{m}$  pinhole, an Omega 682DF22 emission filter, a 645 DRLP02 dichroic mirror, a  $634.54 \pm 5$  nm excitation filter, and a Power Technology ACMO8 635 nm laser operated at 11.2 mW. Using this detector, a microchip CE device with a separation efficiency of 42,000 plates and an etch depth of 20  $\mu\text{m}$ , gave a limit of detection of 9 pM Cy-5. This limit corresponds to the determination of 4560 injected molecules and detection of 900 of these molecules, given a probe volume of 1.6 pL and a probing efficiency of 20%.

## Acknowledgements

I would like to express my special thanks to my supervisor, Dr. D. Jed Harrison for his guidance and support during my Ph.D. program. I am so grateful for his introduction to this fantastic microfluidic world. Without his instruction, I could have never accomplished this thesis work.

I would like to thank Dr. D. Jed Harrison's group members for their helpful discussions. Special thanks go to Christa L. Colyer, Hossein Salimi-Moosavi, Charmaine Xiang-Ming Qiu, Yutao Jiang, Thompson Tang, Gregor Ocvirk and Loranelle Shultz-Lockyear for their helping me through the learning process when I joined this group.

I am greatly appreciated that Dr. Andreas Manz, Dr. Liang Li, Dr. Charles A. Lucy, Dr. Mariusz Klobukowski and Dr. John F. Elliott become my examining committee. Their constructive suggestions are very helpful.

I am grateful to Zhigang Jin of the University of Alberta Biology Department for technical advice and for a supply of fruit flies. Thanks go to Alberta Microelectronic Corporation for device fabrication and Fahima Ouchen for device fabrication training.

I would like to thank the Defense Advanced Research Projects Agency, Defence Research Establishment Suffield and National Sciences and Engineering Research Council for financial support of the projects and the Chemistry Department of the University of Alberta for a Research Fellowship.

## Table of content

	Page
Chapter 1. Introduction	1
1-1. Introduction	2
1-2. Motivation for this study	3
1-3. Genetics analysis with micro-fluidics	4
1-4. Detection methods in micro-fluidics	7
1-5. Capillary Zone Electrophoresis	9
1-6. Capillary gel electrophoresis (CGE)	11
1-6-1. Separation mechanism	12
1-6-2. Gel medium	13
1-7. The basics of DNA and RNA	14
1-8. Reverse transcription and polymerase chain reaction	19
1-8-1. PCR Stringency	20
1-8-2. RT primers	21
1-8-3. PCR primer design	21
1-9. cDNA library construction	23
1-9-1. Preparation of mRNA for cDNA cloning	24
1-9-2. Synthesis of the first strand of cDNA	25
1-9-3. Synthesis of the second strand of cDNA	26
1-9-3-1. Self-priming	27
1-9-3-2. Replacement	27
1-9-3-3. Primed synthesis	27
1-9-4. Molecular cloning of double stranded cDNA	28
1-9-4-1. Homopolymeric Tailing	28
1-9-4-2. Synthetic DNA linkers and adapters	28
1-9-5. Identification of cDNA clones of interest	29
1-10. Scope of the thesis	30
References:	32

Chapter 2. mRNA Isolation and cDNA Synthesis In A Microfluidic Device For Eventual Integration of cDNA Library Construction	37
2-1. Introduction	38
2-2. Experimental	39
2-2-1. Materials	39
2-2-2. Device Fabrication	42
2-2-3. Operation procedure	46
2-2-3-1. mRNA isolation on chip	46
2-2-3-2. mRNA isolation and cDNA synthesis on chip	50
2-3. Results and Discussion	54
2-3-1. Optimizing PCR conditions	54
2-3-1-1. Mg <sup>2+</sup> concentration	54
2-3-1-2. Annealing temperature	55
2-3-1-3. Primer concentration	56
2-3-2. mRNA isolation	57
2-3-3. mRNA isolation and cDNA synthesis	62
2-4 Conclusion	68
References	69
Chapter 3. Red Diode Laser Induced Fluorescence Detection on a Microchip for Capillary Electrophoresis	71
3-1. Introduction	72
3-2. Diode laser	73
3-2-1. Basics of diode lasers	74
3-2-2. Drawbacks of diode laser	75
3-3. Characteristics of the Cy-5 dye	78
3-4. LIF detection of Cy-5 using conventional and confocal optical set up	80
3-4-1. Experimental Section	80
3-4-1-1. Devices	80
3-4-1-2. Materials	80
3-4-1-3. Instrumentation	82

3-4-1-4. Chip operation	84
3-4-2. Results and Discussion	86
3-4-2-1. The performance of conventional two lens optical set up	87
3-4-2-2. The performance of a confocal optical set up	92
3-4-2-2-1. Optimization of filters	92
3-4-2-2-2. Optimization of excitation source	94
3-4-2-2-3. Confocal sectioning power	97
3-4-2-2-4. Limit of detection with optimized parameters	101
3-4-3. Conclusion	104
References	106
Chapter 4. Summary and Future Outlook	109
References	116
Appendix I	117

## List of Tables

	Page
Table 2-1. The conditions for RT	48
Table 2-2. The conditions for PCR	49
Table 3-1. Channel depths and widths	81
Table 3-2. Evaluation of filter sets	93
Table 3-3. Observed and estimated confocal sectioning power	99

## List of figures

	Page
Figure 1-1. Schematic illustration of the CE system	9
Figure 1-2. Schematic representation of capillary zone electrophoresis (CZE)	10
Figure 1-3. Structure of a single DNA strand.	14
Figure 1-4. The hydrogen bonds in A-T and C-G basepairs	16
Figure 1-5. mRNA structure	17
Figure 1-6. The X-ray structure of a complex of ethidium with dinucleoside.	18
Figure 1-7. Schematic illustration of the RT-PCR reaction	19
Figure 1-8. Synthesis of the first strand of cDNA	25
Figure 2-1. CGE and SGE testing the integrity of the TRNA	41
Figure 2-2. The procedure for photolithographic fabrication of glass device	43
Figure 2-3. Layout of the Y-channel fluidic chip	44
Figure 2-4. Y-intersection device for RT	45
Figure 2-5. Cartoon illustrating the affinity purification of mRNA from total RNA	46
Figure 2-6. Cartoon illustrating the affinity purification of mRNA from total RNA & cDNA synthesis	51
Figure 2-7. The peak height of PCR product detected by CGE versus annealing temperature	55
Figure 2-8. The peak height of PCR product detected by CGE versus primer concentration, shown for two independent trials	56
Figure 2-9. Electropherograms of PCR primers and DNA ladder.	57
Figure 2-10. Capillary gel electrophoresis of DNA marker and RT-PCR amplification of bicoid gene isolated on chip	58
Figure 2-11. The peak height observed by CGE for RT-PCR of mRNA captured on chip, is shown as a function of the TRNA mass.	58
Figure 2-12. CGE traces for an RNA marker, for mRNA isolated off chip and on-chip using Dynal beads,	60

Figure 2-13. Capillary gel electrophoresis of DNA marker mixed with PCR amplification of cDNA synthesized on chip from isolated mRNA and PCR amplification of cDNA synthesized on chip from isolated mRNA	62
Figure 2-14. Capillary gel electrophoresis of PCR amplification of cDNA synthesized on chip from mRNA isolated on-chip	63
Figure 2-15. Capillary gel electrophoresis of DNA marker and PCR amplification of cDNA	64
Figure 2-16. The magnetically trapped bead bed inside a 200 $\mu\text{m}$ wide channel	65
Figure 2-17. The magnetically trapped bead bed inside a 70 $\mu\text{m}$ channel	65
Figure 2-18. The peak area of CGE detection of PCR amplification of cDNA synthesized on chip vs. RT reaction temperature	66
Figure 2-19. Electropherograms of Hot start PCR and PCR	67
Figure 3-1. The energy-band diagram of a p-n junction	74
Figure 3-2. The rectangular facet of the laser diode might cause the elliptical cross section of the laser beam.	76
Figure 3-3. The rectangular facet of the laser diode might cause the astigmatism	77
Figure 3-4. The structure of the Cy-5 NHS ester (a) and unreactive Cy-5 (b).	79
Figure 3-5. Schematic layout of microchip designs for COPI and DARPA-NC1 devices	81
Figure 3-6. Conventional optical set up for LIF detection on chip	82
Figure 3-7. Confocal epifluorescence setup for Cy-5 detection on chip	83
Figure 3-8. Schematic illustration of double T injection and single T injection	85
Figure 3-9. Electropherogram of a mixture of 200 $\mu\text{M}$ Cy-5 labeled anti-ovalbumin (Ab*) and 600 $\mu\text{M}$ ovalbumin (Ag)	87
Figure 3-10. The multiple injection of 1 nM Cy-5 using double T injection, with conventional two lens optical set up.	89
Figure 3-11. The calibration curve of Cy-5 using double T injection, with conventional two lens optical set up	89



Figure 3-12. The electropherogram of 0.2 nM of Cy-5 using double T injection with 5 s injection and conventional two lens optical set up	90
Figure 3-13. The multiple injection of 2 nM Cy-5 using single T injection, with conventional two lens optical set up	90
Figure 3- 14. Calibration curve for the Cy-5 with 5s single T injection, with conventional two lens optical set up	91
Figure 3- 15. The electropherogram of 0.2 nM of Cy-5 using single T injection with 5 s injection, with conventional two lens optical set up	91
Figure 3-16. The S/N vs. output power of the laser plot	94
Figure 3-17. The observed laser spot focused in the channel	95
Figure 3-18. Signal-to-noise ratio versus vertical displacement of chip ( $\Delta z$ ) for various pinhole diameters using a 13 $\mu\text{m}$ deep channel	98
Figure 3-19. Signal-to-noise ratio versus vertical displacement of chip ( $\Delta z$ ) for various pinhole diameters using a 20 $\mu\text{m}$ deep channel	98
Figure 3-20. Signal-to-noise ratio versus pinhole size for 13 $\mu\text{m}$ and 20 $\mu\text{m}$ deep channels in Pyrex COPI devices	100
Figure 3-21. Electropherograms of various concentrations of Cy-5 standard solutions in a 20 $\mu\text{m}$ deep, DARPA1-NC device	101
Figure 3-22. Calibration Curve of Cy5 using 10 $\mu\text{m}$ deep channel	103
Figure 3-23. Calibration curve of Cy5 using 20 $\mu\text{m}$ channel depth	103
Figure 4-1. The schematic layout for the device with a dam	111
Figure 4-2. The schematic layout for integrating cDNA library construction on a microfluidic device	111
Figure 4-3. Schematic illustration for construction of cDNA library	113

## List of abbreviations

cDNA	complementary DNA
CDGE	capillary denaturing gel electrophoresis
CE	capillary electrophoresis
CGE	capillary gel electrophoresis
CZE	capillary zone electrophoresis
DNA	deoxyribonucleic acid
EOF	electroosmotic flow
ESI-MS	electrospray mass spectrometry
FITC	fluorescein isothiocyanate isomer I
HEC	hydroxyethyl cellulose
HPMC	hydroxypropylmethyl cellulose
LIF	laser induced fluorescence
LOD	limit of detection
mRNA	messenger RNA
$\mu$ TAS	miniaturized total analysis system
PA	polyacrylamide
PCR	polymerase chain reaction
PEO	poly (ethylene oxide)
RI	refractive index
RNA	ribonucleic acid
rRNA	ribosomal RNA
RT	reverse transcription
TRNA	total RNA
tRNA	transfer RNA

# **Chapter 1. Introduction**

### **1-1. Introduction:**

The concept of the Miniaturized Total Analysis System ( $\mu$ TAS), first suggested by Manz and Widner in 1990<sup>1</sup>, has been developed and applied to a variety of chemical, biological and environmental analysis systems. Planar microfluidic devices form the basis of many of the  $\mu$ TAS concepts that have been presented over the past ten years. While this has proven to be a powerful technology, there remains room for the development of new microfluidic designs and detector methods. This thesis will explore two different aspects of  $\mu$ TAS development. The first of these is the exploration of the technique of forming magnetically trapped bead beds for the capture and purification of messenger RNA. The ultimate goal of this project is the design of a microfluidic chip able to perform complementary DNA (cDNA) library construction. This thesis establishes several of the basic steps required to meet this ambitious goal. In a second project, the issue of sensitivity in detection on-chip was addressed. The goal of this study was to replace the gas-phase lasers used for laser induced fluorescence (LIF) detection with a compact, portable solid-state diode laser.

This introductory chapter will first provide a review of relevant literature on microfluidic devices and detection methods for these devices. Particular attention will be paid to efforts focusing on genetic applications of  $\mu$ TAS. A background introduction to capillary electrophoresis (CE), which forms the basis of many  $\mu$ TAS devices including those utilized in Chapter 3 will be presented. This will be followed by an introduction to molecular biology, and to cDNA cloning in particular.

## **1-2. Motivation for this study:**

The application of  $\mu$ TAS in genetic analysis has been extensive, but the focus has been on performing DNA sequencing<sup>2-8</sup> and polymerase chain reaction (PCR)<sup>9-18</sup>. The technology of cDNA library construction plays an important role in genetic analysis, and may also benefit from integration in a microfluidic system. The rapidly developing technology of planar microfluidics may eventually be able to provide a miniaturized, integrated platform for automated cDNA library construction. It may also be possible to reduce messenger RNA (mRNA) degradation by adventitious RNase, due to the closed nature of an integrated system. Integrating mRNA isolation, followed by cDNA synthesis on a microfluidic device, as presented in this thesis, represents the first two steps towards cDNA library construction on a chip.

This thesis also explores the development of a laser diode based detection method. Laser induced fluorescence (LIF) detection on microfluidic chips has been widely used in DNA separation<sup>2-8</sup>, immunoassay<sup>19-21</sup> and environmental analysis, due to its high sensitivity. The confocal epiluminescent microscope has been demonstrated to provide a very sensitive detection method on chip. To date, gas phase lasers were the most common excitation source used for LIF detection on microfluidic chips<sup>20-23</sup>. Such lasers are bulky and can be fragile, which makes them ill suited to demanding portable devices. Red diode lasers represent a more compact, portable source for LIF on-chip. The exploration of the performance of the diode laser on chip would benefit the construction of the DARPA box, a portable, automated microfluidic platform for immunoassays developed by Harrison's group as a co-contractor to DARPA (Defense Advanced Research Projects

Agency). The DARPA box has since been tested in a field trial, giving a satisfactory performance.

### **1-3. Genetics analysis with micro-fluidics:**

Since the first published demonstrations of capillary electrophoresis on a planar microfluidic glass devices<sup>22, 24</sup>, numerous papers about capillary electrophoresis separations in microfluidic chip have been published, including synchronized cyclic capillary zone electrophoresis<sup>25</sup>, capillary gel electrophoresis<sup>2-4</sup>, micellar electrokinetic chromatography<sup>26</sup>, microchip liquid chromatography<sup>27</sup> and capillary electrochromatography<sup>28</sup>. Recently, the application of  $\mu$ -fluidic devices in genetic analysis has been extensive. DNA separation<sup>2-3</sup>, high throughput DNA sequencing<sup>5, 7</sup> and PCR reactions<sup>9-18</sup> have been demonstrated using  $\mu$ -fluidic devices. Several research groups also reported the integration of PCR with capillary electrophoresis separation on a  $\mu$ -fluidic device<sup>9, 13, 16</sup>, making  $\mu$ -fluidic devices a powerful method in genetic analysis. In general, an attractive feature in utilizing microfabricated devices is the improved analytical performance, which include fast and efficient separations, shorter transport time and lower consumption of chemicals

The application of  $\mu$ -fluidics in the genetic analysis has developed over the last decade. The earlier research was focused on the separation of oligonucleotides and DNA on  $\mu$ -fluidic devices using capillary gel electrophoresis<sup>2-3</sup>. In 1994, the separation of both oligonucleotides and DNA were reported using  $\mu$ -fluidic devices<sup>2-3</sup>. One year later, high-speed DNA sequencing on chip was demonstrated by Mathies's group<sup>4</sup>. Single base resolution up to ~150 bases was achieved in 540 s. The design, fabrication and detection

of 12 different samples in parallel and later a 96 capillary array electrophoresis microplate were demonstrated by the same group<sup>5, 7</sup>. These microfabricated DNA analysis systems allow high-throughput sequencing to take place in a large scale. As a result of the completion of the Human Genome Project, the demand for high-throughput, high-performance DNA sequencing can be expected to increase dramatically. The new  $\mu$ -fluidic devices may soon replace the 96-fused silica capillary array systems introduced in the last 3-4 years.

PCR is a very important tool in molecular biology. The ability to perform PCR using microfabricated devices was an important step in microfluidics and such devices may ultimately replace current methods. Conventional PCR is performed using thermal cyclers. A long thermal cycling time is required due to the large thermal mass of the conventional systems. Miniaturized devices seem to be one way to reduce the long cycling times. Silicon substrates have a very high thermal conductivity, and glass is reasonably thermally conductive. The small sample volumes handled on microfabricated devices are another factor in enhancing the heating and cooling speed of the systems.

A number of groups have investigated microfabricated PCR devices. Early studies demonstrated the faster thermal cycling speed of PCR associated with various designs of the reaction and heating chambers<sup>10-12</sup>. The pre-mixed reagent was added into the microfabricated PCR reaction chambers when PCR took place. The faster cycling speed of these devices illustrated the beneficial elements that the miniaturized devices brought to the PCR world. As an alternative to such batch reaction systems, a continuous flow PCR system was demonstrated by Manz's research group<sup>17-18</sup>. In this device there are three different temperature zones, heated by thermostat copper blocks. As the reagent was

pumped through the chip, it passed repeatedly through the three different zones to provide the thermal cycling required for PCR. The cycle time depended on the length of channel within each temperature zone and the flow rate of the fluid. The cycle number was controlled by the number of repeated passes through the temperature zone. The advantage of this system is that it needs only to heat up the fluid in the channel, not the whole PCR chamber. As a result, short times for heating and cooling were required.

Another aspect of application of microfabricated devices in genetics analysis is the integration of the PCR with capillary electrophoresis separation. Northrup et al<sup>9</sup> demonstrated the first coupling of a silicon and plastic PCR reactor to a glass capillary electrophoresis chip. The PCR chamber was directly linked with the CE chip through a flow channel filled with hydroxyethylcellulose. After 15 minutes for the PCR reaction, the PCR amplification product was immediately injected into the CE chip for separation. The whole PCR-CE analysis was done in 20 minutes. Ramsey's research group<sup>13</sup> later reported the integration of PCR with CGE separation of DNA. PCR reagent was put into one reservoir, and the whole device was thermally cycled. The PCR product was analyzed on CE chip with or without preconcentration. This approach benefited from the integrated analysis, but had slow PCR cycle times due to the need to heat and cool the entire wafer. An improvement was reported recently<sup>29</sup>, in which PCR was performed in a reservoir on-chip by heating the reservoir region alone using a dual Peltier, in which, the cycle time was reduced to 1.25 min. Recent work from Mathies's group<sup>30</sup> showed the PCR amplification of DNA followed by capillary electrophoresis analysis on an integrated device. A 280 nL PCR chamber was etched into a glass substrate and directly connected to a CE channel. A valve and hydrophobic vent, which were actuated using



aluminum pneumatic manifolds that vacuum clamped to the chip, were employed to provide controlled loading for the PCR reaction. After PCR amplification, the manifold was removed from the chip. The platinum electrode and the CGE running buffer were then placed in the reservoirs for injection and separation. A 30 s cycle time was obtained and single molecule amplification was reported using this system.

#### **1-4. Detection method in micro-fluidics:**

LIF detection, though it is not a universal detection method, is still the most powerful detection method applied to  $\mu$ -fluidic devices, due to its tremendous sensitivity. Ocvirk described a confocal epiluminescent optical system used in LIF detection in detail in his thesis<sup>31</sup>. A similar optical set up was employed in Chapter 3. The red diode laser was employed as the source for LIF on chip. The red diode laser has several advantages compared with the gas phase laser. First, it is compact and portable, suitable to the demand of miniaturization. Second, it is a low cost, rugged light source. In addition, the life time for the red laser is longer ( $10^5$  h)<sup>32</sup>. In Chapter 3, the performance of the confocal optical system was tested by using of red diode laser on a microfluidic device.

To date, LIF is the principal detection method in  $\mu$ -fluidics device due to its high sensitivity. However, due to the non-fluorescent nature of most analytes of interest, the need for alternative detection methods that are universal and sensitive is apparent. Absorbance detection is more generally accepted due to its wider applicability, yet absorbance measurements in the small volume within  $\mu$ -fluidics devices is a challenge. Harrison and coworkers reported the fabrication of a planar optical U-cell for both absorbance and fluorescence detection<sup>33</sup>. Using this design, the optical path length was

improved 10 times. However, because of the poor coupling of the optic fiber, a 3 nM fluorescein isothiocyanate isomer I (FITC) detection limit was obtained for fluorescence design. The absorbance detector was limited by the ~200  $\mu\text{m}$  path length. A multi-reflection absorbance detector cell was reported by the same group<sup>34</sup>. The device was fabricated using a three photolithographic mask and three step etching process. Path lengths of 100-300  $\mu\text{m}$  were achieved, giving moderately sensitive detection. Nevertheless, absorbance detection is not the most sensitive technique, even in conventional chromatography and CE.

Electrochemical detection has been demonstrated as another attractive alternative for  $\mu$ -fluidic devices<sup>35-39</sup>. The ability to fabricate microelectrodes using photolithographic methods makes it ideally suited for integration on  $\mu$ -fluidic devices. The principle of electrochemical detection is based upon redox reactions at the surface of an electrode. It is possible to adapt this detection method to  $\mu$ -fluidic devices without loss of sensitivity. Mathies's research group demonstrated the use of electrochemical detection on  $\mu$ -fluidics device<sup>35</sup>. An amperometric detector with a three electrode system was employed for detection. Photolithographic placement of the working electrode outside of the exit of the separation channel minimized the interference caused by the electric field used for separation, giving moderately sensitivity performance. The LOD of this detection system was reported to be in the  $\mu\text{M}$  range for neurotransmitters. Indirect electrochemical detection of DNA fragments was also reported.

Raman spectroscopy has been reported as an on line detector for  $\mu$ -fluidic devices<sup>40</sup>. The detection of 0.2  $\mu\text{M}$  herbicide was achieved using Raman spectroscopy. Unfortunately, the Raman spectrum of water limited the detection limit.

Refractive index (RI) detection is a simple, universal, concentration sensitive method applied in conventional analytical separation, such as chromatography, capillary electrophoresis. Manz's group demonstrated the feasibility of using a hologram-based RI detector in a  $\mu$ -fluidic device<sup>41</sup>. However, it will be necessary to improve the limit of detection from the reported range of 10 mM carbohydrate.

Other detection methods have been reported on  $\mu$ -fluidics device, including chemiluminescence<sup>42</sup>, electrochemiluminescence<sup>43</sup>, electrospray massspectrometry (ESI-MS)<sup>44</sup> and Shah convolution Fourier Transform detection<sup>45</sup>. However, from the sensitivity point of view, these detection methods are far behind those of LIF detection.

### 1-5. Capillary Zone Electrophoresis

Capillary electrophoresis (CE) is a widely used analytical technique, which allows fast and efficient separation of the charged component, consuming sample in the nL

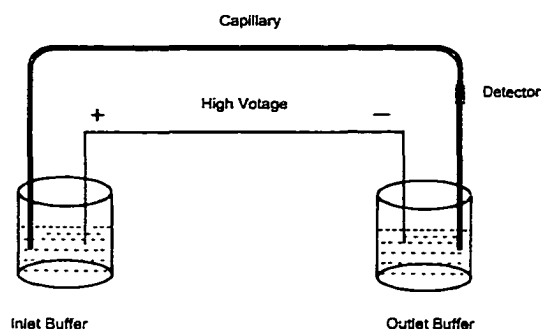


*Figure 1-1. Schematic illustration of the CE system*

range. The differences in electrophoretic mobilities of ions inside the capillaries are the basic element for the separations<sup>46-50</sup>. The simple instrumentation of the CE system (Figure 1-1) attributed to the fast growth of CE in many applications. One high voltage power supply, two buffer reservoirs,

a polyimide coated capillary and a detector are the basic component for the CE

instrument, which could be employed for different mode of capillary electrophoretic

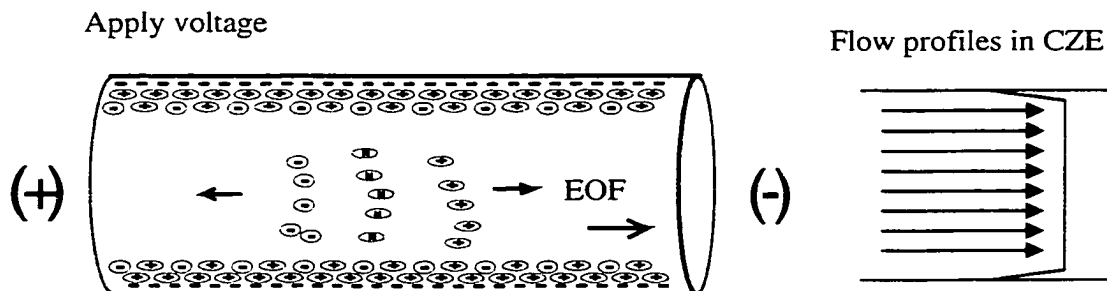


Figure 1-2. Schematic representation of capillary zone electrophoresis (CZE)

separations<sup>51</sup>. Among the several modes of the capillary electrophoretic separations, capillary zone electrophoresis (CZE) is the most commonly used technique (Figure 1-2). The separation is based on the differences in the electrophoretic mobility of the sample in the buffer solution. In other words, the differences in the charge/ size ratio of the sample at a given pH cause the CZE separation. The electrophoretic mobility  $\mu_{ep}$  is given by equation 1-1<sup>52</sup>:

$$\mu_{ep} = \frac{q}{6\pi\eta r} \quad (1-1)$$

Where  $q$  is the effective charge of the sample analyte,  $r$  is the hydrodynamic radius, and  $\eta$  is the medium viscosity.

Most of the capillaries used are made of fused silica, which bears silanol groups on the surface. These silanol groups become ionized in solution and the electrical double layer is formed in the presence of the buffer solution used for CZE. The application of an electrical field induces a migration of fluids through the capillary, which is known as

electroosmotic flow (EOF). The electroosmotic mobility  $\mu_{eo}$ , with units of  $\text{cm}^2/\text{V}\cdot\text{s}$ , is given by equation 1-2<sup>51</sup>:

$$\mu_{eo} = \frac{\epsilon\zeta}{4\pi\eta} \quad (1-2)$$

Where  $\zeta$  is the zeta potential,  $\epsilon$  is the dielectric constant of the solution, and  $\eta$  is the medium viscosity. The velocity  $v$  and migration time  $t$  are given by<sup>51</sup>:

$$v = \frac{(\mu_{eo} + \mu_{ep})V}{L} \quad (1-3)$$

and

$$t = \frac{Ll}{(\mu_{eo} + \mu_{ep})V} \quad (1-4)$$

Where  $V$  is the applied voltage,  $L$  is the length of capillary;  $l$  is the injector-detector distance.

### 1-6. Capillary gel electrophoresis

The rapid, high resolution, high throughput, high sensitivity analysis of RNA, single-stranded (ss) DNA and double-stranded (ds) DNA molecules is a valuable analytical technique in molecular biology. Recently, capillary gel electrophoresis (CGE) has been widely used in DNA sequencing<sup>53-56</sup> during the Human Genome Project. The analysis of the DNA fragments produced by PCR<sup>57-58</sup> has led to the direct detection and quantitation of viruses, diagnosis of genetic diseases and aided in mapping the human genome. For ssDNA and RNA analysis, capillary denaturing gel electrophoresis (CDGE) is employed. A denaturant, such as urea or formamide is added into the gel medium. The

denaturant suppresses the base pairing in the nucleic acids, reducing the secondary structures of the ssDNA and the RNA and achieving good resolution.

### *1-6-1. Separation mechanism*

In free solution, DNA molecules can not be separated using capillary zone electrophoresis because of the linear charge density. For this reason, a sieving medium (gel) has to be introduced into the capillary to achieve DNA separation. Two theories, the Ogston model and the reptation model have been proposed in the past<sup>52</sup> to explain the mechanism of gel electrophoresis.

The Ogston model characterized the gel as a molecular sieve. The mobility of the DNA in the gel medium,  $\mu$ , is given by:

$$\mu = \mu_0^{[-K_r C]} \quad (1-5)$$

where  $\mu_0$  is the mobility of the DNA in free solution,  $K_r$  is the retardation coefficient, which is a function of the size of the DNA and the pore size of the gel, and  $C$  is the concentration of the gel. According to the Ogston model, the mobility of DNA in CGE is dependent on the gel concentration and the DNA size. In a certain concentration of gel medium, the bigger the DNA size, the smaller the mobility will be. However, the Ogston model does not describe the larger DNA molecules, for which the reptation model applies. According to this model, the mobility of DNA is inversely proportional to its size  $N$ :

$$\mu \propto N^{-1} \quad (1-6)$$

In a very high electric field, the DNA molecules become rigid and rod-shaped. The mobility of DNA not only depends on the size of the DNA,  $N$ , but also the electric field,  $E$ . The relationship can be given by:

$$\mu \approx K(N^{-1} + bE^2) \quad (1-7)$$

where  $K$  is a constant and  $b$  is a function of the gel pore size. As the magnitude of the electric field increases (or the DNA size increases), the mobility is no longer related to DNA size, thus there is no separation between small or large DNA molecules. This has limited the magnitudes of field used in DNA separation by CGE to about 300 V/cm.

#### *1-6-2. Gel medium:*

Since the first report of DNA separation with cross-linked polyacrylamide (PA)<sup>59</sup>, several different polymers have been successfully employed in the analysis of DNA<sup>60-64</sup>. There are two kinds of the gel medium employed in CGE for DNA analysis. One is called “chemical gels”<sup>52</sup>, in which the gel medium is chemically cross-linked and may be covalently attached to the wall of the capillary. These gels have a well defined pore size and structure. The resolution, as a result, is good enough to do the DNA sequencing<sup>65</sup>. However, problems such as bubble formation and the degradation of the medium with each use limit the wide application of chemical gels. A search for replaceable “physical gels” was thus initiated.

“Physical gels” refer to noncross-linked, hydrophilic polymer solutions. These gels have low viscosity, which allows replacement of the material as needed without replacement of the capillary. Since they can be pumped out of the capillary at the end of each run, fresh media can be used for each analysis. Linear polyacrylamide has been used

in a number of applications. Dovichi's research group and Karger's research group reported the rapid DNA sequencing by capillary electrophoresis using replaceable linear polyacrylamide<sup>56, 66</sup>. However, these polymers are usually used with a coated capillary. The coating eliminates the EOF, improving reproducibility by eliminating the variability of EOF, and reducing adsorption effects. The other type of replaceable gels are cellulose polymers<sup>67-68</sup>, such as hydroxyethyl cellulose (HEC), hydroxypropylmethyl cellulose (HPMC) and methylcellulose. One advantage of the cellulose polymers is that they can produce dynamic coating of the capillary, which makes the use of uncoated capillaries possible. In addition, a number of other polymers have been tested for analysis of DNA. These include agarose<sup>69-70</sup>, poly (N-acryloylaminoethoxyethanol)<sup>71</sup>, poly (ethylene oxide) (PEO)<sup>64, 72-74</sup> and so on.

In the next chapter, both CGE and CDGE were employed for analyzing the DNA

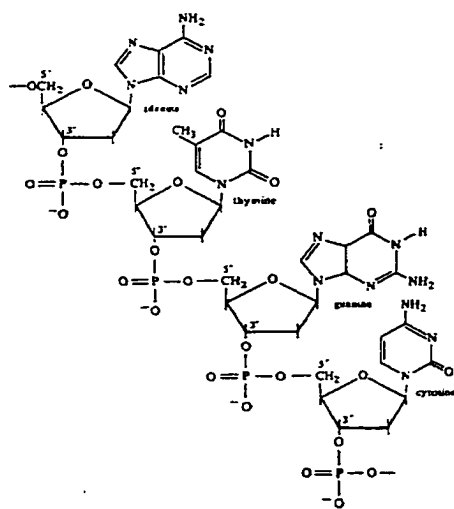


*Figure 1-3. Structure of a single DNA strand. RNA has a similar structure with two exceptions: a hydroxyl replaces hydrogen at the 2'- position of each ribose and uracil replaces thymine.*

fragments produced by PCR and testing the integrity of RNA. HPMC was used as the gel medium for both methods.

### 1-7. The basics of DNA and RNA:

Nucleic acids are linear polymers of nucleotides. A general nucleotide contains a phosphate ion, a five carbon monosaccharide and a heterocyclic base (Fig.1-3). The connecting links in nucleic acids are phosphate ester linkages, which



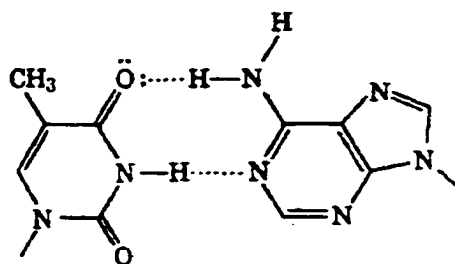
link the 3'-hydroxyl of one sugar with the 5'-hydroxyl of another. The heterocyclic base is attached through an N-glycosidic linkage to C-1' of the sugar unit. There are two classes of nucleic acids, deoxyribonucleic acid (DNA) and ribonucleic acid (RNA). There are two differences between DNA and RNA. DNA contains deoxyribose as its sugar component, and adenine, guanine, cytosine and thymine as its heterocyclic bases. RNA contains ribose and adenine, guanine, cytosine, uracil instead.

DNA has a double-stranded helix structure in nature. The two strands of DNA are held together by the base pairing of the purine and pyrimidine bases. A single base from one strand forms a hydrogen bond with the single base from the other strand. Figure 1-4 shows the structure of the base pairing between two strands of DNA. The A-T base pair forms two hydrogen bonds and the C-G base pair forms three hydrogen bonds (Fig. 1-4). However, the hydrogen bonds contribute little to the stability of the double helix. The base stacking and the hydrophobic interactions are responsible for the double helix stability<sup>75</sup>. In addition, electrostatic interactions also contribute to the stability of the DNA helix. For instance, the melting temperature of duplex DNA increases with the cation concentration because these ions electrostatically shield the anionic phosphate groups from each other. The same explanation applies to the experimental observation that the  $Mg^{2+}$  ion plays an essential role in stabilizing double-stranded DNA.

RNA usually occurs as a single-stranded molecule. It is probably impossible to build a double-stranded helix structure with a ribose in the place of deoxyribose. The extra oxygen may make the duplex structure unstable<sup>76</sup>. RNA has secondary structure due to hydrogen bond formation between bases. This self-annealing of the RNA causes the formation of hairpins, which make the analysis and reverse transcription (RT) of RNA

very difficult. Denaturing of RNA by heat or by adding a chemical denaturant are methods used to reduce the secondary structure of RNA.

adenine pairs with thymine



guanine pairs with cytosine

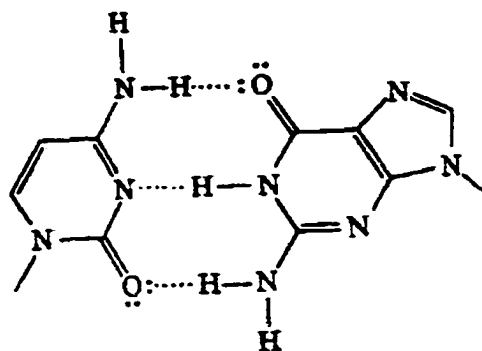


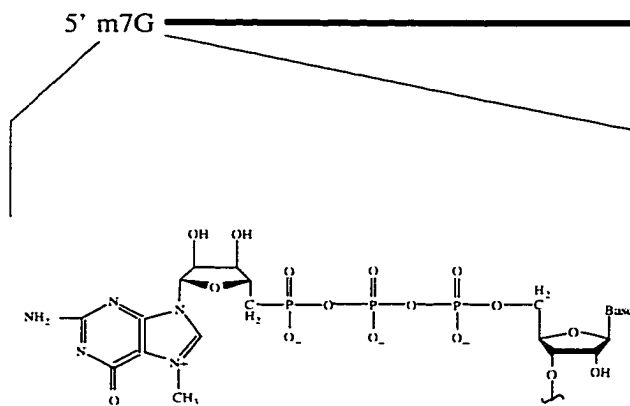
Figure 1-4. The hydrogen bonds in A-T and C-G basepairs

There are three major classes of RNA in total RNA (TRNA): ribosomal RNA (rRNA), transfer RNA (tRNA) and mRNA. About 80-85% of TRNA is rRNA (chiefly 28s, 18s and 5s sedimentation fractions). Most of the remaining 15-20% consists of a variety of low molecular weight species (tRNA and small nuclear RNA). Messenger RNA makes up between 1%-5% of the total cellular RNA. It is heterogeneous in both size and sequence. Reassociation-kinetic analysis indicates that the mRNA of a typical cell is distributed into three frequency classes. A highly abundant class consists of 10-15 differing mRNA sequences, which altogether represent 10-20% of the total mRNA mass. A middle abundance class consisting of 1000-2000 differing mRNA makes up 30-40% of the total mRNA, and a low abundance class consisting of 15,000-20,000 mRNA sequences represents about 50% of the total mRNA.

Most eukaryotic mRNA carries at the 3' end a tail of polyadenylic acid residues

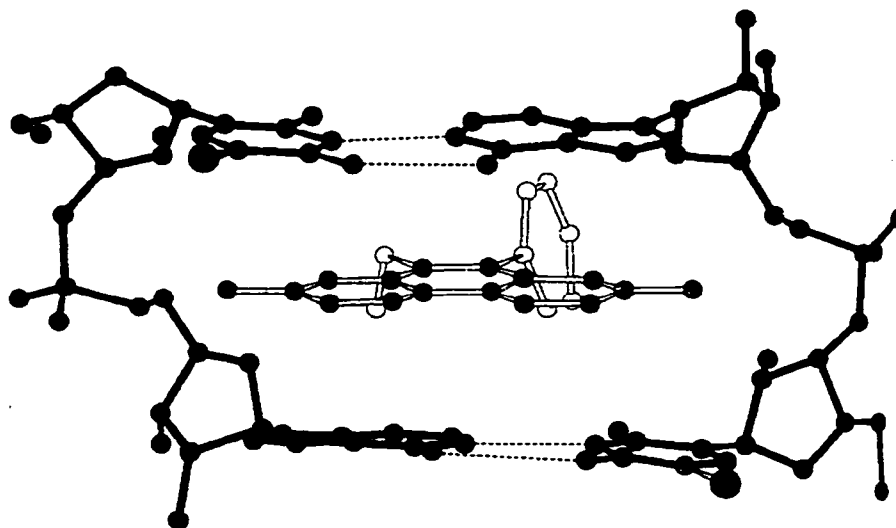
(Figure 1-5), which is long enough to allow mRNA to be purified by affinity chromatography on oligod(T) cellulose. Eukaryotic mRNA also contains another unique structural feature, a 5' cap consisting of an m7G residue linked *via* an inverted 5' to 5' linkage to the body of the mRNA <sup>77</sup>

Figure 1-5. mRNA structure



(Figure 1-5). On the other hand, rRNA and tRNA do not have the 5' cap structures, nor do they have poly(A) tails.

Usually, DNA (RNA) is separated by gel electrophoresis. Ethidium bromide, an intercalating dye, is used to stain DNA for fluorescence detection. The high fluorescence enhancement of the ethidium-DNA complex makes it widely accepted as one of the convenient methods to “label” DNA molecules. Figure 1-6 illustrates the x-ray structure of the complex of ethidium with dinucleotides <sup>78</sup>. Ethidium intercalates between the base pairs of the dinucleotide. For double-stranded DNA, intercalating binding follows the “neighbor-exclusion principle” where every other intercalating site along the length of the DNA double helix remains unoccupied <sup>79-81</sup>. Therefore, at a bound dye to base pair ratio of 1:4, the duplex should be saturated with the intercalating dye. Low ratios will limit the number of bound dye and thus, reduce the sensitivity. High ratios may result in quenching of the fluorescence <sup>82</sup>. Ethidium bromide can be used to detect RNA as well. However, the affinity of the dye for RNA is relatively low and the fluorescent yield is comparatively low.



*Figure 1-6. The X-ray structure of a complex of ethidium with dinucleoside.*

### 1-8. Reverse transcription and polymerase chain reaction:

Sensitive methods for the detection and analysis of RNA molecules are important aspects of most molecular biology studies. Among the commonly used methods, such as *in situ* hybridization, northern blots, S1 nuclease analysis and RNase protection assays, *in situ* hybridization is very sensitive, but is a difficult technique. The other methods lack the sensitivity needed for analysis of the rare transcript or RNA present in low abundance. The adaptation of PCR methodology to the investigation of RNA provided researchers a method featuring speed, efficiency, specificity and sensitivity.

Since RNA can not serve as a template for PCR, reverse transcription is employed to convert the RNA into cDNA, which can be a template for PCR. This two-step technique is referred to as RT-PCR (Figure 1-7). RT-PCR is a highly sensitive tool in the

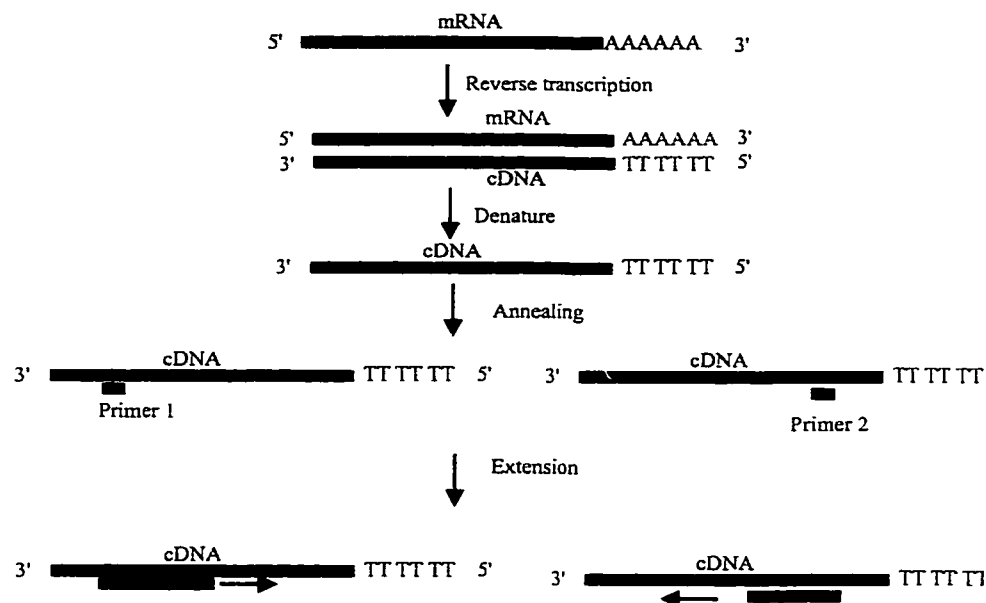


Figure 1-7. Schematic illustration of the RT-PCR reaction

study of gene expression at the RNA level. This technique permits the simultaneous analysis of a large number of mRNAs from a small number of cells<sup>83</sup>. RT-PCR can also be used as a first step in preparing a cDNA library by RT-PCR of all of the mRNA in a sample of cellular RNA. After the RT step, the terminal transferase and dATP will be added into the chamber to synthesize an A tail to the first strand of cDNA. Then PCR will be carried out using T<sub>15</sub> as primer, which will be bound on to the synthetic A tail of first strand cDNA. Such methods have been successful and it is possible to construct a cDNA library from a small number of cells. This is important in situations where only small numbers of cells are available or when the cells of interest can not be propagated<sup>77</sup>.

There are two fundamental aspects of PCR. One is the enormous amplification achieved. Theoretically, after the second cycle, the amplification factor for the PCR reaction is  $2^{n-1}$ , where n is the cycle number. With such extreme sensitivity in PCR, contamination must be carefully avoided. The other aspect is the specificity. Since the target region is defined by the flanking primers, the primers will only be specifically hybridized to a certain region of template DNA under annealing conditions. With such extremely sensitivity and selectivity, PCR has had a profound impact upon molecular biology.

#### *1-8-1. PCR Stringency*

Stringency relates to the number of mismatched basepairs that can be tolerated when two nucleic acid molecules come together to form a double-stranded molecule. Stringency is affected by several variables, including the temperature, salt concentration and pH of the hybridization reaction<sup>84-85</sup>. The higher the stringency of the reaction, the

less likely it is for mismatched basepairs to stay together as a stable double-stranded molecule<sup>84</sup>. Under conditions of low stringency, a false-positive reaction might happen. Thus to avoid false-positive reactions, hybridization conditions particularly ionic strength, pH and temperature, must be carefully controlled.

### *1-8-2. RT primers*

In RT, only a single primer is required. There are three types of primers that may be used for reverse transcription, oligo(dT)<sub>12-18</sub>, random hexanucleotides and specific oligonucleotide sequences. Oligo(dT)<sub>12-18</sub> binds to the endogenous poly (A) tail at the 3' end of mammalian mRNA. This primer most frequently produces a full length cDNA product, unless hairpin structure interferes with the reverse transcription. Random hexanucleotides can bind to mRNA template at any complementary site and will give partial length (short) cDNA. Template secondary structure means that the structure near the 5' end is often not reverse transcribed, so the random primers are often better at ensuring some partial length representing of the 5' end will be present. Specific oligonucleotide sequences can be used to selectively prime the RNA of interest. In chapter 2, since the eventual goal is to build cDNA library, the oligo(dT)<sub>12-18</sub> primer is the best choice for RT primer.

### *1-8-3. PCR primer design*

The specificity of the PCR reaction depends on the primers. Choosing an effective primer for PCR is crucial in practice. The following factors are important.

- Primers should be 17 to 30 bases in length. Longer primers may cause poor annealing efficiency for PCR, while shorter primers may effect the specificity of PCR.
- The GC content is close to 50%. A low GC content of the primer might cause a lower melting temperature.
- A sequence with long runs of a single nucleotide should be avoided.
- Primers which may form significant secondary structure are undesirable.
- There should be no complementary binding between the two primers.

When TRNA is extracted from tissue using Trizol reagent, it is possible that the extract may be contaminated with genomic DNA. PCR can not discriminate between cDNA targets synthesized by reverse transcription and genomic contamination. The critical aspect in RT-PCR primer choice, with respect to minimizing the problems associated with DNA contamination, is to design primers that will cross the intron/exon boundary in genomic DNA. This will result in a PCR product from genomic contamination that will be larger in size than the product generated from cDNA. In this thesis *Drosophila Melanogaster* was used as the mRNA source. The sequence information showed that the two 22 bp primers selected for the PCR amplification of the bicoid mRNA gene (2456 bp) would give a 699 bp RT-PCR product, while the bicoid genomic DNA (5130 bp) would give a 1214 bp PCR product. As a result, the CGE detection of the PCR product would distinguish the PCR amplification of cDNA from that of contaminated genomic DNA. The sequence information for bicoid mRNA and bicoid genomic DNA are given in Appendix I.



### 1-9. cDNA library construction

Genomic DNA and mRNA provide two sources of genetic information. To supplement information obtained by studying clones of genomic DNA, it is essential to be able to clone the expressed RNA products encoded by genomic DNA. This has been accomplished by using viral reverse transcriptase to synthesize complementary DNA (cDNA) copies of RNA<sup>86</sup>. Introns (non-coding sequences) will be spliced out during formation of mRNA, so that it will contain a contiguous coding region. Thus, cDNA lacks the intron sequences that are usually present in corresponding genomic DNA. The position of intron/exon boundaries can be assigned by comparison with the cDNA sequence if the sequence of genomic DNA is known. In the field of functional genomics, cDNA cloning is carried out if information about temporally regulated gene expression in development or in tissue-specific gene expression is needed<sup>87</sup>. It is also possible to screen a cDNA library to identify cDNA clones from mRNA molecules present in one cell type but absent in another cell type, by using differential screening procedures.

There are three major classes of RNA in TRNA: rRNA, tRNA and mRNA. To construct a cDNA library, mRNA is first isolated from TRNA and then serves as a template for cDNA synthesis (reverse transcription). A typical mammalian cell contains about 20 pg of RNA ( $3.6 \times 10^{10}$  nucleotides), so that the content of mRNA within the cell is approximately  $5 \times 10^8$  nucleotides (assuming that mRNA represents about 1.5% of the RNA in the cell)<sup>86</sup>. Because the average mRNA has a size of about 2000 nucleotides, this means there are approximately 400,000 mRNA molecules per cell. It has been estimated that there are more than 10,000 and possibly as many as 20,000 different mRNA's per cell, with any given mRNA represented from one to thousands of times per cell.

The technology for preparing useful cDNA libraries has advanced remarkably.

These technical advances include:

1. Simple and effective methods for isolating intact RNA.
2. Better quality preparations of many enzymes required for converting RNA to cDNA clones.
3. Better methods for converting single-stranded to double-stranded cDNA with ends suitable for ligating to a vector.
4. The availability of more efficiently cloning vectors.

As a consequence, the construction of cDNA libraries is now feasible for most laboratories.

#### *1-9-1. Preparation of mRNA for cDNA cloning*

It is possible to isolate mRNA from TRNA using oligodT coated solid phase support. Since mRNA has a poly A tail it will be captured, while rRNA and tRNA, which don not have a poly A tail, will be washed away. To construct a cDNA library, mRNA must serve as a template for reverse transcription. Clearly, the higher the concentration of the sequences of interest in the starting mRNA, the easier the task of isolating relevant cDNA clones becomes. Therefore, it is worthwhile to ensure that sufficient, high quality mRNA is available. Since the cDNA library cannot be better than the mRNA from which it is derived, it is important to check the integrity of the preparation of mRNA before it is used as a template for first strand cDNA synthesis. Typically isolated mRNA is analyzed by gel electrophoresis to assess the quality.

### 1-9-2. Synthesis of the first strand of cDNA

A schematic illustration of synthesis of the first strand of cDNA is shown in Fig.1-8. There are two different reverse transcriptase used during first strand cDNA synthesis: Avian reverse transcriptase, which is purified from particles of an avian retrovirus, and

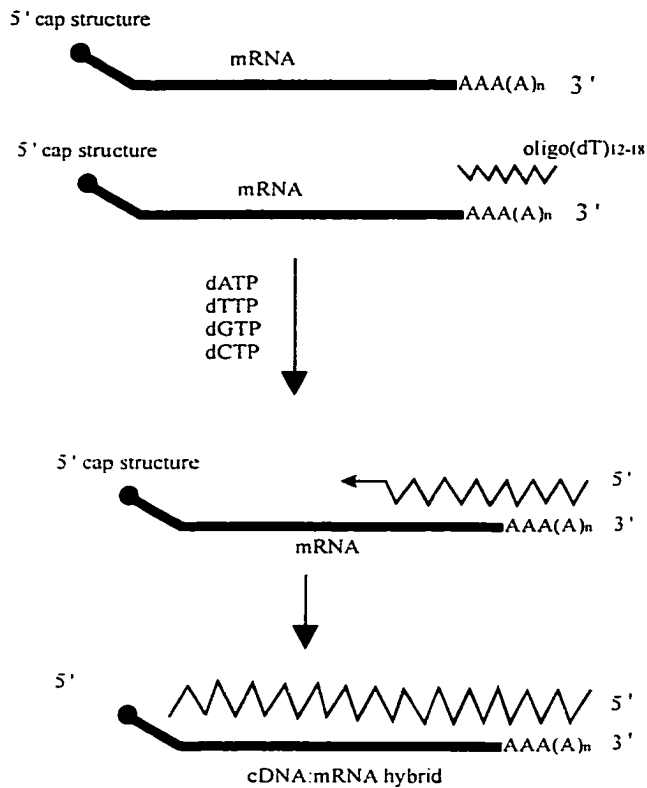


Figure 1-8. Synthesis of the first strand of cDNA using an oligo(dT) primer and reverse transcriptase.

murine reverse transcriptase, which is isolated from a strain of *E. coli* that expresses a cloned copy of the reverse transcriptase gene of the Moloney murine leukemia virus. The avian enzyme consists of two polypeptide subunits that carry several enzymatic activities: RNA-dependant synthesis of DNA, DNA-dependant synthesis of DNA, and endonucleolytic attack on the RNA moiety of DNA:RNA hybrids followed by processive exonucleolytic removal of ribonucleoside triphosphates

(rNTPs). The high level of RNase H activity tends to suppress the yield of cDNA and to restrict its length when avian enzyme is used to synthesize cDNA. The murine enzyme consists of a single polypeptide subunit that carries out both RNA- and DNA-dependant synthesis of DNA, but has a reduced capacity to degrade RNA in DNA:RNA hybrids.

Preparations of murine reverse transcriptase lack the contaminating endonuclease activity. Thus, the murine enzyme, is a safer choice when attempting to obtain full-length cDNA copies of mRNAs larger than 2-3 kb in length. For cloning cDNA, a primer is required to initiate synthesis of DNA. The most frequently used primer is oligo(dT)<sub>12-18</sub>, which binds to the poly (A) tails of mRNA. The primer is added to the reaction mix in large excess, so that each molecule of mRNA binds several molecules of oligo(dT)<sub>12-18</sub>. Priming of cDNA synthesis probably begins from the most proximal of these bonded primers and is very efficient.

The secondary structure (hairpin formation) of mRNA plays an important role in cDNA synthesis. The length of the cDNA synthesized by reverse transcription is limited by the mRNA secondary structure. Because both enzymes mentioned above need fairly low temperature for reverse transcription, the presence of hairpin is a significant problem. Thus a denaturing step for mRNA is important before use, mRNA is first denatured by applying high temperature, then it is cooled on ice to reduce hairpin formation. However, some hairpins return during cooling, resulting in poor quality of cDNA. Therefore, enzymes which work in a higher temperature range would be beneficial, although the cost could be high.

### *1-9-3. Synthesis of the second strand of cDNA*

There are three methods to synthesize second strand cDNA. self-priming, replacement and primed synthesis of the second strand of cDNA.

### *1-9-3-1. Self-priming:*

The 3' end of single stranded cDNA is capable of forming hairpin structures that can be used to prime the synthesis of the second strand of cDNA by reverse transcriptase. To allow these structures to form, it is necessary to denature the DNA:RNA hybrid molecules by boiling or hydrolyzing RNA with OH<sup>-</sup>.

### *1-9-3-2. Replacement:*

In this method, the product of first-strand synthesis, the cDNA:mRNA hybrid is used as a template for a nick-translation reaction. Rnase H produces nicks and gaps in the mRNA strand of the hybrid, creating a series of RNA primers that are used by *E. coli* DNA polymerase I during the synthesis of the second strand of cDNA. Most cDNA libraries are constructed using a replacement reaction to synthesize the second strand of cDNA.

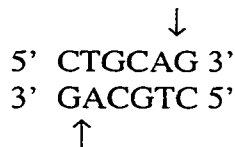
### *1-9-3-3. Primed synthesis:*

Sometimes, if it is necessary to clone the 5'-terminal sequences of eukaryotic mRNA, the primed synthesis method is used. After completion of the first strand cDNA synthesis, terminal transferase can be used to add homopolymeric tails of dC residues (often referred to homopolymeric tracts) to free 3'-hydroxyl groups. This tail is then hybridized to oligo(dG), which serves as primer for synthesis of a full-length second strand of cDNA. The 5' cap structure of mRNA may be removed before second strand cDNA synthesis.

#### *1-9-4. Molecular cloning of double stranded cDNA*

##### *1-9-4-1. Homopolymeric Tailing*

One of the most commonly used procedures for cloning cDNA is to add the complementary homopolymeric tracts to double-stranded cDNA and to the plasmid vector. The vector and the double-stranded cDNA are then joined by hydrogen bonding between the complimentary homopolymers to form open circular hybrid molecules capable of transforming *E. coli*. Usually, all cDNA cloning is carried out by homopolymetic dG:dC tailing: dC residues are added to the double-stranded cDNA, and complementary dG residues are added to a plasmid vector that is digested with *Pst*I. This enzyme cleaves the sequence



leaving protruding 3' termini that are ideal substrates for addition of homopolymeric tails.

##### *1-9-4-2. Synthetic DNA linkers and adapters*

Unlike the homopolymeric tailing method, synthetic linkers containing one or more restriction sites provide an alternative method for joining double-stranded cDNA to both plasmid and bacteriophage  $\lambda$  vectors. Double-stranded cDNA is treated with specific enzymes to generate blunt-ended cDNA molecules, which are then incubated with linker molecules in the presence of ligase enzyme to generate cDNA molecules carrying a polymeric linker sequence at their termini. These molecules are then cleaved at a

restriction site in the linker, purified and ligated to a vector, which has been cleaved with a restriction enzyme that generates cohesive termini compatible with those of the linker.

#### *1-9-5. Identification of cDNA clones of interest*

There are three methods to screen cDNA libraries: nucleic acid hybridization, immunological detection of specific antigens and sib selection of cDNA clones (dividing a large cDNA cloning into several small pool of cDNA, then screening these sibling pools). Nucleic acid hybridization is the most commonly used and reliable method of screening cDNA libraries. This method allows large numbers of clones to be analyzed simultaneously and rapidly, does not require a full-length of cDNA clone or the synthesis of antigenically or biologically active product in the host cell. Immunological detection of specific antigens can be used to screen the cDNA libraries constructed using an expression vector. A specific antibody directed against the protein of interest is employed to screen the detritus of bacterial lysis.

Hybrid selection and production of biologically active molecules are two methods involved in sib selection of cDNA clones. These two methods are based on the concept of dividing a large cDNA library into a manageable number of pools, each consisting of between 10 and 100 clones. These pools are then tested for the sequence of interest. The lower complexity of each pool means a larger surface area is available per clone, so that relatively less sensitive detection methods can be applied to an analysis of complete cDNA library.

**1-10. Scope of the thesis:**

Automation, and the power to integrate multi-functional elements within a microfluidic device are among the main driving forces for the rapid development of miniaturized systems. Their applications for genetic analysis have been an area of active interest.

In Chapter 2, we develop some of the individual components required to ultimately create an integrated microfluidic device for complementary DNA (cDNA) library construction. The first two steps required include the isolation and purification of messenger RNA (mRNA), followed by first strand synthesis of cDNA using reverse transcription (RT). We describe the use of paramagnetic oligo-dT beads for mRNA capture within the microfluidic channels. A simple Y-intersection flow design mixes beads and total RNA (TRNA) on-chip to allow capture of the mRNA, and uses a magnetic field to trap the beads. Initial designs show a capture efficiency of about 26 % compared to conventional methods. The RT reaction was performed for 2 hours from 30 °C to 45 °C on mRNA bound to the bead bed within the channel and 35 °C gave the best result. The bead-cDNA complex was then released from the chip and polymerase chain reaction was employed to amplify the cDNA bound to the beads. Capillary gel electrophoresis detection of the PCR product indicated that mRNA isolation and cDNA synthesis could be done on chip.

In Chapter 3, a highly sensitive laser induced fluorescence (LIF) detection system based on a 635 nm laser diode and cyanine-5 (Cy-5) dye, is described for use with a planar, microfluidic, capillary electrophoresis (CE) chip. A confocal, epiluminescent detection system utilizing a photomultiplier tube gave optimum results with a 400  $\mu\text{m}$



pinhole, an Omega 682DF22 emission filter, a 645 DRLP02 dichroic mirror, a  $634.54 \pm 5$  nm excitation filter, and a Power Technology ACMO8 635 nm laser operated at 11.2 mW. Using this detector, a microchip CE device with a separation efficiency of 42,000 plates and an etch depth of 20  $\mu\text{m}$ , gave a limit of detection of 9 pM for Cy-5. This limit corresponds to the determination of 4560 injected molecules and detection of 900 of these molecules, given a probe volume of 1.6 pL and a probing efficiency of 20%. In contrast, a conventional two lens fluorescence detector yield a limit of detection of 0.1 nM Cy-5.

Chapter 4 provides a brief summary of the previous chapters and future work. The optimization of the flow design and heating elements to improve the on-chip capture and RT efficiency will be discussed briefly. Such optimization could be used either to increase the amount of mRNA captured or to improve the RT reaction conditions.

**References:**

1. A. Manz, N. Graber, H. M. Widmer, *Sensor and Actuators, B1* **1990**, 244-248.
2. A. T. Woolley, R. A. Mathies, *Proc. Natl. Acad. Sci. USA*, **1994**, *91*, 11348-11352.
3. C. S. Effenhauser, A. Paulus, A. Manz, H. M. Widmer, *Anal. Chem.* **1994**, *66*, 2949-2953.
4. A. T. Woolley, R. A. Mathies, *Anal. Chem.* **1995**, *67*, 3676-3680.
5. A. T. Woolley, G. F. Sensabaugh, R. A. Mathies, *Anal. Chem.* **1997**, *69*, 2181-2186.
6. R. M. McCormick, R. J. Nelson, M. G. Alonso-Amigo, D. J. Benvegna, H. H. Hooper, *Anal. Chem.* **1997**, *69*, 2626-2630.
7. Y. Shi, P. C. Simpson, J. R. Scherer, D. Wexler, C. Skibola, M. T. Smith, R. A. Mathies, *Anal. Chem.* **1999**, *71*, 5354-5361.
8. O. Salas-Solano, D. Schmalzing, L. Koutny, S. Buonocore, A. Adourian, P. Matsudaira, D. Ehrlich, *Anal. Chem.* **2000**, *72*, 3129-3137.
9. A. T. Woolley, D. Hadley, P. Landre, A. J. deMello, R. A. Mathies, M. A. Northrup, *Anal. Chem.* **1996**, *68*, 4081-4086.
10. J. Cheng, M. A. Shoffner, K. R. Mitchelson, L. J. Kricka, P. Wilding, *J. Chromatogr. A* **1996**, *732*, 151-158.
11. J. Cheng, M. A. Shoffner, G. E. Hvichia, L. J. Kricka, P. Wilding, *Nucleic Acids Research* **1996**, *24*, 380-385.
12. J. Cheng, L. C. Waters, P. Fortina, G. Hvichia, S. C. Jacobson, J. M. Ramsey, L. J. Kricka, P. Wilding, *Anal. Biochem.* **1998**, *257*, 101-106.
13. L. C. Waters, S. C. Jacobson, N. Kroutchinina, J. Khandurina, R. S. Foote, J. M. Ramsey, *Anal. Chem.* **1998**, *70*, 158-162.
14. M. Sofi Ibrahim, R. S. Lofts, P. B. Jahrling, E. A. Henschel, V. W. Weedn, M. A. Northrup, P. Belgrader, *Anal. Chem.* **1998**, *70*, 2013-2017.
15. R. P. Oda, M. A. Strausbauch, A. F. R. Huhmer, N. Borson, S. R. Jurens, J. Craighead, P. J. Wettstein, B. Eckloff, B. Kline, J. P. Landers, *Anal. Chem.* **1998**, *70*, 4361-4368.

16. L. C. Waters, S. C. Jacobson, N. Kroutchinina, J. Khandurina, R. S. Foote, J. M. Ramsey, *Anal. Chem.* **1998**, *70*, 5172-5176.
17. M. U. Kopp, M. B. Luechinger, A. Manz, in: D. J. Harrison, A. Van den Berg (Editors), *μTAS' 98*, Kluwer, Dordrecht, **1998**, p7.
18. M. U. Kopp, A. J. deMello, A. Manz, *Science* **1998**, *280*,1046.
19. L. B. Koutny, D. Schmalzing, T. A. Talor, M. Fuchs, *Anal. Chem.* **1996**, *69*, 18-22.
20. N. Chiem, D. J. Harrison, *Anal. Chem.* **1997**, *69*, 373-378.
21. N. Chiem, D. J. Harrison, *Clin. Chem.* **1998**, *44*, 591-598.
22. D. J. Harrison, A. Manz, Z. Fan, H. Ludi, H. M. Widmer, *Anal. Chem.* **1992**, *64*, 1926-1932.
23. D. J. Harrison, K. Fluri, K. Seiler, Z. Fan, C. S. Effenhauser, A. Manz, *Science* **1993**, *261*, 895-897.
24. A. Manz, D. J. Harrison, E. Verpoorte, J. C. Fettinger, A. Paulus, H. Ludi, H. M. Widmer, *J. Chromatogr.* **1992**, *593*, 253-258.
25. N. Burggraf, A. Manz, C. S. Effenhauser, E. Verpoorte, N. F. deRooij, H. M. Widmer, *J. High Res. Chromatogr.* **1993**, *16*, 594.
26. A. W. Moore, S. C. Jacobson, J. M. Ramsey, *Anal. Chem.* **1995**, *67*, 4184.
27. G. Ocvirk, E. Verpoorte, A. Manz, M. Grasserbauer, H. M. Widmer, *Anal. Methods Instrum.* **1995**, *2*, 74.
28. S. C. Jacobson, R. Hergenroder, L. B. Koutny, J. M. Ramsey, *Anal. Chem.* **1994**, *66*, 2369-2373.
29. J. Khandurina, T. E. McKnight, S. C. Jacobson, L. C. Waters, R. S. Foote, J. M. Ramsey, *Anal. Chem.* **2000**, *72*, 2995-3000.
30. E. T. Lagally, I. Medintz, R. A. Mathies, *Anal. Chem.* **2001**, *73*, 565-570.
31. G. Ocvirk, *Ph. D. Dissertation*, University of Alberta, **1999**.
32. T. Imasaka, N. Ishibashi, *Anal. Chem.* **1990**, *62*, 363A-371A.
33. Z. Liang, N. Chiem, G. Ocvirk, T. Tang, K. Fluri, D. J. Harrison, *Anal. Chem.* **1996**, *68*, 1040-1046.
34. H. Salimi-Moosavi, Y. Jiang, L. Lester, G. McKinnon, D. J. Harrison, *Electrophoresis* **2000**, *21*, 1291-1299.
35. A. T. Wooley, K. Lao, A. N. Glazer, R. A. Mathies, *Anal. Chem.* **1998**, *70*, 684-688.

36. J. Wang, B. Tian, E. Sahlin, *Anal. Chem.* **1999**, *71*, 5436-5440.
37. R. Tantra, A. Manz, *Anal. Chem.* **2000**, *72*, 2875-2878.
38. J. Wang, R. Polsky, B. Tian, M. P. Chatrathi, *Anal. Chem.* **2000**, *72*, 5285-5289.
39. R. S. Martin, A. J. Gawron, S. M. Lunte, C. S. Henry, *Anal. Chem.* **2000**, *72*, 3196-3202.
40. P. A. Walker, M. D. Morris, M. A. Burns, B. N. Johnson, *Anal. Chem.* **1998**, *70*, 3766-3769.
41. N. Burggraf, B. Krattiger, A. J. de Mello, N. F. de Rooij, A. Manz, *Analyst* **1998**, *123*, 1443-1447.
42. S. D. Mangru, D. J. Harrison, *Electrophoresis* **1998**, *19*, 2301-2307.
43. A. Arora, A. J. de Mello, A. Manz, *Anal. Commun.* **1997**, *34*, 393-395.
44. G. A. Schultz, T. N. Corso, S. J. Prosser, S. Zhang, *Anal. Chem.* **2000**, *72*, 4058-4063.
45. Y. C. Kwok, A. Manz, in: A. Van den Berg, W. Olthuis, P. Bergveld (Editors), *μTAS' 2000*, Kluwer, Dordrecht, **2000**, 603-606.
46. J. W. Jorgenson, K. D. Lucas, *Anal. Chem.* **1981**, *53*, 1298.
47. J. W. Jorgenson, K. D. Lucas, *Science* **1983**, *222*, 266.
48. A. G. Ewing, R. A. Wallingford, T. M. Olefirowicz, *Anal. Chem.* **1989**, *61*, 292A.
49. M. J. Gordon, X. Huang, S. L. Pentony, R. N. Zare, *Science* **1989**, *242*, 224.
50. P. D. Grossman, J. C. Colburn, H. H. Lauer, R. G. Nielsen, R. Riggin, G. S. Sittampalam, E. C. Rickard, *Anal. Chem.* **1989**, *61*, 1186.
51. S. F. Y. Li, *Capillary Electrophoresis: principles, practice and applications*, Elsevier, Amsterdam, The Netherlands, **1993**.
52. J. P. Landers, *Handbook of Capillary Electrophoresis*, 2nd Ed., CRC Press, Boca Raton, USA, **1997**.
53. H. Swerdlow, J. Z. Zhang, D. Y. Chen, H. R. Harken, R. Grey, S. Wu, N. J. Dovichi, C. Fuller, *Anal. Chem.* **1991**, *63*, 2835-2841.
54. K. Ueno, E. S. Yeung, *Anal. Chem.* **1994**, *66*, 1424-1431.
55. J. Bashkin, D. Roach, J. Leong, M. Bartosiewicz, D. Barker, R. G. Johnston, *J. Capillary Electrophor.* **1996**, *3*, 61-68.
56. E. Carriho, M. C. Ruiz-Martinez, J. Berka, I. Smirnov, W. Goetzinger, A. W. Miller, D. Brady, B. L. Karger, *Anal. Chem.* **1996**, *68*, 3305-3313.

57. R. K. Saiki, S. J. Scharf, F. Faloona, K. B. Mullis, G. T. Hom, H. A. Erlich, N. Amheim, *Science* **1985**, *230*, 1350.
58. H. E. Schwartz, K. J. Ulfelder, *Anal. Chem.* **1992**, *64*, 1737.
59. A. S. Cohen, D. R. Najarian, A. Paulus, A. Guttman, J. A. Smith, B. L. Karger. *Proc. Natl. Acad. Sci. U. S. A.* **1988**, *85*, 9660-9663.
60. M. G. Harrington, T. E. Zewert, *Electrophoresis* **1994**, *15*, 195-199.
61. N. Chen, L. Wu, A. Palm, T. Srichaiyo, S. Hjerten, *Electrophoresis* **1996**, *17*, 1443-1450.
62. K. W. Talmadge, M. Zhu, L. Olech, C. Siebert, *J. Chromatogr., A* **1996**, *744*, 347-354.
63. J. Berka, Y. F. Pariat, O. Muller, K. Hebenbrock, D. N. Heiger, F. Foret. B. L. Karger, *Electrophoresis* **1995**, *16*, 377-388.
64. N. Zhang, E. S. Yeung, *Anal. Chem.* **1996**, *68*, 2927-2931.
65. J. Yan, N. Best, J. Z. Zhang, H. Ren, R. Jiang, J. Hou, N. J. Dovichi, *Electrophoresis* **1996**, *17*, 1037-1045.
66. J. Z. Zhang, Y. Fang, J. Y. Hou, H. J. Ren, R. Jiang, P. Roos, N. J. Dovichi, *Anal. Chem.* **1995**, *67*, 4589-4593.
67. A. Chrambach, A. Aldroubi, *Electrophoresis* **1993**, *14*, 18-22.
68. P. D. Grossman, D. S. Soane, *Biopolymers* **1991**, *31*, 1221-1228.
69. P. Bocek, A. Chrambach, *Electrophoresis* **1991**, *12*, 1059.
70. P. Bocek, A. Chrambach, *Electrophoresis* **1992**, *13*, 31.
71. M. Chiari, M. Nesi, P. G. Righetti, *Electrophoresis* **1994**, *5*, 616.
72. H. T. Chang, E. S. Yeung, *J. Chromatogr., B* **1995**, *669*, 113-123.
73. H. S. Chen, H. T. Chang, *Electrophoresis* **1998**, *18*, 3149-3153.
74. H. S. Chen, H. T. Chang, *Anal. Chem.* **1999**, *71*, 2033-2036.
75. D. Voet, J. G. Voet, *Biochemistry*, 2nd Ed., John Wiley & Sons, New York, **1995**.
76. R. H. Tamarin, *Principles of Genetics*, 2nd edition. Prindle, Weber & Schmidt, Boston, MA, USA. **1986**.
77. C. R. Newton, A. Graham. *PCR*, 2nd Ed. Oxford, OX, UK: BIOS Scientific Publishers; New York: Springer, **1997**.
78. C. C. Tsai, S. C. Jain, H. M. Sobell, *Proc. Natl. Acad. Sci.* **1975**, *72*, 629.

79. D. M. Crothers, *Biopolymers* **1968**, *6*, 575-584.
80. Q. Gao, L. D. Williams, M. Egli, D. Rabinovich, S. L. Chen, G. J. Quigley, A. Rich, *Proc. Acad. Sci. U.S.A.* **1991**, *88*, 2422-2426.
81. H. S. Rye, M. A. Quesada, M. A. Peck, R. A. Mathies, A. N. Glazer, *Nucleic Acids Res.* **1991**, *19*, 327-333.
82. X. M. Yan, W. K. Gace, T. M. Yoshida, R. C. Habbersett, N. Velappan, J. H. Jett. R. A. Keller, B. L. Marrone, *Anal. Chem.* **1999**, *71*, 5470-5480.
83. C. A. Brenner, A. W. Tam, P. A. Nelson, E. G. Engelman, N. Suzuki, K. E. Fry, J. W. Larrick, *Biotechniques* **1989**, *7*, 1096.
84. R. J. Britten, and E. H. Davidson. Hybridization strategy, P. 3-14 In B. D. Hames and S. J. Higgins (ed.), *Nucleic Acid Hybridization: A practical Approach*. IRL Press. Oxford, **1985**.
85. J. Sambrook, E. F. Fritsch, T. Maniatis. *Molecular Cloning: A laboratory Manual*. 2nd ed., Cold Spring Harbor Laboratory. Cold Spring Harbor, N. Y. **1989**.
86. L. G. Davis, W. M. Kuehl, J. F. Battey, *Basic Methods in Molecular Biology*, 2nd ed., Appleton & Lange Paramount Publishing Business and Professional Group, Norwalk. Connecticut, USA. **1994**.
87. R.W. Old, S.B. Primrose, *Principles of Gene Manipulation*, 5th ed., Blackwell Science Ltd., Oxford and Northampton. **1994**, ch. 6.

**Chapter 2. mRNA Isolation and cDNA Synthesis  
In A Microfluidic Device For Eventual Integration  
of cDNA Library Construction**

A version of part of this chapter has appeared in G. Jiang, D.J. Harrison, *The Analyst*, **2000**, *125*, 2176-2179.

## 2-1. Introduction

In this chapter, we describe the first demonstration of the use of Dynal beads with a poly-T tail for capture of messenger RNA (mRNA) from isolated total RNA (TRNA) and cDNA synthesis in a flowing stream, within a microchip. Complimentary DNA (cDNA) library construction plays an important role in molecular biology. The analysis of a cDNA library should give sufficient information to understand gene regulation in relation to different levels of gene expression and in terms of tissue-specific gene expression<sup>1-2</sup>. In addition, cDNA lacks the intron sequences that are usually present in corresponding genomic DNA. The position of intron/exon boundaries can thus be assigned by a comparison of a cDNA sequence with the sequence of genomic DNA. Several steps are involved in cDNA library construction, including mRNA isolation, fractionation of mRNA by size in some procedures, first strand cDNA synthesis, second strand cDNA synthesis, molecular cloning of double-stranded cDNA and the final identification of cDNA clones of interest<sup>3</sup>. However, the technology for preparing useful cDNA libraries is laborious and tedious.

Planar microfluidic devices are capable of performing sample preparation, chemical and biochemical reactions, separations and analysis, thus creating a laboratory on a chip<sup>4-5</sup>. Their application in genetic analysis has been extensive, but the focus has been on performing the polymerase chain reaction (PCR) and/or separation<sup>6-8</sup>.

Planar microfluidics<sup>4</sup> may eventually be able to provide a miniaturized, integrated platform for automated cDNA library construction. It may also be possible to reduce mRNA degradation by adventitious RNase, due to the closed nature of an integrated



system. Recently, Fan *et al.*<sup>9</sup> have described the use of paramagnetic Dynal beads for dynamic DNA hybridization within a microfluidic device using external magnetic fields for bead trapping. Synthetic DNA samples with a poly-A tail were used to demonstrate the hybridization. Ahn and co-workers<sup>10</sup> have integrated magnetic traps within microfluidic silicon devices for performing immunoassays. Dynal beads<sup>11-12</sup> have been extensively used for RNA preparation<sup>13-16</sup>, DNA and RNA hybridization<sup>17, 18</sup>, solid phase sequencing<sup>19-21</sup>, protein and gene regulation<sup>22-27</sup>, and solid phase cDNA library construction<sup>28-30</sup>. The efficiency of cDNA library construction is improved by creating a reusable pool of first-strand cDNA coupled to paramagnetic beads<sup>28, 29</sup>. Conventionally, in order to construct a relatively complete cDNA library, 10 µg of mRNA is required as starting material, which exceeds the capability of a typical chip device. However, Lambert *et al.* constructed a cDNA library from 5 ng of mRNA using paramagnetic beads and PCR<sup>30</sup>. This suggests it will be possible to perform cDNA library construction on chip with small amounts of mRNA.

## **2-2. Experimental**

### *2-2-1. Materials*

The PCR primers (fly1, TGCATTGATATTGGTTCGATTC<sup>31</sup>, fly2, CACATGCACA TGCAGTATCCTT<sup>31</sup>) and DNA marker (ΦX174 RF DNA/*Hae* III fragments) were from Life Technologies (Burlington, ON, Canada). Paramagnetic oligo-(dT)<sub>25</sub> beads (Dynal beads, supplied as a suspension containing 3.3x10<sup>8</sup> beads/mL with a bead diameter of 2.8 µm), RT-PCR kit and RNA marker (0.28-6.6 kb) were purchased from Dynal Inc. (Lake Success, NY, USA), Perkin-Elmer (Mississauga, ON, Canada)

and Sigma, respectively. The mRNA binding buffer (20 mM Tris-HCl (pH 7.5, Sigma), 1.0 M LiCl (Sigma), 2 mM EDTA (Sigma)), washing buffer (10 mM Tris-HCL (pH 7.5), 0.15 M LiCl, 1 mM EDTA), and elution solution (10 mM Tris-HCl (pH 7.5)) were prepared using diethylpyrocarbonate-treated water (DEPC, Amersham Pharmacia Biotech, Inc. Québec, Canada). The running buffers used for capillary gel electrophoresis (CGE) detection of DNA and RNA were 0.5 x Tris-Borate-EDTA buffer (TBE; 45 mM Tris (Fisher Scientific), 45 mM Boric-acid (BDH, Toronto, ON, Canada), 1mM EDTA) and 1 x MOPS-EDTA-Sodium Acetate buffer (Sigma, 40 mM MOPS, 10 mM Sodium Acetate, 1 mM EDTA) with 1 M formaldehyde (Sigma), respectively. Ethidium bromide (Molecular Probe Inc., Eugene, OR, USA) was employed to stain DNA and RNA when using CGE for detection.

A Progene Thermo-cycler (Mandel Scientific Company Ltd., Guelph, ON, Canada) was used to perform RT-PCR. A syringe pump (Harvard Apparatus, Québec, Canada) was applied at the end of the channel on the chip to create a negative pressure. The magnets (D38428) used to trap the beads were from Edmund Scientific (Barrington, New Jersey, USA). CGE was performed on a Beckman P/ACE 5000 equipped with a 488 nm laser module LIF detector, 580DF40 (Omega) filter and 488 nm notch filter. A 27 cm (20 cm to detector) long, 50  $\mu\text{m}$  i.d. fused silica capillary filled with 0.4% hydroxypropylmethyl-cellulose (HPMC, Sigma), operated at 5 or 10 kV, was used for detection of RT-PCR product (699 bp) with a 5 kV, 5 s sample injection. A 47 cm (40 cm to detector) long, 50  $\mu\text{m}$  i.d. fused silica capillary filled with 0.15% denaturing (formaldehyde) HPMC, operated at 15 kV, was used for detection of mRNA isolated directly from the chip, with a 10 kV, 5 s sample injection.

Total RNA was extracted using Trizol reagent (Life Technologies) from *Drosophila Melanogaster* in this study. Adult *Drosophila Melanogaster* (850 mg) and 8 mL Trizol reagent were put into a Glass-Teflon homogenizer. After homogenizing and incubating, 1.6 mL of chloroform (Sigma) was added to achieve phase separation. The colorless, aqueous RNA phase was transferred to a 15 mL centrifuge tube, 4 mL of isopropyl alcohol (Sigma) was added to precipitate RNA, then 8 mL 75% ethanol (Sigma) was used to wash the RNA pellet. The RNA was dissolved into DEPC-treated water after being air-dried. The integrity of the total RNA was checked by both denaturing CGE and denaturing slab gel electrophoresis (Figure 2-1). Both methods

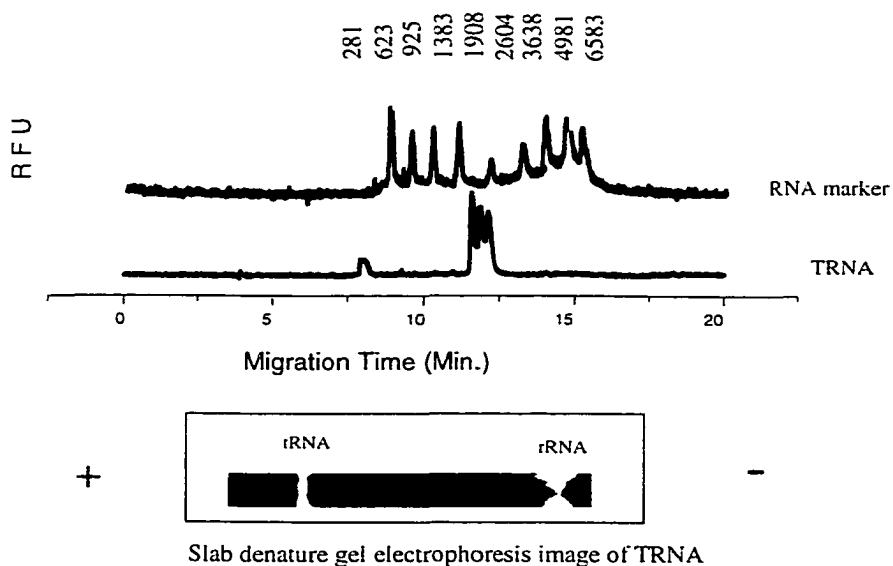


*Figure 2-1. Capillary denaturing electrophoresis and slab denaturing gel electrophoresis testing the integrity of the TRNA*

illustrated that the TRNA was intact and had good integrity. Whole body extraction of TRNA from *Drosophila Melanogaster* typically produces a three bands by CGE.

Extractions from embryos or the ovum give the characteristic two peak profile, representing 18s and 28s rRNA, that is seen for most organisms. The concentration of the TRNA was measured by Pharmacia Gene Quant (LKB Biochrom, England). The yield for the TRNA extraction was 0.5% weight ratio of TRNA to *Drosophila Melanogaster*.

### 2-2-2. Device Fabrication

There are several steps involved in device fabrication, such as metal deposition, photolithography, etching and bonding. Figure 2-2 illustrates a single mask fabrication process. The glass substrate, which was ultrasonically cleaned with acetone, deionized water, was coated with a Cr film by vapor deposition to form an adherent layer. Au film was then deposited on the Cr-glass substrate to serve as a mask for the HF/HNO<sub>3</sub>/H<sub>2</sub>O etching of glass substrate. The trace organics were then removed in H<sub>2</sub>SO<sub>4</sub> (98%): H<sub>2</sub>O<sub>2</sub> (30%) at a volume ratio of 3:1. A layer of positive photoresist was then spin coated on the Au-Cr-glass substrate (Fig.2-2, a) with a Solitec Photoresist Coater/Developer. After soft baked at 120 °C for 30 min., aligned with the master mask, which was manufactured by the Precision Photomask (Ottawa, Canada) with L-Edit designed layout, the substrate was exposed to the UV light for couple seconds (Fig.2-2, b). The exposed photoresist was then removed by the developer (Fig.2-2, c). After hard baking of the substrate at 120 °C for 30 min, the exposed Au, Cr were removed by gold-etchant and Cr-etchant, respectively (Fig.2-2, d, e). The exposed glass was then etched by HF/HNO<sub>3</sub>/H<sub>2</sub>O, the depth of the etching could be controlled by the etching time (Fig.2-2, f). The unexposed photoresist, metal (Au-Cr) layer were then removed afterwards by using acetone, Au-etchant and Cr-etchant respectively (Fig.2-2, g). After drilling 1.9 mm diameter access

holes in the cover plate, it was thermally bonded to the etched glass substrate to form an enclosed fluidic device. The bonding conditions are illustrated as following:

For Pyrex glass, the temperature was held at 550 °C for 30 min, 610 °C for 30 min, 635 °C for 30 min and 650 °C for 6 hours; For 0211 glass, the temperature was held at 440 °C for 30 min, 473 °C for 30 min, 592 °C for 6 hours and 473 °C for 30 min.

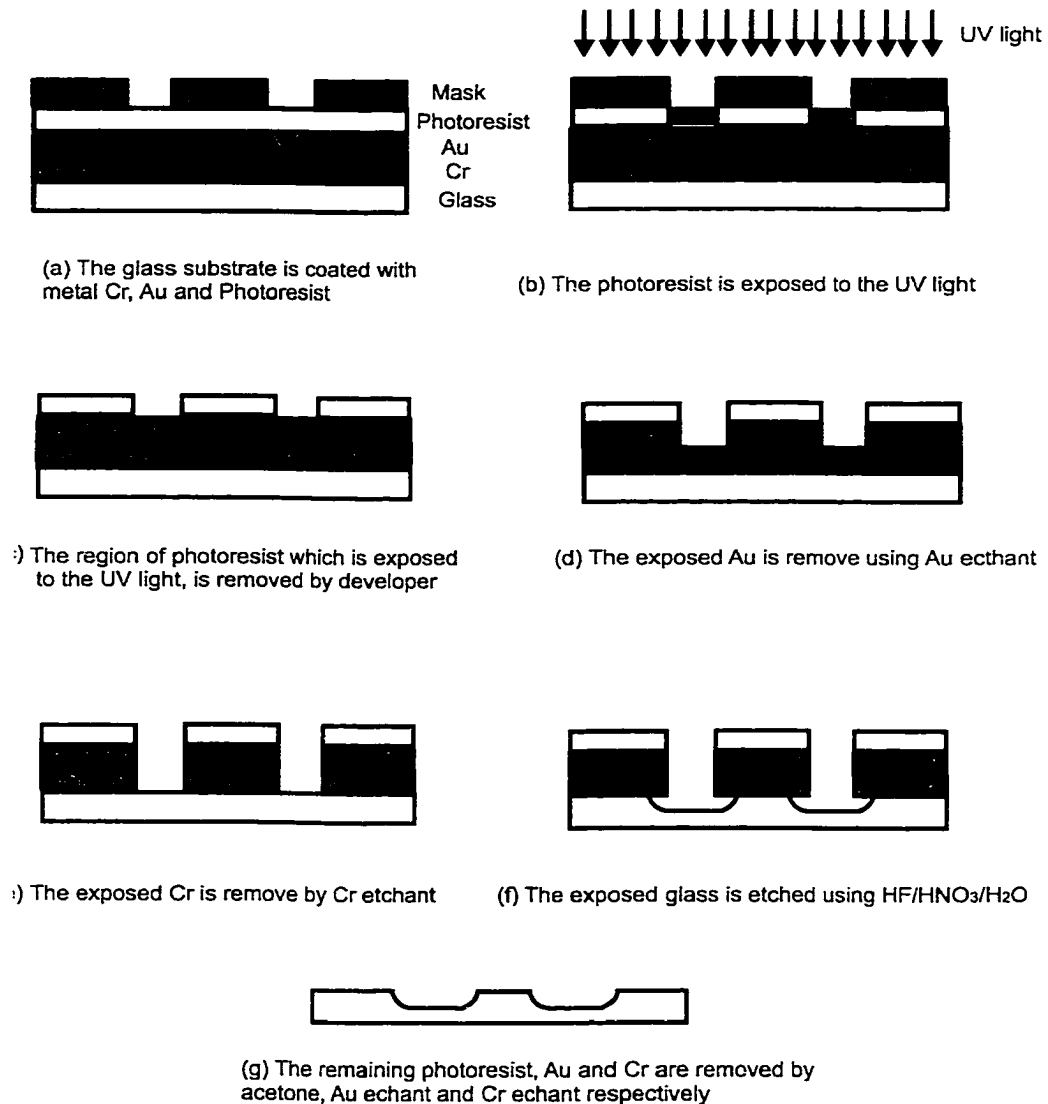
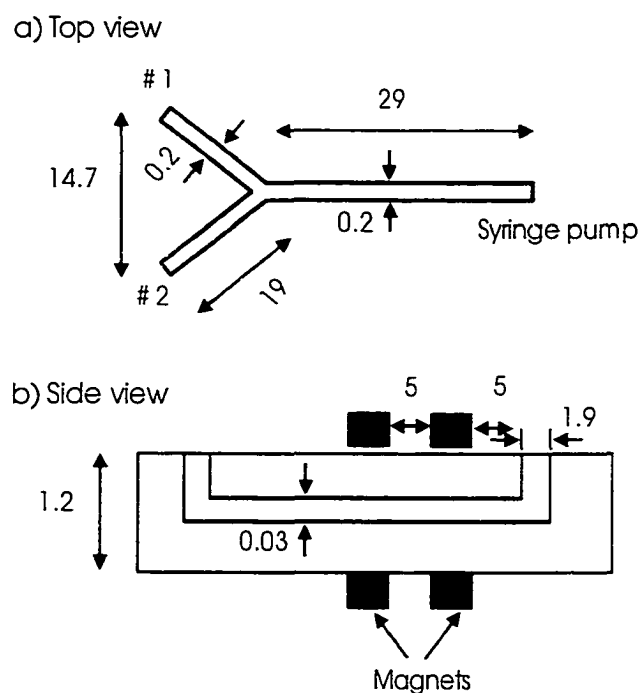


Figure 2-2. The procedure for photolithographic fabrication of glass device.

Two devices with different feature width were used. One is for mRNA isolation on chip (Figure 2-3)<sup>32</sup>, and the another is for mRNA isolation and cDNA synthesis (Figure 2-4). The device channels were etched 30  $\mu\text{m}$  deep with a 200 (150)  $\mu\text{m}$  feature width in the mask, giving about 260 (226)  $\mu\text{m}$  width at the top. A simple Y-intersection fluidic device was employed (Figure 2-3, 2-4). One set of magnets (D38428, Edmund Scientific, Barrington, New Jersey, USA) were placed along the channel to capture the mRNA loaded beads (bead-mRNA). A syringe pump (Harvard Apparatus, Québec, Canada) was connected to the end of the channel to draw the solution through the channel. The adhesive heater strip (HK5565R10.0L12B, MOD-TRONIC, Brampton, Ontario, Canada) was placed underneath the device (Fig.2-4) to adjust the temperature.



*Figure 2-3. Layout of the Y-channel fluidic chip, fabricated in 0.6 mm thick Corning 0211 glass. Dimensions are indicated in mm. A syringe pump was operated in negative pressure mode to draw solution from reservoirs #1 and #2.*

The heater was connected to a home made power supply via a temperature controller (16A3030992, MOD-TRONIC, Brampton, Ontario, Canada). A Resistive Temperature Detector (RTD, S651PDZ40B, MOD-TRONIC, Brampton, Ontario, Canada) was placed on the top of the device, above the heater, to monitor the temperature and provide feedback to the controller. The chip device was heated at 180 °C in the oven for 5 hours before use, in order to sterilize it.

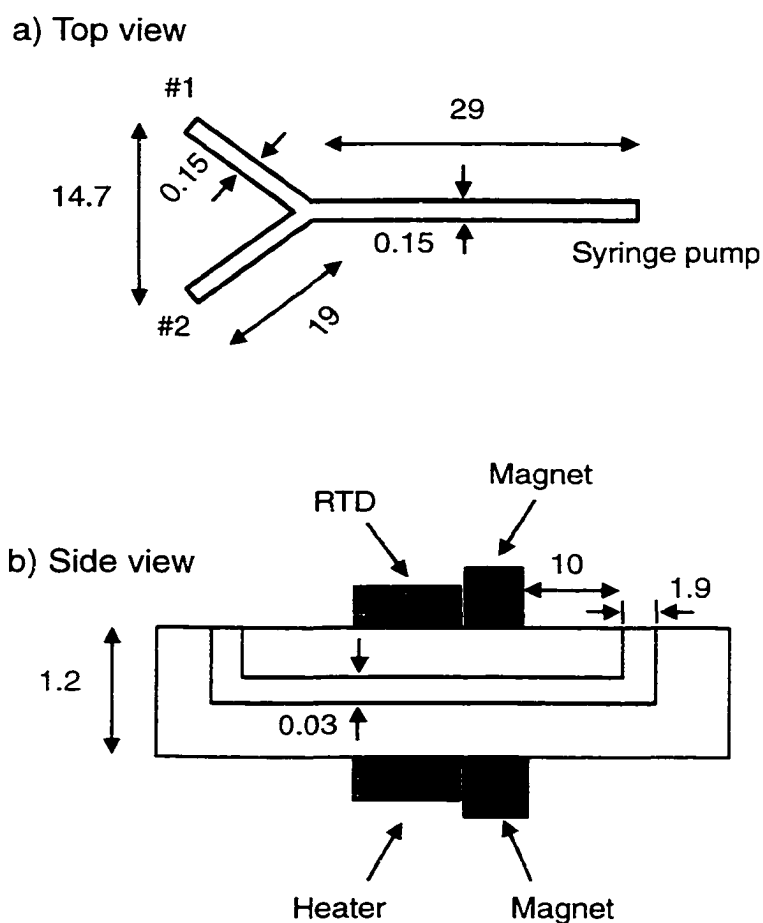


*Figure 2-4. Y-intersection device for mixing of beads, sample and RT reagents. Magnetic Oligo(dT) beads are trapped by magnets. A resistive heater is placed underneath the channel with a resistive temperature detector (RTD) above the channel. The RTD is connected to a temperature controller that operates the heater. A syringe pump was employed to drive the solution through the chip. Dimensions are indicated in mm.*

### 2-2-3. Operation procedure

#### 2-2-3-1. mRNA isolation on chip

##### a) Introducing TRNA and beads on chip

Throughout the text the volume of the original bead slurry is reported. This volume was always further diluted before introduction to the chip. The beads were washed twice using binding buffer, then diluted in 0.5 x binding buffer to form a slurry 10 times lower in concentration than the original slurry. Typically, the TRNA was diluted in 0.5 x binding buffer to 0.17  $\mu\text{g}/\mu\text{L}$ , heated at 65 °C for 5 min., then cooled on ice to denature. After rinsing the channel with DEPC-treated water, reservoir #1 was filled with 10-100  $\mu\text{L}$  of the diluted Dynal bead slurry, while the other was filled with TRNA solution. Two sets of magnets were placed along the channel: the first set to capture the beads; and the second set to capture escaped beads. A syringe pump was connected to the end of the channel and a flow rate of 2  $\mu\text{L}/\text{min}$  was applied. Figure 2-5 illustrates the

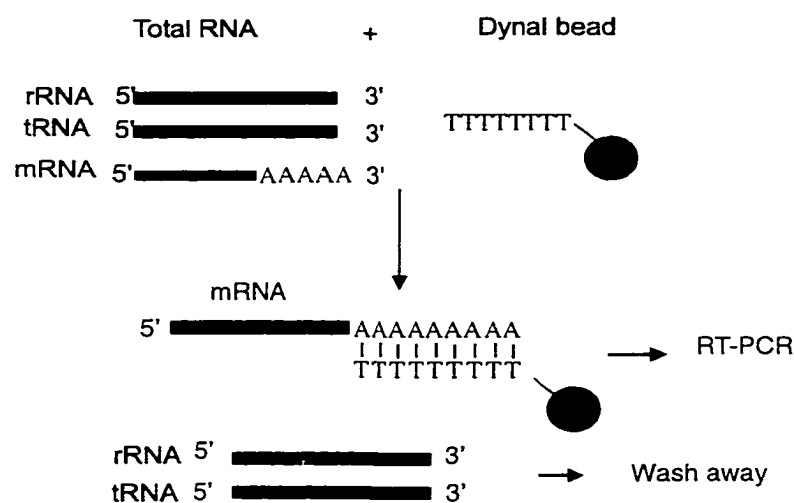


Figure 2-5. Cartoon illustrating the affinity purification of mRNA from total RNA using paramagnetic, poly-T coated Dynal beads. Reverse transcription-polymerase chain reaction. RT-PCR, may then be used to amplify the presence of a target gene.



protocol for mRNA isolation from total RNA (TRNA), which was extracted from *Drosophila Melanogaster*. Dynal beads oligo-d(T)<sub>25</sub>, which are uniform, 25 nucleotide long chains of deoxythymidines covalently linked to their surfaces via a 5' linker group, are used to capture mRNA from TRNA using mRNA binding buffer. Most mRNA has a poly-A tail, which will hybridize with the poly-T chain of the Dynal beads. Transfer RNA (tRNA) and ribosomal RNA (rRNA), which do not have the poly-A tail, are removed with a washing buffer. This protocol is conventionally performed in microcentrifuge tubes using a magnetic field for trapping the beads. The procedure may be adapted to mRNA isolation in a flowing stream within a simple microfluidic device. One inlet was used for sample, the other for a slurry of the Dynal beads. A syringe pump was operated in negative pressure mode to draw the solution from the two upstream reservoirs toward the Y-intersection. Laminar flow would prevent significant mixing of the two streams. However, the magnets placed downstream trap the Dynal beads across the width of the channel, forcing the TRNA stream to mix with the beads and be captured. Typically, 2-6  $\mu\text{L}$  of Dynal beads (original slurry) was used; about 1-3% of the quantity used off-chip. The maximum mRNA capture capacity of the Dynal beads is about 0.01  $\mu\text{g}/\mu\text{L}$  of original bead slurry<sup>12</sup>. Adjusting the flow rate was crucial for the experiment, since the beads did not remain in place when the flow rate was too high. The maximum usable flow rate was 4  $\mu\text{L}/\text{min}$ . About 20 min was required to pull the beads and sample through the chip at 2  $\mu\text{L}/\text{min}$ . After the TRNA and bead solutions in the reservoirs were all delivered into the channel, the flow was stopped.

b). RT-PCR amplification of bicoid gene:

The mRNA loaded beads (bead-mRNA) are brought to the exit reservoir using the magnet and transferred to a microvial using a gel-loading micro pipet tip. The bead-mRNA were washed with washing buffer and the isolated mRNA strands were reverse transcribed into cDNA. The bicoid gene was then amplified by PCR. This RT-PCR process took place in a single reaction tube. Reverse transcription solution (20  $\mu\text{L}$ ) was placed in the tube, which contained bead-mRNA from a chip, 5 mM  $\text{MgCl}_2$ , 50 mM KCl, 10 mM Tris-HCl, 1 mM dGTP, 1 mM dATP, 1 mM dTTP, 1 mM dCTP, 1 U/ $\mu\text{L}$  RNase inhibitor, 2.5 U/ $\mu\text{L}$  MuLV Reverse Transcriptase and 2.5  $\mu\text{M}$  oligod(T)<sub>16</sub>. The tube was incubated at room temperature for 10 minutes, to allow the extension of oligod(T)<sub>16</sub> by reverse transcriptase. These extended primers (oligodT) remains annealed to the RNA template upon raising the reaction temperature to 42 °C<sup>33</sup>. The tube was incubated in the Thermal Cycler as follows (Table 2-1):

Table 2-1. The conditions for RT:

Step	Temperature	Duration
Reverse transcribe	42 °C	60 Minutes
Denature	99 °C	5 Minutes
Cool	5°C	5 Minutes

After the RT step, the tube was removed from the Thermal Cycler. Then 78  $\mu\text{L}$  of a PCR master mix, which contained 4  $\mu\text{L}$  25 mM  $\text{MgCl}_2$ , 8  $\mu\text{L}$  10x PCR buffer (500 mM KCl, 100 mM Tris-HCl), 65.5  $\mu\text{L}$  DEPC-H<sub>2</sub>O and 0.5  $\mu\text{L}$  5 U/ $\mu\text{L}$  AmpliTaq DNA Polymerase, together with 1  $\mu\text{L}$  30  $\mu\text{M}$  fly1 primer and 1  $\mu\text{L}$  30  $\mu\text{M}$  fly 2 primer, were added into the

RT tube to give a 100  $\mu$ L final volume. The tube was then placed into a Thermal cycler to run PCR cycles as follows (Table 2-2):

Table 2-2. The conditions for PCR

Initial step, 1 cycle	35 cycles each		Final step
	Melt	Anneal-Extend	
120 second, 95 °C	60 second, 95 °C	60 second, 60 °C	7 minutes, 72 °C

c). Capillary gel electrophoresis (CGE) detection of PCR product.

The 35 cycle PCR product was detected using a Beckman P/ACE 5000 equipped with a 488 nm laser module LIF detector, for CGE detection. A 27 cm long, 50  $\mu$ m i.d. fused silica capillary filled with 0.4% hydroxy-propylmethyl-cellulose (HPMC, Sigma) using pressure separation mode, operated at 5 or 10 kV, was used for detection of PCR product (699 bp) with a 5 kV, 5 s sample injection. Ethidium bromide, which was used to stain DNA molecules during the DNA separation, was added into 0.4% HPMC gel and 0.5x TBE running buffer with a concentration of 1.5  $\mu$ g/mL. A 580DF40 (Omega) filter and 488 nm notch filter were used, since the ethidium bromide-DNA complex will give maximum fluorescence at 600 nm.

d). Denaturing capillary gel electrophoresis detection of mRNA

In order to check the integrity of mRNA isolated on chip, denaturing capillary gel electrophoresis was employed to detect the mRNA isolated from the device. A 47 cm long, 50  $\mu$ m i.d. fused silica capillary filled with 0.15% denaturing (formaldehyde) HPMC, operated at 15 kV, was used for detection of RNA (mRNA, tRNA, rRNA)

marker) with a 10 kV, 5 s sample injection. Unlike the CGE detection of PCR products, ethidium bromide was not added into the gel and buffers in this case. The sample was mixed with the RNA loading buffer (62.5% deionized formamide, 1.14 M formaldehyde, 1.25x MOPS-EDTA-sodium acetate buffer, 200 µg/mL bromphenol blue, 200 µg/mL xylene cyanole and 50 µg/mL ethidium bromide, Sigma) in a ratio of 2 to 3. Just before loading, it was heated to 65 °C for 10 minutes, then chilled on ice. A 488 nm laser module LIF detector with 580DF40 (Omega) filter and 488 nm notch filter were used for fluorescence detection.

### *2-2-3-2. mRNA isolation and cDNA synthesis on chip*

#### a).mRNA isolation on chip.

The Dynal beads were washed twice using binding buffer, then diluted in 0.5 x binding buffer to form a slurry 4 times lower in concentration than the original slurry. Typically, the TRNA was diluted in 0.5 x binding buffer to 0.5 µg/µL, heated at 70 °C for 5 min., then cooled on ice to denature. After rinsing the channel first with DEPC-treated water, then with 0.5x binding buffer, reservoir #1 was filled with 80 µL of the diluted Dynal bead slurry, while the other was filled with 80 µL TRNA solution. One set of magnets were placed along the channel to capture the bead-mRNA. A syringe pump was connected to the end of the channel and a flow rate of 1.5 µL/min was set for a 30 min period. The volume of fluid within the syringe pump was checked and found to be consistent with the flow rate setting. Figure 2-6 illustrates the protocol for mRNA isolation and RT reaction on chip. Dynal beads Oligod(T)<sub>25</sub> are used to capture mRNA from TRNA. The poly A tail of mRNA will hybridize with poly T chain of the Dynal

beads through hydrogen bonding. The beads and captured mRNA were trapped by the magnetic field created by the magnets.

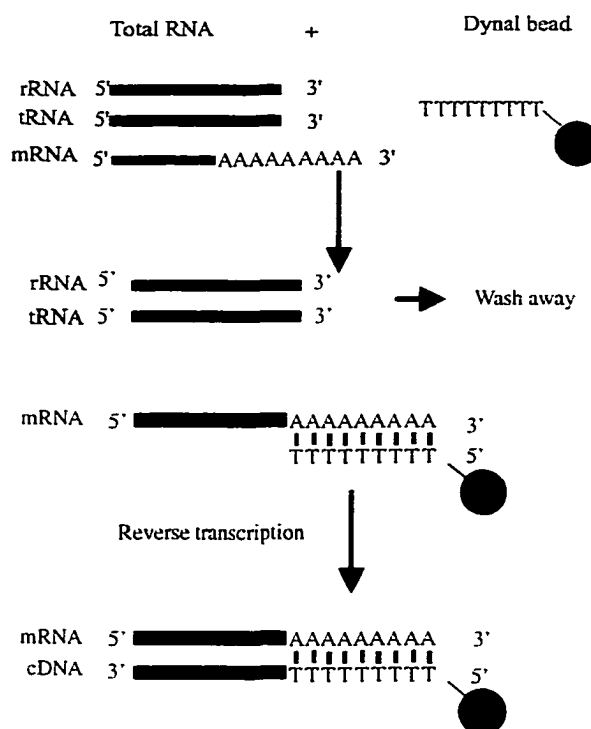


*Figure 2-6. Cartoon illustrating the affinity purification of mRNA from total RNA & cDNA synthesis using paramagnetic, poly-T coated Dynal beads. Polymerase chain reaction, PCR, may then be used to amplify the presence of a target gene.*

#### b). Washing step prior to on-chip RT

The rRNA and tRNA do not have the poly-A tail. As a result, they will not hybridize on the surface of the Dynal beads and are washed away (Figure 2-6). The remaining solution in both reservoirs in step (a) was then removed and the reservoirs were washed with DEPC-treated water three times, followed by three rinses with washing buffer. After both reservoirs were filled with washing buffer, a 1  $\mu\text{L}/\text{min}$  flow rate was applied for 1 min with the syringe pump. The flow was then stopped and the magnets

were normally moved back and forth along the channel to enhance the washing efficiency. Then the 1  $\mu\text{L}/\text{min}$  flow was restarted for 1 min with the magnets fixed in position. This procedure was repeated 10 times, giving a total flow time of 10 min. During the washing steps, extreme caution must be taken not to introduce air bubbles while changing solutions in the reservoirs.

c). Washing the bed using RT buffer:

The EDTA in the washing buffer will bind to the  $\text{Mg}^{2+}$  in the RT buffer, as a result, reverse transcription may not occur. The EDTA was eliminated by introducing RT buffer (5mM  $\text{MgCl}_2$ , 50 mM KCl, 10 mM Tris-HCl, 1 mM dATP, 1 mM dTTP, 1 mM dCTP, 1mM dGTP, 1 U/ $\mu\text{L}$  RNase inhibitor and 2.5  $\mu\text{M}$  oligo(dT)<sub>16</sub>) to wash all reservoirs, channels and the bead bed. The remaining solution in both reservoirs was removed and the reservoirs were first washed with DEPC-treated water three times, then with RT buffer three times. After both reservoirs were filled with RT buffer, a 1  $\mu\text{L}/\text{min}$  flow rate was applied for 1 min with the syringe pump. Then the flow was stopped and the magnets were moved back and forth along the channel to enhance the washing efficiency. Then the 1  $\mu\text{L}/\text{min}$  flow was restarted for 1 min. The same procedure was repeated 10 times, giving a total flow time of 10 min.

d). cDNA synthesis on chip (RT reaction).

1  $\mu\text{L}$  MuLV Reverse Transcriptase per 10  $\mu\text{L}$  RT buffer was added into both reservoirs. The adhesive heater strip was placed underneath the device (Fig.2-4) to adjust the temperature. The heater was connected to a home made power supply via a

temperature controller. An RTD was placed on the top of the device, above the heater, to monitor the temperature and provide feedback to the controller. The reaction temperature was set to 35 °C. A flow rate of 0.5 µL/min was applied for 5 min. Then the flow was stopped and the magnets were moved back and forth along the channel. Then the 0.5 µL/min flow was restarted for 5 min with the magnets fixed in place. The same procedure was repeated 24 times. The total reaction time was 2 hours. The beads with hybridized cDNA were brought to the exit reservoir using the magnet while flow was stopped. They were then transferred into a PCR reaction vial using a gel-loading micro pipet tip.

e). PCR amplification:

PCR mix was added into PCR reaction vials along with the beads with hybridized cDNA obtained from the device. Each 20 µL PCR mix contains 0.3 µM fly1 primer, 0.3 µM fly2 primer, 2 mM MgCl<sub>2</sub>, 50 mM KCl, 10 mM Tris-HCl, 0.2 mM dATP, 0.2 mM dTTP, 0.2 mM dCTP, 0.2mM dGTP, and 1 U AmpliTAQ DNA polymerase. PCR amplifications were performed for 35 cycles using a Progene Thermo-cycler. Each cycle consisted of denaturation for 1 min at 94 °C, annealing at 60 °C for 1 min and extension for 1 min at 72 °C. In order to reduce the non-specific amplifications, hot start PCR (the vial is raised to 94 °C before adding the DNA polymerase) was employed for all PCR amplifications.

f). CGE detection:

The 35 cycle PCR product was detected using Beckman P/ACE 5000 equipped with a 488 nm laser module LIF detector, 580DF40 (Omega) filter and 488 nm notch filter for

CGE detection. A 27 cm long, 50  $\mu\text{m}$  i.d. fused silica capillary filled with 0.4% hydroxy-propylmethyl-cellulose (HPMC, Sigma), operated at 10 kV, was used for detection of PCR product (699 bp) with a 5 kV, 5 s sample injection. The Ethidium bromide concentration in both the 0.4% HPMC gel and 0.5x TBE buffer was 1.5  $\mu\text{g}/\text{mL}$ .

## **2-3. Results and Discussion**

### *2-3-1. Optimizing PCR conditions*

#### *2-3-1-1. $\text{Mg}^{2+}$ concentration*

$\text{Mg}^{2+}$  affects the PCR reaction in the following manner:

- 1). It forms a soluble complex with dNTP, which is essential for dNTP incorporation.
- 2). It stimulates polymerase activity.
- 3). It increases the melting temperature ( $T_m$ ) of double-stranded DNA and the primer/template interaction.

The concentration of  $\text{Mg}^{2+}$  can have a dramatic effect on the specificity and yield of PCR. Insufficient  $\text{Mg}^{2+}$  leads to low yield, while excess  $\text{Mg}^{2+}$  will result in the accumulation of non-specific products. The optimal  $\text{Mg}^{2+}$  concentration has to be determined by experiment. The  $\text{Mg}^{2+}$  concentration was varied from 1 to 4.5 mM. The product peak height increased up to 2 mM. However, above 2 mM multiple product peaks were observed. Therefore, 2 mM  $\text{Mg}^{2+}$  concentration was used in all PCR experiments.



### 2-3-1-2. Annealing temperature

The annealing temperature for PCR varies for the different primers. The suitable annealing temperatures are approximately related to the melting temperature of the primers ( $T_m$ ). The formula is :

$$T_m = 81.5 + 16.6(\text{Log}[\text{Molar Na}^+]) + 41(\%GC) - 675/\text{primer length} \quad \text{for primer} > 10 \text{ base}$$

For the PCR amplification used in this study,  $\text{Na}^+$  is 0.05 M and the primer length is 22 bases.  $T_m$  for the fly1 primer (%GC=36) was calculated to be 44 °C, and for the fly2 primer (%GC=45) it was 48 °C. Five annealing temperatures (45-65 °C) were tested in this study (Figure 2-7). A 60 °C annealing temperature was chosen in the following PCR amplifications because it gave maximum PCR yield.

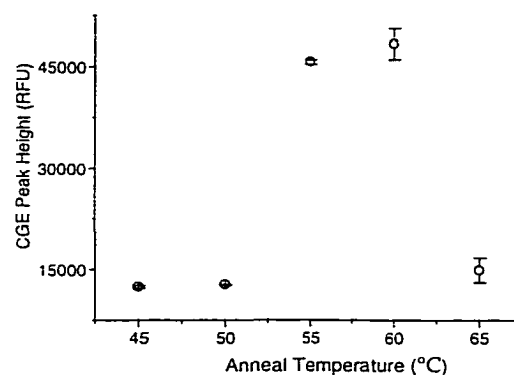
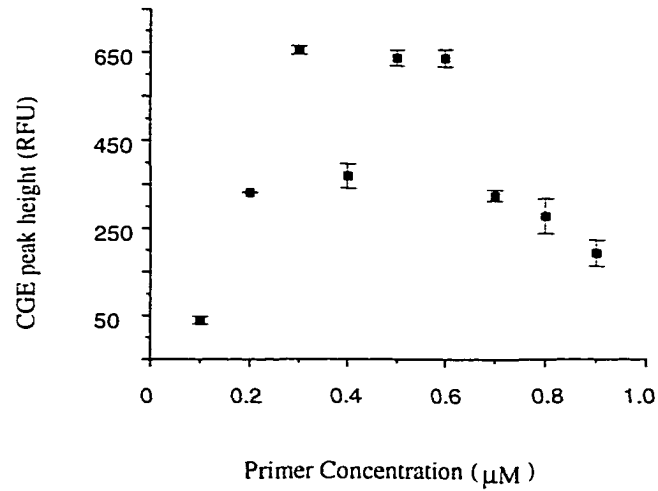


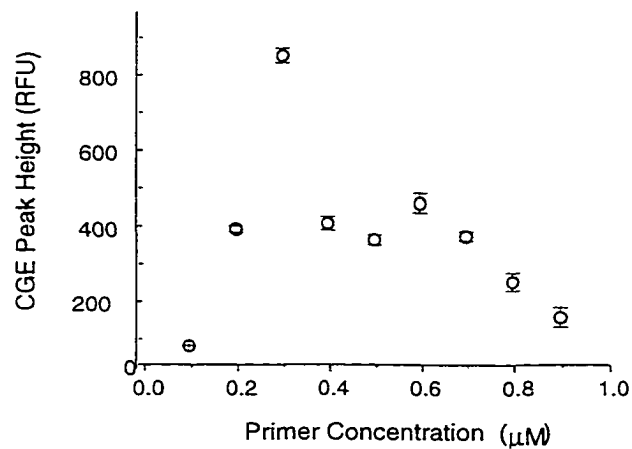
Figure 2-7. The peak height of PCR product detected by CGE versus annealing temperature. Error bars show the standard deviation of 3 replicate CE runs on one sample.

2-3-1-3. *Primer concentration:*

The Primer concentration has an effect on the PCR amplification efficiency. Figure 2-8 shows the relationship between the primer concentration and the PCR product peak



(a)



(b)

Figure 2-8. The peak height of PCR product detected by CGE versus primer concentration, shown for two independent trials. Error bars show the standard deviation of 3 replicate CE runs on one sample.

height detected by CGE. The results illustrated that both insufficient and excess primer concentration give lower PCR yield. Insufficient primers in the PCR mix might cause low annealing efficiency during PCR amplification, while excess primer may cause competition between the target and primer, and as a result reduce the annealing efficiency. The optimal primer concentration was chosen as 0.3  $\mu\text{M}$  since at this concentration, the PCR amplification yield was a maximum.

### 2-3-2. mRNA isolation

The primers used for PCR defined a 699 basepair long DNA fragment from the bicoid gene (2.6 kb), which is a rare gene in *Drosophila Melanogaster*. That is, the mRNA for the gene is in low abundance. The electropherograms of the primers shown in

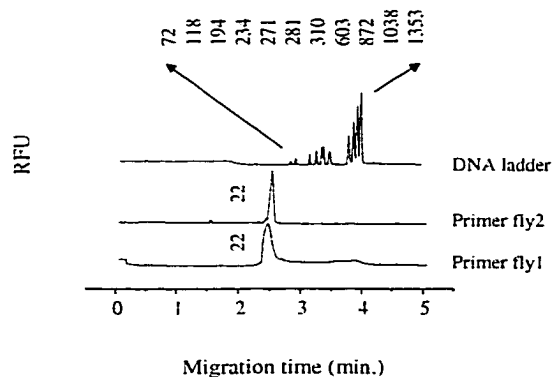


Figure 2-9. Electropherograms of PCR primers and DNA ladder.

Figure 2-9 illustrates that only short DNA oligomers are present in the commercially prepared primers. Capillary gel electrophoresis was employed to detect the PCR product. Figure 2-10 shows the electropherograms of a standard DNA marker, and of the RT-PCR product of

mRNA isolated on chip. Observation of the 699 bp RT-PCR product showed that the rare bicoid gene could be captured by Dynal beads on a chip device. Trace A shows the electropherogram of 50 ng/ $\mu\text{L}$  DNA marker. Trace B illustrates the electropherogram of the RT-PCR product (699 bp), prepared from 5  $\mu\text{g}$  TRNA and 3  $\mu\text{L}$  of original bead slurry introduced on-chip. Trace C shows the RT-PCR product prepared

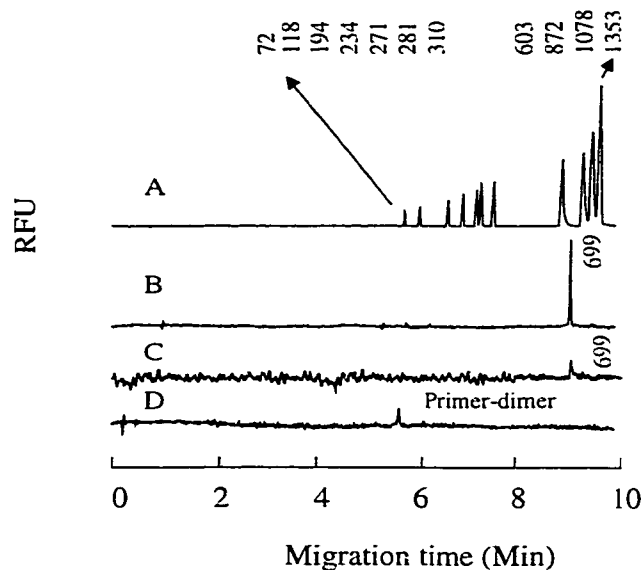


Figure 2-10. Capillary gel electrophoresis of A) standard DNA  $\Phi$ X174 RF DNA/Hae III fragments (intensity  $\times 0.1$  for comparison); B) RT-PCR amplification of bicoid gene isolated on chip from 5  $\mu$ g of TRNA; C) as in B except isolated from 0.85  $\mu$ g of TRNA; D) RT-PCR of blank sample showing only primer-dimer formation.

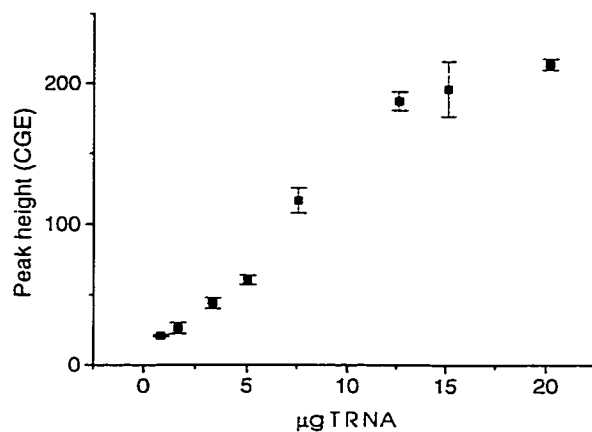
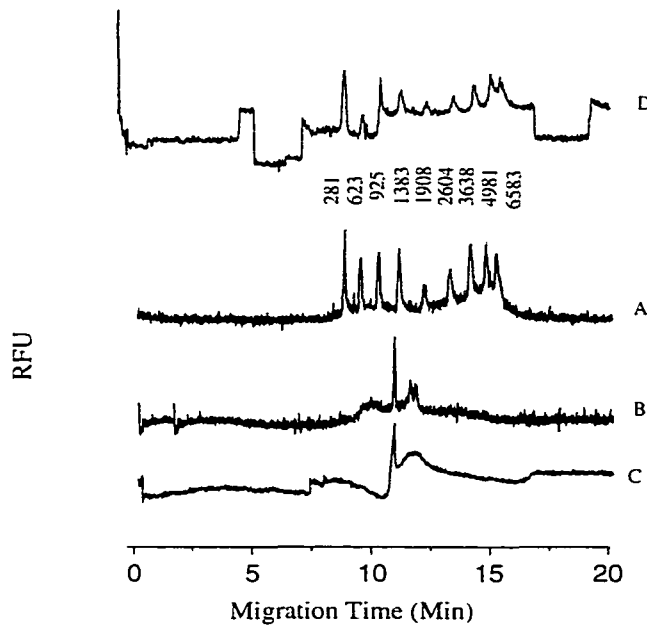


Figure 2-11. The peak height observed by CGE for the rare bicoid gene, obtained by RT-PCR of mRNA captured on chip, is shown as a function of the TRNA mass. The bead slurry volume was constant at 6  $\mu$ L of the original slurry, giving a maximum mRNA capacity of about 60 ng. Error bars show the standard deviation of 3 replicate CE runs on one sample.

from 0.85  $\mu\text{g}$  of TRNA and 6  $\mu\text{L}$  of the original bead slurry. A negative control for the RT-PCR reaction (Trace D) shows that when no mRNA template was present, no 699 bp peak was detected. The control confirms that the 699 bp RT-PCR product was from the mRNA template isolated on chip. Figure 2-11 shows the relationship between the RT-PCR product peak height by CGE and the amount of TRNA introduced to the chip. The amount of beads was constant at 6  $\mu\text{L}$  (original slurry), so the plot illustrates that the more TRNA in the device, the more signal could be detected by CGE after RT-PCR. Using this simple Y-intersection design required a minimum of 0.85  $\mu\text{g}$  of TRNA and 6  $\mu\text{L}$  of original bead slurry to capture and detect the rare bicoid gene with RT-PCR.

Though the amplified mRNA could be detected by CGE, we know little about the integrity of mRNA captured on chip. Clearly the integrity plays an important role in cDNA library construction. A preliminary evaluation of the mRNA integrity was done by performing denaturing capillary gel electrophoresis to directly detect mRNA isolated on the chip, without the use of RT-PCR amplification. About 44 mRNA capture trials (20  $\mu\text{L}$  original bead slurry, 34  $\mu\text{g}$  TRNA each trial (3 h.)) had to be run on chip and pooled into one sample in order to accumulate sufficient mRNA for this direct electrophoresis assay. Figure 2-12 shows the detection of unamplified mRNA isolated on chip. Trace A shows the electropherogram of a standard RNA marker. Trace B shows mRNA isolated with Dynal beads off-chip in a conventional fashion. Trace C shows mRNA isolated with Dynal beads on-chip. A comparison of traces A and D shows that there can be significant variation in the baseline between runs. This arises because each injected gel is different. These baseline variations cause a bigger problem at low concentrations where the S/N ratio is low. In comparing trace B and trace C we ascribe a

large part of the difference to the gel baseline noise. When off-chip isolated mRNA was



*Figure 2-12. Capillary gel electrophoresis (CGE) traces for an RNA marker, for mRNA isolated off chip using Dynal beads, and for mRNA isolated on chip using Dynal beads. The on chip results were obtained by pooling 44 runs. The baseline variations observed were typical of run-to-run differences seen with CGE in our hands.*

allowed to age in  $-20^{\circ}\text{C}$  for one week, the two sharp peaks at about 12 min became broader and poorly resolved. This change is presumably due to partially degradation of the mRNA. Comparison of trace C with B suggests that degradation of on-chip isolated mRNA occurred during the analysis. However, the component at 11 min remains intact and a reasonable amount of the material at 12 min must still be intact. Since it required ten days to acquire the 44 on-chip samples, we

believe most of the degradation occurred after isolation, during storage at  $-20^{\circ}\text{C}$ . Consequently, the on-chip isolation of mRNA should produce mRNA suitable for constructing a cDNA library. Further, the broad peak located around 1.8 kbp in trace C showed that abundant mRNA can also be captured on-chip.

The efficiency of capturing mRNA on the chip is an important parameter describing the device performance. RT-PCR of mRNA samples isolated on-chip compared to conventional isolation in a centrifuge tube indicated a 50% capture

efficiency for the rare bicoid gene. However, RT-PCR is known to exhibit extremely poor quantitative accuracy, with 5–90% efficiency for the RT step resulting from small changes in the concentration of mRNA and various salts<sup>34,35</sup>. Consequently, we performed a direct measurement of the total mRNA captured on-chip using CGE. It was necessary to pool 44 replicate mRNA capture experiments into one sample to obtain enough for a CGE run. This experiment was performed twice, giving a value of 26% for on-chip vs. off-chip capture efficiency of total mRNA in both tests. Given the well known variability of RT-PCR<sup>35</sup>, these two estimates of efficiency (26% and 50%) are in agreement, with much greater confidence attached to the lower value. These yields suggest a better fluid flow design may be needed to obtain a more efficient capture bed. Nevertheless, the current device is capable of capturing at least the 5 ng of mRNA required for cDNA library construction using the method of Lambert et al.<sup>29</sup>, as outlined below. Fig. 2-11 shows the device required a minimum of 0.85  $\mu\text{g}$  TRNA in order to detect the rare bicoid gene by RT-PCR. We estimate that between 9–40 ng of mRNA was present in the minimum TRNA sample, given that the fraction of mRNA in TRNA lies between 1–5%, depending upon tissue type. In fact, off-chip isolation of mRNA with the Dynal beads gives a value of 1.3%. Using this value of 1.3% and the lower value for the measured on-chip capture efficiency of 26%, the amount of mRNA we estimate is captured at the detection limit in Fig. 2-11 is 2.8 ng. At 10  $\mu\text{g}$  TRNA, near the saturation point seen in Fig. 2-11, the amount of mRNA captured can similarly be estimated to be 34 ng. Consequently, the microfluidic device performance is sufficient to capture more than the 5 ng amounts of total mRNA required<sup>29</sup>.

### 2-3-3. mRNA isolation and cDNA synthesis

The electropherograms shown in Figure 2-13 illustrate that we are able to do on-chip mRNA isolation and on-chip cDNA synthesis. Observation of the 699 bp PCR product showed that the rare bicoid gene could be captured by Dynal beads and cDNA synthesis could be done on a chip device. Trace A shows the electropherogram of the DNA marker, mixed with the PCR amplification product of cDNA. The cDNA was synthesized on chip from mRNA isolated from 10  $\mu$ g of TRNA using 5  $\mu$ L of the original Dynal bead slurry on chip. Trace B illustrates the electropherogram of the PCR product

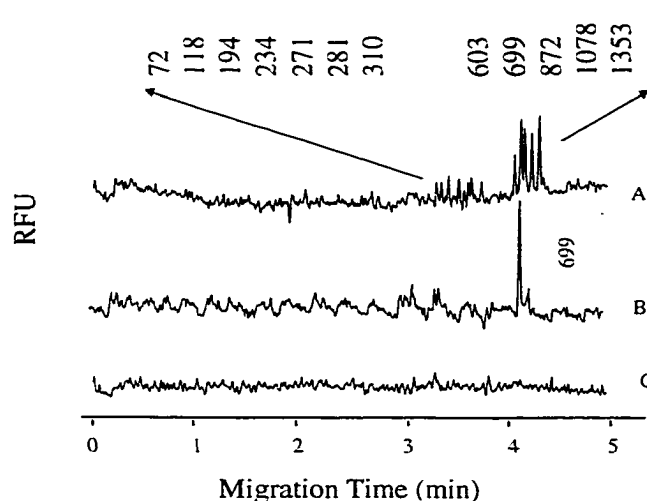


*Figure 2-13. Capillary gel electrophoresis of A) DNA marker mixed with PCR amplification of cDNA synthesized on chip from isolated mRNA; B) PCR amplification of cDNA synthesized on chip from isolated mRNA, Dilution with the DNA marker solution reduced the 699 peak in trace A; C) Negative control for PCR.*

without the DNA marker added. Dilution with the DNA marker solution reduced the 699 peak in trace A. A negative control for the PCR reaction (Trace C) showed that when only mRNA template was introduced to the PCR reaction without the RT step, no PCR product was observed. The negative control confirms that the 699 bp PCR product was from the cDNA template synthesized on chip.



During initial attempts to perform RT on chip, the magnetic bed was not disturbed by movement of the magnets and there was no PCR product peak using CGE detection (Figure 2-14). Several possible sources for this failure were considered:

1. The mRNA isolated on chip was degraded.
2. The cDNA synthesis on chip failed.
3. The PCR amplification failed.
4. The CGE detection of the PCR product was not successful.

In each PCR amplification, a positive control for PCR was run together with the sample, in different PCR tubes. Observation with CGE of the positive control product illustrated that both the PCR and CGE steps were functioning. The mRNA isolated on chip previously (Fig.2-12) showed good integrity and could be amplified by off-chip RT-PCR. As a result we concluded the RT reaction step was not functioning properly on-chip. We

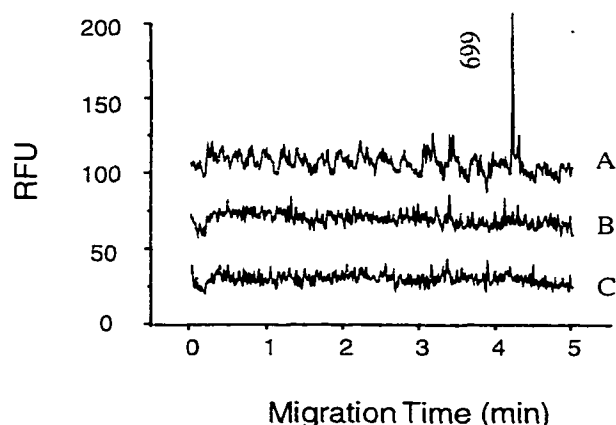


Figure 2-14. Capillary gel electrophoresis of A) PCR amplification of cDNA synthesized on chip from mRNA isolated on-chip; B) PCR amplification of cDNA synthesized on chip from mRNA isolated on-chip without moving magnets to cause mixing; C) Negative control for PCR

attempted to optimize the on-chip RT reaction by varying the concentration of the reverse transcriptase, evaluating various  $Mg^{2+}$  concentrations, trying different reaction temperatures and increasing the reaction time. Unfortunately, none of these efforts gave a PCR amplification product. A further set of tests was then performed. In one study, mRNA was isolated on-chip, followed by off-chip RT and

PCR. In another, off-chip mRNA isolation was performed on Dynal beads. These were then introduced into the chip and on-chip RT was performed, followed by PCR. Observation of the PCR product of both experiments, shown in Figure 2-15, illustrated that each on-chip step functioned when performed independently. However, when the two steps were combined, no cDNA was available for PCR amplification.

We noted that for the two independent steps, the washing steps for the mRNA prior to performing RT was done off chip. When the mRNA isolation and cDNA synthesis were combined together on chip, the washing steps were carried out on chip. These

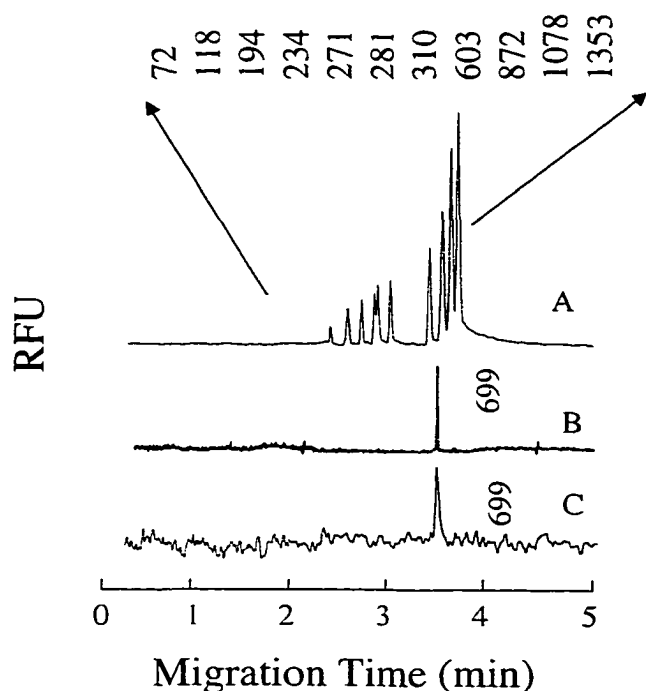
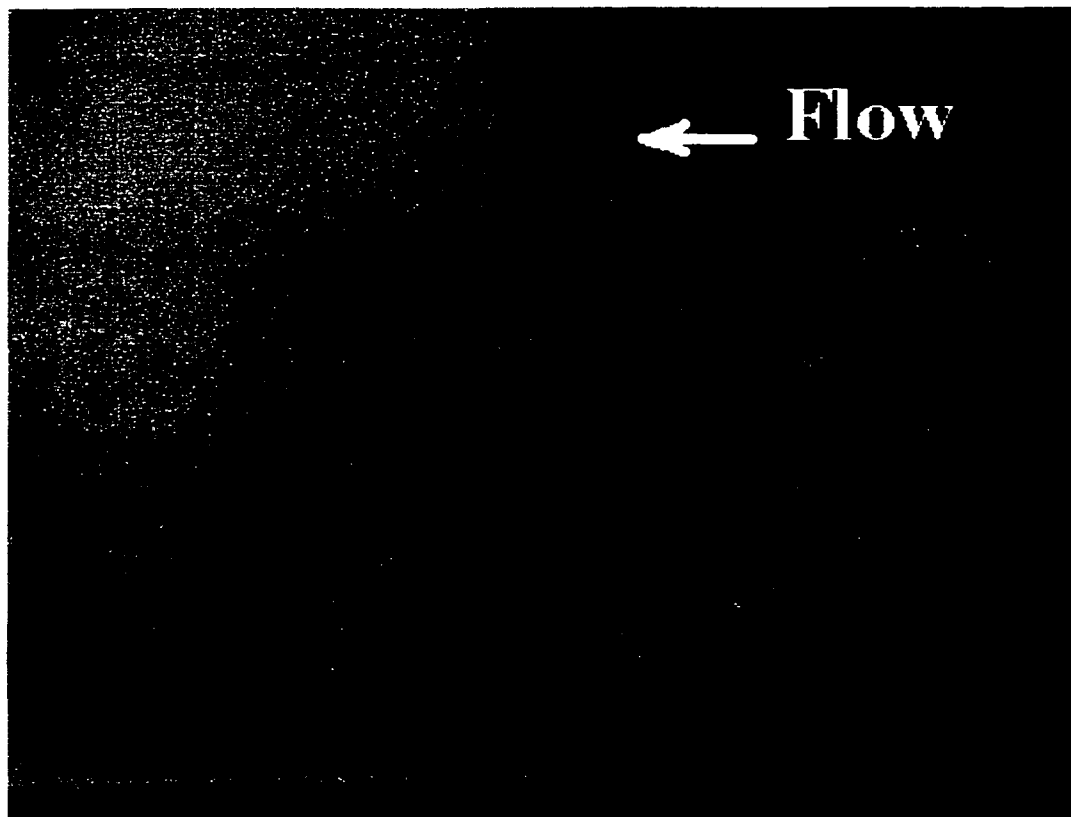
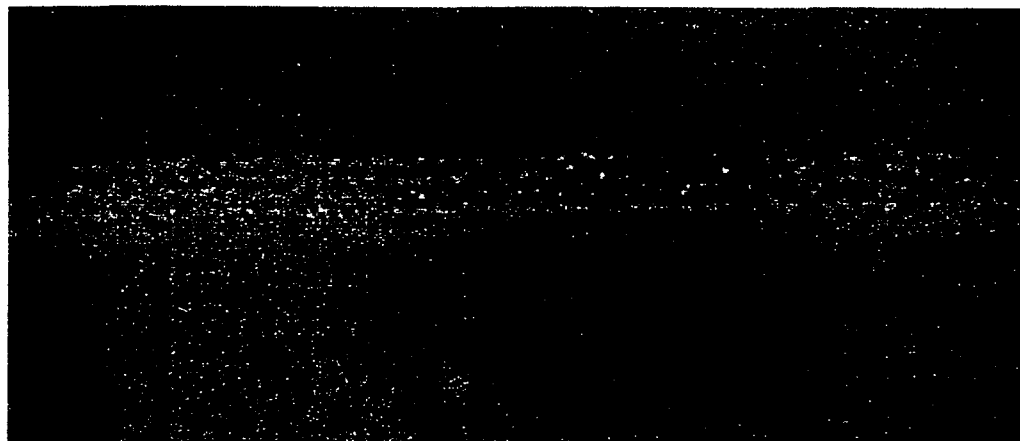


Figure 2-15. Capillary gel electrophoresis of A) DNA marker; B). PCR amplification of cDNA synthesized off chip from on-chip isolated mRNA ; C) PCR amplification of cDNA synthesized on chip from off-chip isolated mRNA.

observations suggested that off-chip washing was much more efficient than on chip washing. At this stage we considered that the magnetically trapped bead bed might not be compact enough, which could cause inefficient washing. The images of two trapped bead beds shown in Figure 2-16 and Figure 2-17 illustrated that the bead bed was in fact poorly packed. The wider channel shown in Fig. 2-16 was employed in this study.



*Figure 2-16. The magnetically trapped bead bed inside a 200  $\mu\text{m}$  wide channel, 30  $\mu\text{m}$  deep.*



*Figure 2-17. The magnetically trapped bead bed inside a channel with a 70  $\mu\text{m}$  channel width and 10  $\mu\text{m}$  depth.*

When the pressure was applied, open flow channels formed, creating a phenomenon known as channeling. The washing fluid could thus pass through the bed zone without permeating the denser portion of the bed. Most of the beads were not in contact with the fluid delivered into the reaction channel, causing inefficient washing and mixing. The magnetically trapped bed structure shown in Fig. 2-17 might be better for washing. The beads are lined up in rows inside the channel, offering a better chance for contact with the washing fluid. Unfortunately, as much as  $\sim 50 \mu\text{L}$  of solution must be introduced into the channel, so that a very long time will be involved if the narrow channel is employed. Therefore, the wider channel was a better choice. However, this means the channeling problem will have to be addressed.

We concluded the bed needed to be disturbed during the washing steps in order to properly clean it and mix the RT reagents. Another on-chip mRNA isolation and cDNA synthesis study was carried out while moving the magnets along the channel about 5 mm to stir the bed during washing and while delivering the RT mixture. Observation of the

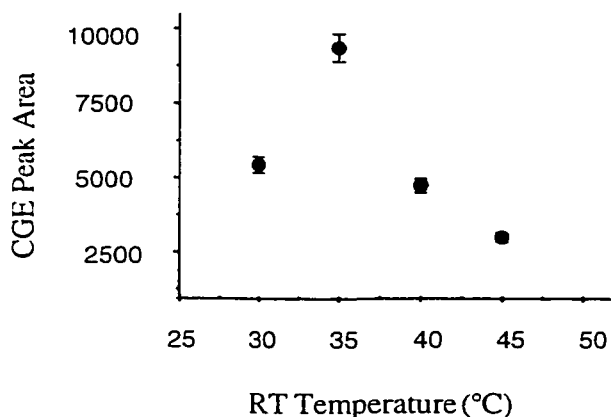


*Figure 2-18. The peak area of CGE detection of PCR amplification of cDNA synthesized on chip vs. RT reaction temperature. Error bars show the standard deviation of 3 replicate CE runs on one sample.*

PCR amplification product (Figure 2-13, 2-14) illustrated that the movement of the magnets during washing and delivering steps were the key element required to enhance the on-chip mixing efficiency, which is consistent with the observation of channeling in bead bed structures.

Figure 2-18 shows the relationship

between the PCR product peak area by CGE and the on-chip RT temperature. In order to elucidate the optimal temperature, we performed off chip mRNA isolation, then the bead-mRNA were introduced and trapped in the channel with magnets, and the RT reaction was performed at four different temperatures. This study showed that 35 °C was the best temperature for the RT reaction on chip. Since the temperature sensor was placed on top of the chip device and the heater was placed right underneath the chip device (Figure 2-4), it is not easy to estimate the real temperature in the channel. There is a temperature gradient across the chip substrate, making the temperature in the channel lie between the temperature of the heating point and the temperature at the sensor point. The optimal temperature for the RT reaction off-chip was 42 °C, at which the enzyme has its optimal

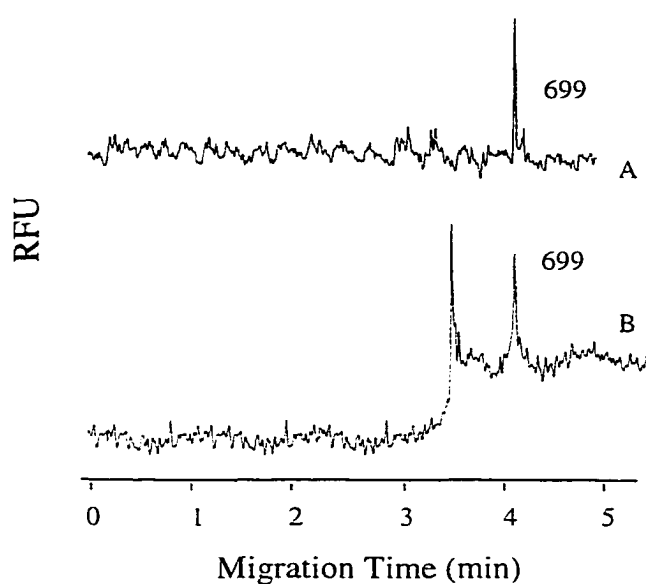


*Figure 2-19. Electropherograms of A). Hot start PCR of the cDNA synthesized on-chip from on-chip isolated mRNA; B). PCR of the cDNA synthesized on-chip from on-chip isolated mRNA.*

activity. This suggests that the temperature inside the channel was around 42 °C when the temperature sensor showed 35 °C at the chip surface.

Some primer-dimer peak was occasionally observed in the routine PCR amplification of the cDNA formed by on-chip synthesis. The use of hot start PCR eliminated the primer-dimer peak as shown in Figure 2-19.

## **2-4 Conclusion**

The present data shows that mRNA can be isolated from total RNA and RT reaction could be done on chip using a magnetic bead based collection technique. The device is sufficiently robust to be used with realistic mRNA samples. The mRNA isolated is intact, and both rare genes and abundant genes can be isolated. The quantity of mRNA isolated is sufficient for subsequent cDNA library formation. Optimization of the flow design and heating elements to improve the on-chip capture and RT efficiency would be beneficial. Such optimization could be used either to increase the amount of mRNA captured or to improve the RT reaction condition. This functional mRNA isolation and cDNA synthesis element is suitable for interfacing to PCR and electrophoresis elements also integrated within a chip, and represents the first step towards the design of an on chip cDNA library construction device.

## References

1. L. G. Davis, W. M. Kuehl, J. F. Battey, *Basic Methods in Molecular Biology*, Appleton & Lange Paramount Publishing Business and Professional Group, Norwalk, Connecticut, USA, 2nd ed. **1994**
2. R.W. Old, S. B. Primrose, *Principles of Gene Manipulation*, Blackwell Science Ltd., Oxford and Northampton, 5th ed. **1994**, ch. 6.
3. J. Sambrook, E. F. Fritsch, T. Maniatis, *Molecular Cloning, A Laboratory Manual*, Cold Spring Harbor Laboratory Press, USA, 2nd ed. **1989**, ch. 8.
4. G. H. W. Sanders, A. Manz, *Trends in Analytical Chemistry* **2000**, *19*, 364-377.
5. N.H. Chiem, D.J. Harrison, *Clin. Chem.* **1998**, *44*, 591-598.
6. A. T. Woolley, R. A. Mathies, *Proc. Natl. Acad. Sci. USA* **1994**, *91*, 11348-11352.
7. A. T. Woolley, D. Hadley, P. Landre, A. J. deMello, R. A. Mathies, M. A. Northrup, *Anal. Chem.* **1996**, *68*, 4081-4086.
8. L. C. Waters, S. C. Jacobson, N. Kroutchinina, J. Khandurina, R. S. Foote, J. M. Ramsey, *Anal. Chem.* **1998**, *70*, 158-162.
9. Z. H. Fan, S. Mangru, R. Granzow, P. Heaney, W. Ho, Q. Dong, R. Kumar, *Anal. Chem.* **1999**, *71*, 4851-4859.
10. C. H. Ahn, T. Henderson, W. Heineman, B. Halsall, in: *Proceedings of the  $\mu$ TAS '98*, 225-230, Kluwer Academic Publishers, Dordrecht, The Nertherland, **1998**.
11. *Biomagnetic Techniques in Molecular Biology*, Technical handbook, 3rd Ed, Dynal. Oslo, Norway, **1998**.
12. *Protocol of Dynal bead mRNA purification*, Dynal A. S. Oslo, Norway, **1998**.
13. C. Ainsworth, *Plant Mol. Biol. Reporter* **1994**, *12*, 198-203.
14. J.D.B. Faulkner, N.P. Minton, *Biotechniques* **1993**, *14*, 718-720.
15. E. Hornes, L. Korsnes, *Genet. Anal. -Tech. Appl. (GATA)* **1990**, *7*, 145-150.
16. K.S. Jakobsen, E. Breivold, E. Hornes, *Nucleic Acids Res.* **1990**, *18*, 3669.
17. J. G. Morgan, G. M. Dolganov, S. E. Robbins, L. M. Hinton, M. Lovett, *Nucleic Acids Res.* **1992**, *20*, 5173-5179.
18. J. E. Parrish, D. L. Nelson, *Genet. Anal.-Tech. Appl.* **1993**, *10*, 29-41.
19. T. Hultman, S. Bergh, T. Moks, M. Uhlen, *Biotechniques* **1991**, *10*, 84-93.

20. T. Hultman, S. Stahl, E. Hornes, M. Uhlen, *Nucleic Acids Res.* **1989**, *17*, 4937-4946.
21. H. Kaneoka, D. R. Lee, K. C. Hsu, G. C. Sharp, R. W. Hoffman, *Biotechniques* **1991**, *10*, 30-34.
22. C. T. Ashley Jr., K. D. Wilkinson, D. Reines, S. T. Warren, *Science* **1993**, *262*, 563-566.
23. C. S. Baker, A. Perry, J. L. Bannister, M. T. Weinrich, R. B. Abernethy, J. Calambokidis, J. Lien, R. H. Lambersten, J. Urban Ramirez, O. Vasquez, P. J. Clapham, A. Alling, S. J. O'Brien, S. R. Palumbi, *Proc. Natl. Acad. Sci. USA* **1993**, *90*, 8239-8243.
24. O. S. Gabrielsen, E. Hornes, L. Korsnes, A. Ruet. T. B. Oyen, *Nucleic Acids Res.* **1989**, *17*, 6253-6267.
25. J. P. Quinn, J. McAllister, *Nucleic Acids Res.* **1993**, *21*, 1637-1641.
26. L. Ren, H. Chen. E. A. Sternberg, *Biotechniques* **1994**, *16*, 852-855.
27. R. Sandaltzopoulos, C. Mitchelmore, E. Bonte, G. Wall, P. B. Becker, *Nucleic Acids Res.* **1995**, *23*, 2478-2487.
28. Y-H. Lee, V.D. Vacquier, *Anal. Biochem.* **1992**, *206*, 206-207.
29. K. N. Lambert and V. M. Williamson, *Nucleic Acids Res.* **1993**, *21*, 775-776.
30. I. Raineri, C. Moroni and H. P. Senn, *Nucleic Acids Res.* **1991**, *19*, 4010.
31. Z. Jin, Dept. of Biological Sciences, University of Alberta, Personal communication
32. G. Jiang, D.J. Harrison, *Analyst* **2000**, *125*, 2176-2179.
33. *Protocols for reverse transcription of RNA and PCR amplification of cDNA*, PE Biosystems, USA, **1996**.
34. W. M. Freeman, S.J. Walker and K.E. Vrana, *Biotechniques* **1999**, *26*, 112.
35. F. Ferre, A. Marchese, P. Pezzoli, S. Griffin, E. Buxton and V. Boyer. *The Polymerase Chain Reaction*, ed. K.B. Mullis, F. Ferre and R. A. Gibbs, Birkhauser, Boston, **1994**, 67-88.



# **Chapter 3. Red Diode Laser Induced Fluorescence Detection on A Microchip for Capillary Electrophoresis**

A version of this chapter has appeared in G. Jiang, S. Attiya, G. Ocvirk, W. E. Lee, D. J. Harrison, *Biosensors & Bioelectronics*, **2000**, vol. 14, 861-869.

### 3-1. Introduction

Planar microfluidic devices utilizing electrokinetic pumping may provide a powerful tool for automating the fluid handling steps required in many biological assays<sup>1-8</sup>. Such systems offer an alternative to biosensors for the detection of biological threat agents, or else complement such sensors by transporting the sample and reagent to the detector<sup>1-2, 6-7</sup>. The Harrison laboratory has developed microfluidic devices<sup>9-10</sup> capable of performing immunoassays which can be applied to the determination of threat agents. In these devices, samples and immunoreagents are mixed within 30-60  $\mu\text{m}$  wide flow channels, allowed to react homogeneously, then electrophoretically separated in order to determine the sample concentration<sup>9</sup>. These devices provide a means to automate immunoassays in the field, performing an analysis within 1-5 minutes. Reagent consumption on the order of 0.1-10 nl per assay has been achieved, which is of critical importance for reduced maintenance of a field-based instrument<sup>11</sup>.

To date, gas phase lasers were the most common excitation source used for laser induced fluorescence (LIF) detection on microfluidic chips<sup>1, 5, 7, 9</sup>. Such lasers are bulky and can be fragile, which makes them ill suited to field applications. Yet LIF is so sensitive that it is one of the most preferred detection methods on-chip. The red diode laser family represents a more compact, portable source for LIF on a chip, as has been made clear by the fact that diode lasers have been used previously in capillary electrophoresis (CE)<sup>12</sup>. Ligler and coworkers have shown they can also be used with optical fiber immuno-sensors in the field<sup>13-14</sup>. Early studies showed the promise of these lasers for detection in CE, but detection limits were poor<sup>15-20</sup>. However, the concentration detection limits have since improved to 50-100 pM with a red diode laser

<sup>21-23</sup> and  $\sim 3$  pM in aqueous solutions using a gas phase  $\text{Ar}^+$  ion pumped solid state Ti/sapphire laser <sup>24</sup>.

In this chapter we examine the use of cyanine-5 (Cy-5) dye with a 635 nm diode laser and a microfluidic chip. The optimal parameters needed to obtain good detection limits with a confocal, epiluminescent microscope are reported. This microscope design was selected because it produced the best detection limits obtained on a chip when using a 488 nm LIF source <sup>25</sup>.

### 3-2 Diode laser

Semiconductor laser diodes have many advantages over other types of lasers. Compared to gas or dye lasers, the diode laser offers a considerably smaller size, higher efficiency, lower cost and the unique ability to be modulated up to gigahertz rates by simply changing the driving current through the device <sup>26</sup>. Thus, diode lasers have found acceptance in a wide range of applications, for example, optical communication, optical sensors and optical disc systems <sup>27</sup>. The red diode laser has seen significant development. Kressel *et al.* developed the  $\text{Al}_x\text{Ga}_{1-x}\text{As}$  visible and IR-light-emitting semiconductor laser in 1970. Unfortunately, the laser only operated at 73 K with 50% power conversion efficiency <sup>28-29</sup>. In 1976, Colemann and coworkers made the pulsed room temperature operation of  $\text{In}_{1-x}\text{Ga}_x\text{P}_{1-z}\text{As}_z$  double heterojunction lasers (6470  $\Delta$ ) possible. However, the large diode size, thick active region and poor heat sinking caused low quantum efficiency (5%) and poor performance <sup>30</sup>. An increasing demand for short wavelength laser light sources for use in optical information processing and plastic fiber communication systems has stimulated research on 600 nm wavelength range visible laser diode. In 1985, Usui *et al.* reported 671 nm room temperature continuous-wave (cw) operation of an

InGaAsP/InGaP laser. They successfully reduced the thermal resistance of the diode and the threshold current density<sup>31-32</sup>. The same year, Ikeda *et al.* and Kobayashi *et al.* achieved cw operation of a GaInP/AlGaInP laser at room temperature with 671 nm emission wavelength<sup>33-34</sup>. Then in the 1990's, the 635 nm diode laser became commercially available. In this chapter, the 635 nm red diode laser was employed as the excitation light source for LIF detection.

### 3-2-1. Basics of diode lasers

There are two factors required to operate a laser<sup>35</sup>:

1. A gain medium that can amplify the electromagnetic radiation propagating inside it.
2. A feedback mechanism that can define the electromagnetic field through the well

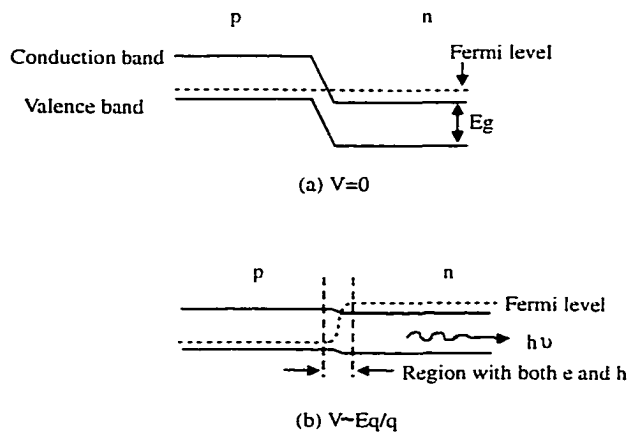


Figure 3-1. The energy-band diagram of a p-n junction at a) zero bias and b) Forward bias. The Radiative recombination of the electrons and holes in the narrow overlapping region generates light.

defined optical modes.

In semiconductor lasers, semiconductor materials are used as a gain medium. The optical feedback is obtained by using cleaved facets that form a Fabry-Perot cavity, and mode confinements are achieved through dielectric waveguiding.

The p-n junction, which is formed by bringing a p-type and an n-type semiconductor into contact with each

other, is the heart of the diode laser<sup>36</sup>. Figure 3-1 illustrates an energy-band diagram of the p-n junction of the semiconductor laser. When there is no external applied field, the p-

n junction is at equilibrium. Diffusion of the electrons from the n side to the p side and diffusion of the holes from p to n sides are opposed by the built-in electric field across the p-n junction. The field arises from the equilibration of the negatively charged acceptors on the p side with the positively charged donors on the n side. When the p-n junction is forward biased by applying an external voltage, the built-in electric field is reduced, making diffusion of the electrons and holes possible <sup>35</sup>. The recombination of the electron and holes gives off photons. Of course, the photons could be adsorbed again to give electron-hole pairs. However, when the external voltage exceeds a critical value a condition known as population inversion is achieved, in which the rate of the photon emission exceeds that of absorption. Laser irradiation is thus obtained.

### *3-2-2. Drawbacks of diode laser*

Laser diodes have certain shortcomings. Of these, the elliptical cross section of the laser beam and the diode's intrinsic astigmatism are the most likely to cause problems in an application.

The elliptical cross section of the beam is a result of the rectangular shape of the beam emission facet of the laser diode. This characteristic prevents the beam from being entirely collimated, allowing for quasi-collimation only <sup>37</sup>. Wave optics theory tells us that a beam output from a small aperture has, in one given direction, a full divergent angle  $\theta$  given by

$$\theta = 4\lambda / \pi d \quad (3-1)$$

where  $\lambda$  is the wavelength and  $d$  is the size of the aperture in this direction. The difference in  $\theta_x$  and  $\theta_y$  causes the laser diode beam to have an elliptical cross section, as

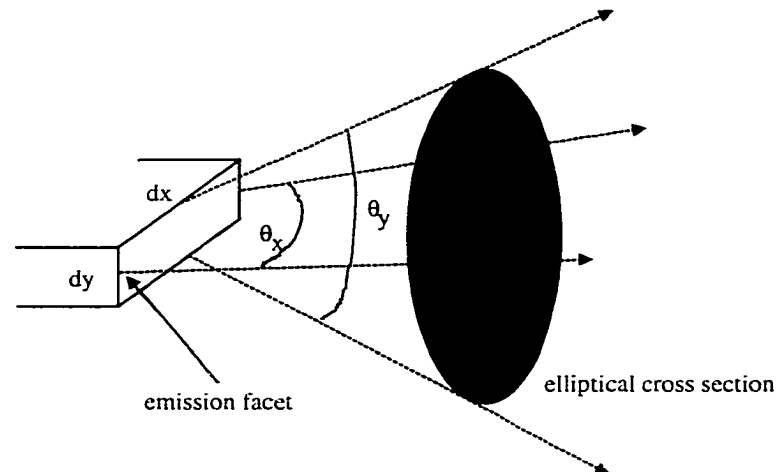


*Figure 3-2. The rectangular facet of the laser diode might cause the elliptical cross section of the laser beam.*

shown in Fig.3-2. Universal characterization of this problem is made impossible by the differences between index-guided and gain-guided diodes, as well as by the individual characteristics of each laser diode <sup>37</sup>.

### Astigmatism

Astigmatism is, in fact, another result of the rectangular facet of the laser diode. As illustrated in Fig.3-3, the beam emitted from a small facet is equivalent to the beam emitted by an imaginary point source P, whose position can be located by tracing the beam backwards. It can be seen immediately that  $P_x$  is located behind  $P_y$ , because  $\theta_x$  is smaller than  $\theta_y$ . This phenomenon is called astigmatism, and the distance between  $P_x$  and  $P_y$  is the numerical description of astigmatism.

The existence of astigmatism means that when using a single, standard aspheric lens the beam can be collimated only in one direction, either in the X direction or in the Y

direction, because  $P_x$  and  $P_y$  can not simultaneously converge at the focal point of the collimating lens.

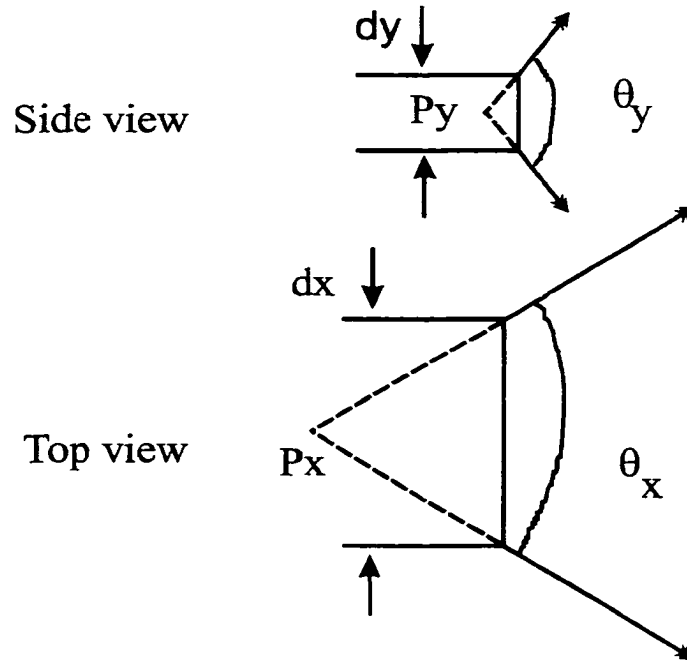


*Figure 3-3. The rectangular facet of the laser diode might cause the astigmatism.*

The most commonly used method to circularize the elliptical beam and to correct astigmatism is to use a pair of correcting prisms and a very weak cylindrical lens. The prisms can enlarge or reduce the beam size in one direction while keeping the beam size in another direction unchanged. By properly adjusting the angles of the prisms, a circular beam can be obtained. The cylindrical lens, on the other hand, can collimate the beam in one direction, while not altering the divergent angle in the other direction. By using a cylindrical lens with the right focal length, astigmatism can be corrected. The beam corrected using this method still has residual astigmatism and high beam wavefront distortion. However, this is an inexpensive method with low loss of power. An alternative method is to use a single mode fiber coupled to a collimating lens. The quality and spatial

characteristics of the beam output from the fiber can be totally determined by the surface quality and shape of the output end of the fiber. The elliptical cross section and astigmatism of the beam before entering the fiber does not affect the spatial characteristics of the beam output from the fiber. The fiber core has a circular cross section, so as a result the output beam has a circular cross section with constant divergent angle in any radial direction. Because the divergent angle of the beam is a constant in any radial direction, the beam output from the fiber has no astigmatism. However, the relatively high cost of alignment systems for launching into the fiber and the 50-80% power losses in the coupling step limit the wide application of this method.

### **3-3. Characteristics of the Cy-5 dye**

Cy-5 is a fluorescent dye, which is widely used for detection in cell biology assays, antibody, DNA and protein labeling<sup>38-48</sup>. The maximum excitation wavelength is 649 nm and the maximum emission wavelength is 670 nm. The reactive N-hydroxy succinimide (NHS) esters (Fig. 3-4) of the Cy-5 are used to conjugate to biomolecules containing aliphatic amino groups. In this chapter, we used an unreactive form of Cy-5 dye (Fig. 3-4), if not otherwise mentioned, to test the performance of the optical detector.



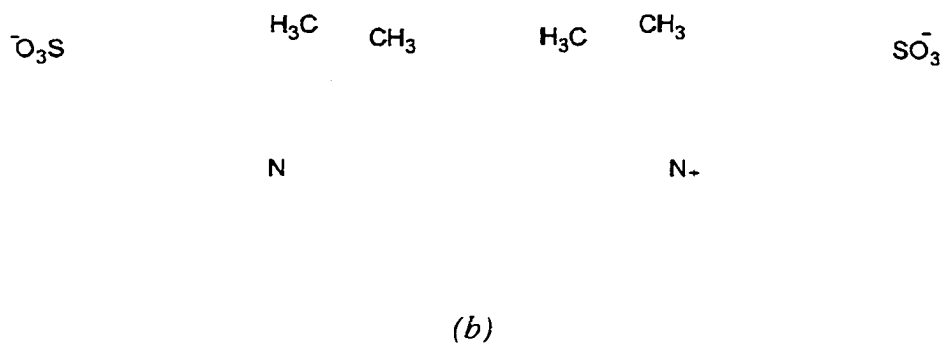
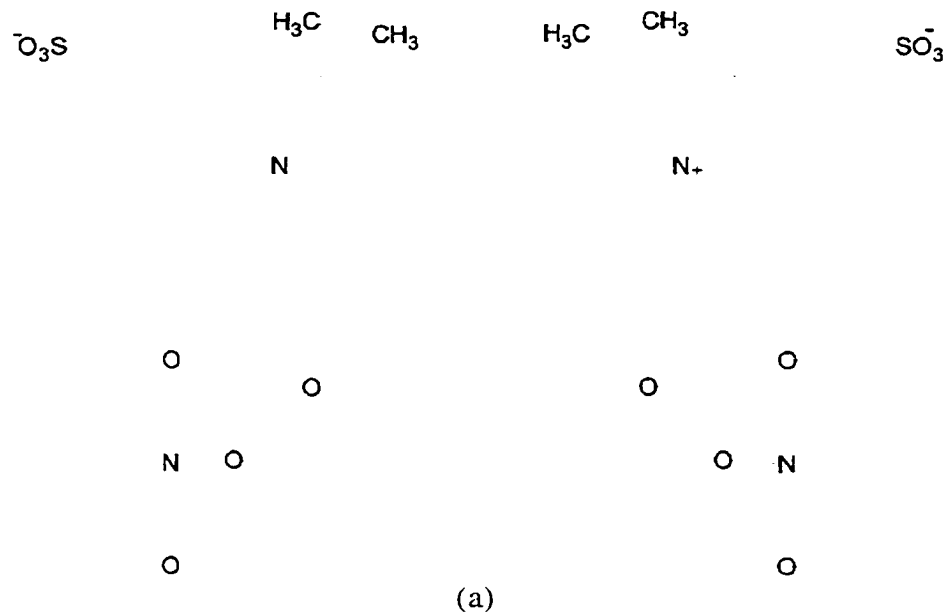


*Figure 3-4. The structure of the Cy-5 NHS ester (a) and unreactive Cy-5 (b).*

### **3-4. LIF detection of Cy-5 using conventional and confocal optical set up**

#### *3-4-1. Experimental Section*

##### *3-4-1-1. Devices*

Microchannels were isotropically etched in 3" x 3" Pyrex glass (Paragon Optical, Reading, PA) and 4" x 4" 0211 glass (Corning, Corning, NY) as described previously<sup>4, 10</sup>. After drilling 1.9 mm diameter access holes in the cover plate, it was thermally bonded to the etched glass wafer to form an enclosed fluidic device. The chip layouts used in this study, COPI<sup>1, 10, 49</sup> and DARPA-NC1<sup>11</sup>, are depicted in Figure 3-5. The device channels were etched either 13 or 20  $\mu\text{m}$  deep, giving the channel width at the top indicated in Table 3-1. Pyrex COPI devices were used for all optical optimization procedures. Corning 0211 DARPA-NC1 devices were used for measuring the limit of detection and the separation efficiency observed for a Cy-5 standard.

##### *3-4-1-2. Materials*

The unreactive Cy-5 standard dye was from Beckman Instruments (Fullerton, CA), (L+) lactic acid and boric acid were from Sigma (St. Louis, MO) and Baker (Phillipsburg, N.J.), respectively. Water from a Milli-Q UV Plus Ultra-pure system (Millipore, Mississauga, ON, Canada) was used for all solutions. A borate buffer containing 0.2 mM (L+) lactic acid and 15 mM boric acid was adjusted to pH 10.6 with 1 M NaOH. A  $10^{-7}$  M stock solution of Cy-5 dye was prepared by dissolving 200 pmole of dye in 2 ml water. All solutions used with Cy-5 were prepared by dilution of the stock solution in pH 10.6 boric acid buffers. Chicken egg ovalbumin and anti-ovalbumin were from Sigma (St. Louis, MO). The antibody was labeled with bifunctional Cy-5 (Amersham Life Science, Pittsburgh, PA.) using an affinity protected labeling procedure described elsewhere<sup>50</sup>. A

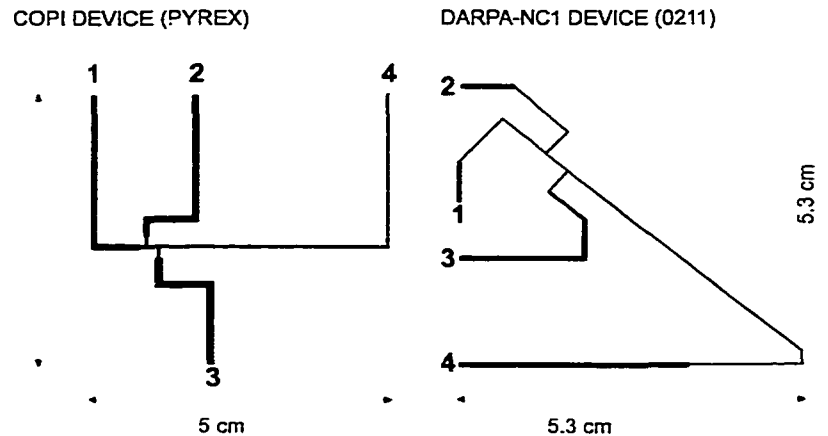


Figure 3-5. Schematic layout of microchip designs for COPI and DARPA-NC1 devices. Reservoir junctions are indicated by their names. The double T injector offset is  $100\ \mu\text{m}$  in COPI, and  $491\ \mu\text{m}$  in DARPA-NC1 device; they are exaggerated here for clarity. The narrow lines in the figure refer to channels with narrow feature width, the wide lines refer to channels with wide feature width (Table 3-1).

Table 3-1. Channel depths and widths<sup>(a)</sup>.

Device	Depth ( $\mu\text{m}$ )	Feature width <sup>(b)</sup>		Etched width	
		Wide ( $\mu\text{m}$ )	Narrow ( $\mu\text{m}$ )	Wide ( $\mu\text{m}$ )	Narrow ( $\mu\text{m}$ )
COPI	13	210	25	260	78
COPI	20	210	25	284	96
DARPA-NC1	13	210	26	240	65
DARPA-NC1	20	210	26	270	75

(a) Channels are approximately trapezoidal in cross-sectional shape, with the etched width defining the upper width and the feature width defining the lower width.

Dimensions were measured with a surface profilometer.

(b) Feature width defines the dimension on the photolithographic patterning mask.

pH 8.5 buffer was prepared with 20 mM boric acid, NaOH added to adjust pH, and 20 mM NaCl. All chemicals used were reagent grade, and all solutions were filtered using 0.22  $\mu\text{m}$  pore cellulose acetate syringe filters (Millipore, Bedford, MA) before use.

### 3-4-1-3. Instrumentation

A previously described<sup>3, 4, 49</sup> computer-controlled power supply system (-15 kV, MJ Series, Glassman High voltage, Whitehouse station, N.J.) with high voltage relays (30

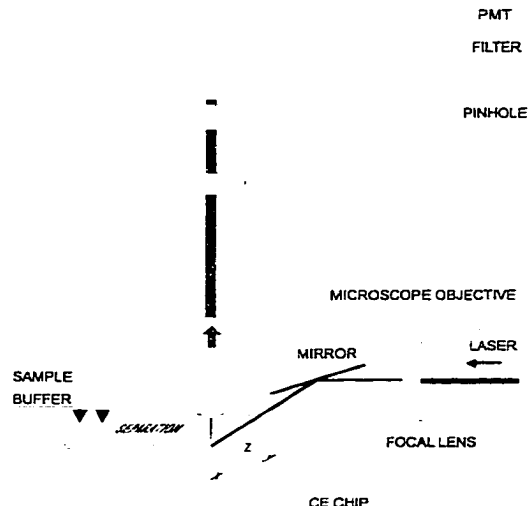
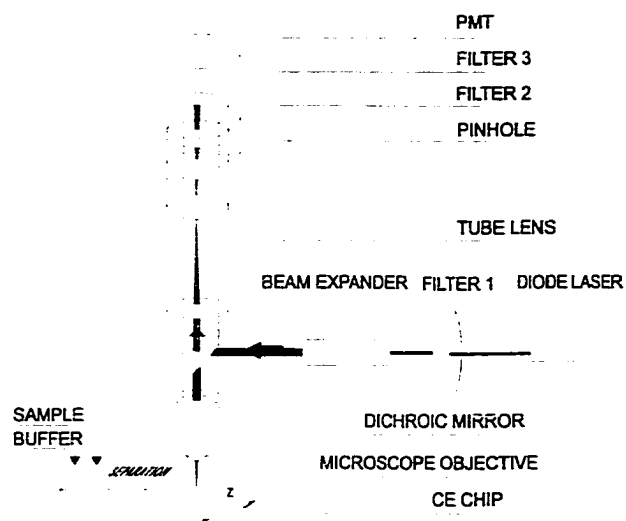


Figure 3-6. conventional optical set up for LIF detection on chip

kV, Kilovac, Santa Barbara, CA) was used for voltage control. Two types of optical arrangement were employed for comparison. A conventional two lens set up (Figure 3-6) in which the laser focus lens and the fluorescence collection lens are separate, and the epiluminescent confocal optical set up shown in Figure 3-7 were compared. The chip was mounted onto an X-Y-Z translation stage (Newport 423, Irvine, CA). A power adjustable 635 nm diode laser (ACM08 (635-15) X 12,

Power Technology Inc., Mabelvale, AR), was used as the exciting laser source. When using the conventional optical set up, the laser light was focused by a lens with a 15 cm focal length, then reflected by a mirror on to the detection spot of the channel. The fluorescence signal was collected using a 25 x microscope objective, an 800  $\mu\text{m}$  pinhole, a 670DF40 emission filter and a photomultiplier tube (PMT, Hamamatsu R1477; bias:



*Figure 3-7. Confocal epifluorescence setup for Cy-5 detection on chip.*

900 V). The confocal optical set up shown in Figure 3-7 is similar to that described previously for a 488 nm source<sup>25</sup>. The laser light passed through an optional filter 1, a beam expander (optional, 10-20 x Zoom, Edmund Scientific Company, N.J.), then was reflected by a dichroic mirror (Omega, Battleboro, VT) and focused in the channel by a 0.6 N.A., 40x, 4.9 mm focal length, 3.3 mm

working distance microscope objective (Planachromat LDN 1.2-A, Carl Zeiss, Jena, Germany). The 670 nm (peak max.) fluorescence signal, collected by the microscope objective, was passed through the dichroic mirror, then was focused by the tube lens (Achromat, Newport PAC064,  $f=200$  mm) onto a pinhole located at the focal point, then was detected by a PMT. Filter 2 and Filter 3 (optional) were inserted above the pinhole for spectral filtering. Optical filters were purchased from Melles Griot (03FIL024,  $\lambda_{\text{max}}=634.54$  nm, FWHM=10 nm), Omega Optical (670DF40, 682DF22, 645DRLP02, 670DRLP02; Battleboro, VT) and Beckman (675DF20; Fullerton, CA). A 665 nm long pass filter was from Rolyn Optics (RG665, Covina, CA). The laser power was measured using a Model 835 optical power meter (Newport). The PMT current was converted to a voltage using a  $10^8$  gain trans-impedance amplifier, filtered with an 8th order, active, 25 Hz, low-pass noise filter, then acquired with a computer with sampling rate of 50 Hz.

A Beckman P/ACE 5000 equipped with a 635 nm LIF detector and a 27 cm long, 50  $\mu\text{m}$  i.d. fused silica capillary operated at 20 kV, was used for comparative studies. The pressure injection mode (0.5 psi) was used for 10 s for sample introduction.

#### *3-4-1-4. Chip operation*

All devices were conditioned with 0.1 M NaOH for 30 minutes before use. The chip was then filled with Cy-5 solution after an intermediate rinsing step with boric buffer for 5 minutes. The dye or buffer solutions were flushed through the separation channel by applying vacuum at the separation waste port, resulting in a linear flow velocity,  $u$ , of 3.8  $\mu\text{L}/\text{min}$ . The flow rate was measured by determining the volume delivered over a 2 h period. The pinhole was positioned in the XY plane with a pinhole translator (Newport LP-1-XYZ) in order to obtain maximum fluorescence signals for a given dye concentration. The maximum background corrected fluorescence signal at a given Cy-5 concentration was found by monitoring the response for Cy-5 and buffer solutions ( $u = 3.8 \mu\text{L} / \text{min}$ ), while translating the chip vertically.

#### The conditions for conventional two lens system

Both double T and single T injection modes shown in Figure 3-8 were employed in this study. For a double T injection, an injection voltage of -2 kV was applied from sample (S) to sample waste (SW) for 30 s to fill the injection channel with the sample. Once filled, a 5 s injection time was applied to form the injection plug within the double T segment. A separation voltage of -4 kV was subsequently applied from the buffer (B) to the separation waste (BW) reservoirs, while the other channels were left floating. For a

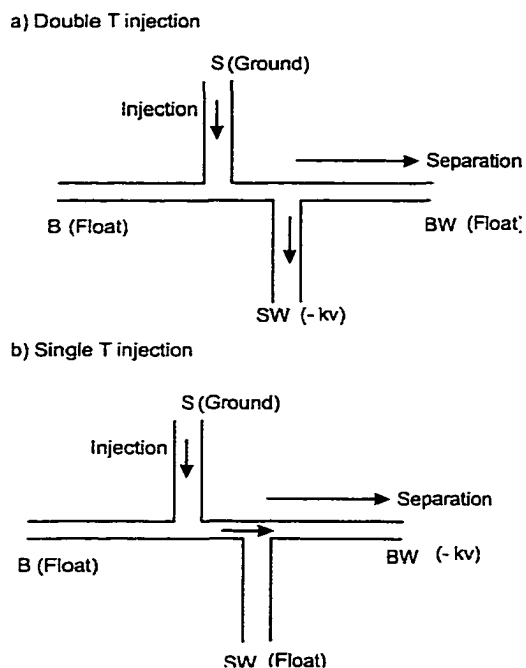


*Figure 3-8. Schematic illustration of double T injection and single T injection.*

Northampton, USA).

single T injection, a voltage of -2 kV was applied from sample (S) to sample waste (SW) for 30 s to fill the channels, a voltage of -2 kV was applied from sample (S) to separation waste (BW) for 5 s to form the injection plug. A separation voltage of -4 kV was subsequently applied from the buffer (B) to the separation waste (BW) reservoirs. All data in this section was smoothed using a 13 point Savitzky-Golay smoothing algorithm, included in Origin 5.0 software (Microcal software,

### The conditions for confocal optical system

The sectioning power study was done in continuous-flow mode. First, the chip was filled with buffer; the background data were collected while vertically scanning the chip from 40  $\mu\text{m}$  below the focal plane to 40  $\mu\text{m}$  above the plane in 1  $\mu\text{m}$  steps. Then  $10^{-8}$  M Cy-5 fluorescence signals were collected in the same way. The background corrected fluorescence signals in continuous flow experiments are the average of 3000 data points. The reported noise levels represent the standard deviation of the buffer background fluorescence ( $n = 3000$ ). Signal to noise ratios, S/N, were determined by dividing the background corrected fluorescence signal by the standard deviation. For the evaluation of detection limits by capillary electrophoresis, the sample reservoir was filled with Cy-5

dye, and the others with buffer. A double T geometry, if not otherwise mentioned, was employed for injection, and an injection voltage of -2 kV was applied from sample to sample waste for an injection time of 10 s for all experiments. A separation voltage of -4 kV was subsequently applied from the buffer to the separation waste reservoirs. All data was smoothed using a 21-point box smooth algorithm, included in Igor Pro (Wavemetrics, Lake Oswego, OR).

In both optical systems, the  $S/N$  for each electropherogram was calculated by dividing the average peak height above background by the standard deviation in the background, determined from the portion of the electropherogram ( $\Delta t = 10\text{ s}$ ) before the peak. The  $S/N$  versus concentration of Cy-5 plot will be referred to as the calibration curve throughout the whole text. The calibration curve was forced through the origin point and the limit of detection was obtained by extrapolated to a  $S/N$  of 3.

Solutions of antigen and Cy-5 labeled antibody were placed in the sample reservoir 5 min after mixing them together. An injection voltage of -1.2 kV was applied from sample to sample-waste reservoirs in DARPA-NC1 for 3 s, after an initial 1 min flush. Separation was performed with -6 kV applied from the pH 8.5 borate buffer reservoir to separation waste.

### *3-4-2. Results and Discussion*

Separation of antibodies (Ab) from their antigen complexes using capillary electrophoresis can be a challenge, and the separation efficiency depends on the specific antigen/Ab pair<sup>51-54</sup>. The labeling dyes used often play a role, since they will change the charge to size ratio of the labeled compound. For this reason we evaluated our ability to separate Cy-5-labeled antibody to ovalbumin (Ab\*) from the ovalbumin-Ab\* complex.



Ovalbumin (Ov) is a commonly used simulant for protein toxins in environmental trials. Figure 3-9 shows the separation of a mixture of 200  $\mu\text{M}$  Ab\* and 600  $\mu\text{M}$  Ov, within a 13  $\mu\text{m}$  deep DARPA–NCI device. The free Ab\* eluted at 23 s, so the later eluting peak can be assigned to the antibody-antigen complex<sup>11,50</sup>. The high concentration of Ov was needed because of the low affinity constant of this monoclonal antibody<sup>50</sup>.

The results illustrate that the Cy-5/635 nm laser diode combination can be used for the LIF determination of immunoreaction products on a microfluidic chip. Optimization of the limits of detection (LOD) of this system was required for it to be used effectively<sup>22</sup>. The relevant elements of our optimization study are discussed below. Key features included the choice of optical detection design the optical filter set, laser spot size, confocal pinhole choice and the volume of the detection channel.

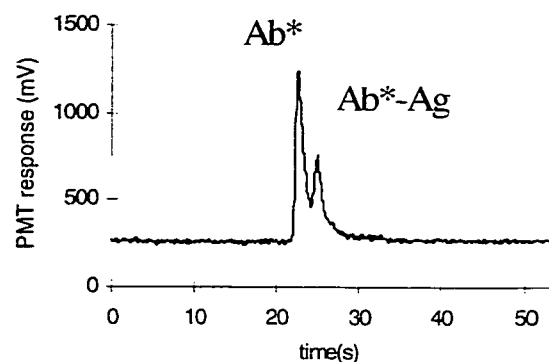


*Figure 3-9. Electropherogram of a mixture of 200  $\mu\text{M}$  Cy-5 labeled anti-ovalbumin (Ab\*) and 600  $\mu\text{M}$  ovalbumin (Ag) obtained in DARPA –NCI.<sup>58</sup>*

#### *3-4-2-1. The performance of conventional two lens optical set up*

The limit of detection of Cy-5 with a 635 nm diode laser was tested using our conventional two lens optical set up first. Both double T injection and single T injection were employed for sample introduction (Figure 3-8). The double T geometry of the injector design will define the sample plug introduced in the separation channel. The

injection time usually will not affect the length of the sample plug if no sample leakage problem occurs. The single T injection was applied when it was necessary to improve the sensitivity. Obviously, the longer the injection time, the longer was the sample plug introduced into the separation channel. Figure 3-10 illustrates the electropherograms of multiple injections of 1 nM Cy-5 using the double T injector. The peak height reproducibility calculated as the relative standard deviation (RSD) was 0.7%. A plot of S/N versus concentration, hereafter referred to as a calibration curve is shown in Figure 3-11. The limit of detection of 0.12 nM Cy-5 could be obtained by extrapolating to a S/N equal to 3. Figure 3-12 shows the electropherogram of 0.2 nM Cy-5 using a double T injection, yielding S/N of 7.5. The 0.82 s of the full width at half maximum (FWHM) of the peak was measured by Origin 5.0 software after Gaussian fitting. The same tests for the Cy-5 were carried out using the single T injection mode. Multiple injection of 2 nM Cy-5 dye (Figure 3-13) illustrated that if the injection time was carefully controlled, the peak height reproducibility (RSD 1.5%) for the single T mode could be good too. The limit of detection (LOD) of the Cy-5 was also tested using the single T. The calibration curve shown in Figure 3-14 gave an LOD of 0.11 nM. Figure 3-15 shows the electropherogram of 0.2 nM Cy-5 using a 5 s single T injection. The S/N was 7.6. The LOD is limited by this two-lens optical set up. A focusing lens with long focal length (15 cm) was employed in this conventional set up system, resulting in a relatively large excitation spot diameter and high background scattering. A small numerical aperture (N.A.) microscope objective was also employed, making the fluorescence collection efficiency relatively low.

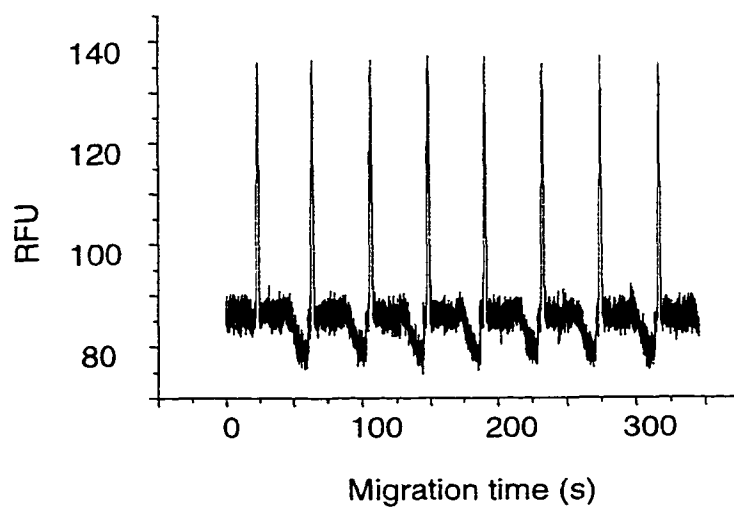


*Figure 3-10. The multiple injection of 1 nM Cy-5 using double T injection, with conventional two lens optical set up.*

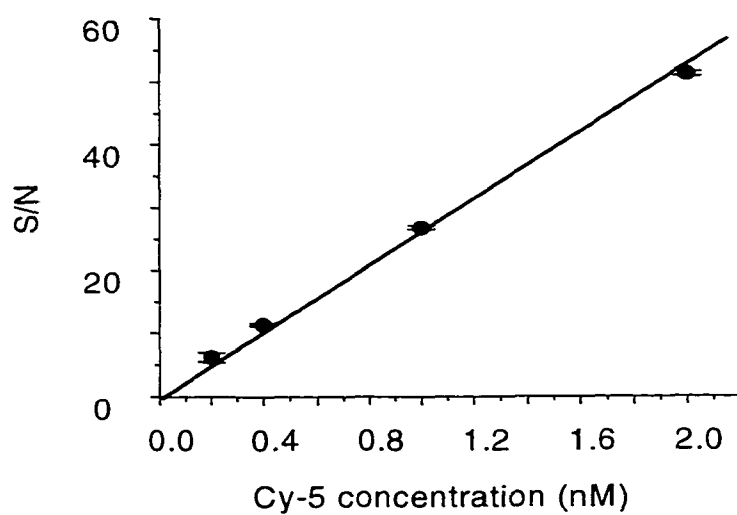


*Figure 3-11. The calibration curve of Cy-5 using double T injection, with conventional two lens optical set up.*

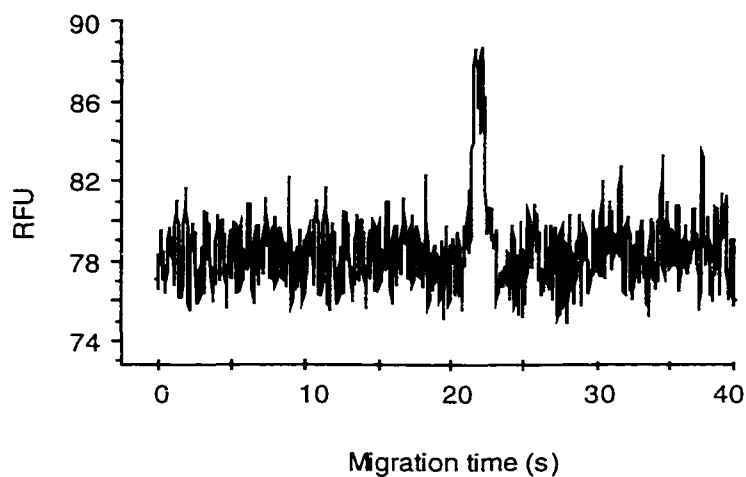


*Figure 3-12. The electropherogram of 0.2 nM of Cy-5 using double T injection with 5 s injection and conventional two lens optical set up.*

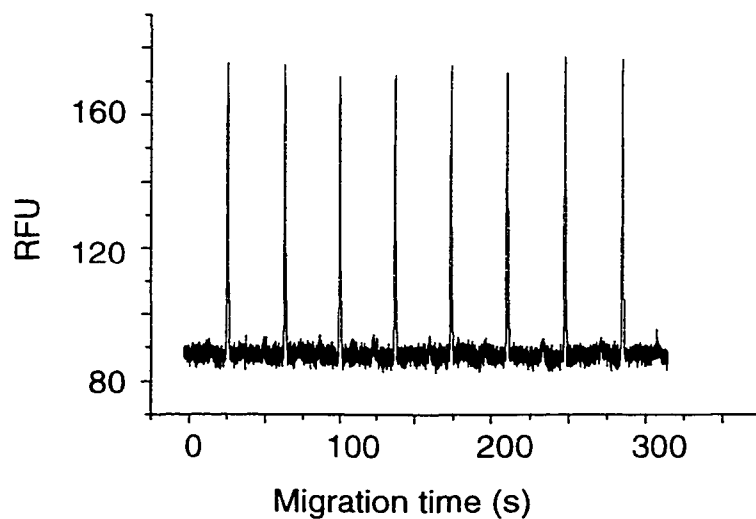


*Figure 3-13. The multiple injection of 2 nM Cy-5 using single T injection, with conventional two lens optical set up.*

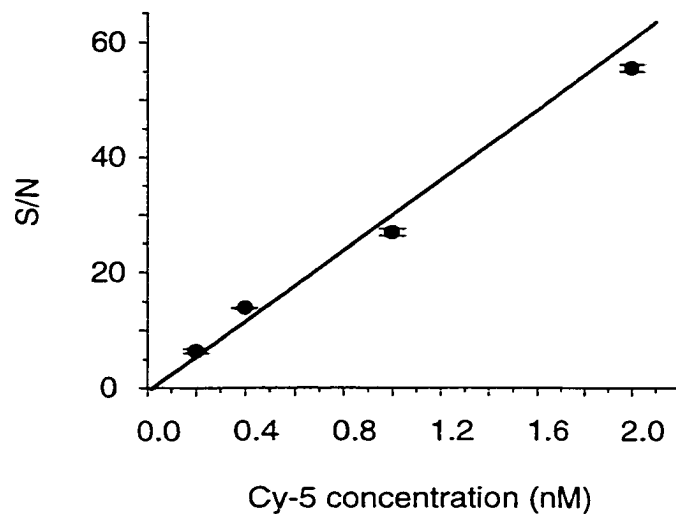


*Figure 3- 14. Calibration curve for the Cy-5 with 5s single T injection, with conventional two lens optical set up.*

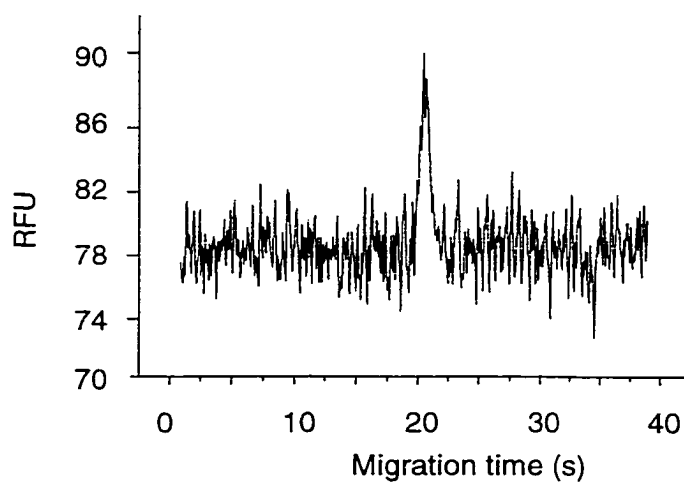


*Figure 3- 15. The electropherogram of 0.2 nM of Cy-5 using single T injection with 5 s injection, with conventional two lens optical set up.*

### *3-4-2-2. The performance of a confocal optical set up*

A confocal epiluminescent microscope use a high N.A. microscope objective could be used instead to increase the collection efficiency. The use of a small pinhole and a high magnification lens creates a confocal system that will reduce the collection of background scatter, which should provide a lower LOD. Ocvirk<sup>25</sup> illustrated that a minimum 10-fold sensitivity was gained by using a confocal microscope for detection of fluorescein on a chip device. Therefore, we evaluated a confocal epiluminescent optical set up to test the LOD of Cy-5 when using the diode laser.

#### *3-4-2-2-1. Optimization of Filters*

Because the epiluminescent design can be sensitive to scattering, the choice of optical filters can be important. A number of filter sets were examined. Filter selection was difficult due to the small Stokes shift of the Cy-5 dye. Table 3-2 indicates the filter sets examined. The specific locations of the filters are indicated in Figure 3-7. The lowest detectable concentration we actually observed is given, along with the LOD extrapolated from higher concentrations. Our first choice of a 645DRLP02 dichroic mirror and a 670DF40 filter was intended to maximize the throughput of the emission filter for the emission spectrum of the dye. However, this set allowed so much excitation radiation to reach the detector that no fluorescence signal was observed. Use of the 682DF22 filter instead allowed us to observe fluorescence. Increasing the emission filter rejection power with a 655 nm long pass filter improved the LOD further; however, we noted that the laser source could still be viewed through the long pass filter alone. By instead using a laser line selection filter ( $634.54 \pm 5$  nm) between the laser and the excitation optics, the best LOD was obtained. This result indicates the background

emission of the laser at wavelengths considerably longer than 635 nm was significant compared to the dye's emission intensity. Mank and Yeung<sup>22</sup> also report it was necessary to use a rejection filter in the excitation path of a 670 nm diode laser. It is worth noting that this filter combination (row three of Table 3-2) provided the greatest value of sensitivity divided by noise of all the filter sets tested. With the exception of the data in Table 3-2, this filter set was used for all subsequent studies.

The data in Table 3-2 shows that use of the 670DRLP02 dichroic mirror, instead of the 645 DRLP02 mirror, resulted in somewhat poorer LOD regardless of the other filter sets selected. Although the 670 mirror rejects more of the reflected 635 nm line than the 645 mirror, the improved transmission of the emitted light is apparently a more important factor, since the emission filters remove the laser line. The last two rows in Table 3-2

Table 3-2. Evaluation of filter sets <sup>(a)</sup> :					
Filter 1	Dichroic mirror	Filter 2	Filter 3	Minimum detected Cy-5 concentration (nM)	LOD <sup>(b)</sup> (nM)
None	645DRLP02	682DF22	None	0.5	0.30 <sup>(c)</sup>
None	645DRLP02	682DF22	655 long pass		0.20
634.54±5 nm	645DRLP02	682DF22	None	0.1	0.15 <sup>(c)</sup>
634.54±5 nm	670DRLP02	682DF22	655 long pass	0.5	0.30
634.54±5 nm	670DRLP02	675DF20	655 long pass		0.25
634.54±5 nm	670DRLP02	670DF40	655 long pass	0.5	0.21
634.54±5 nm	670DRLP02	670DF40	None	0.2	1.5 <sup>(c)</sup>

(a) refer to Figure 2 for location of filters. This study was performed using a 200 µm diameter pinhole, 11.2 mW laser power and a 13 µm deep COPI device.

(b) Limit of detection (LOD) extrapolated from replicate measurements (n=5) at 1 nM Cy-5, except where marked (c).

(c) Extrapolated from plot of five different concentrations ranging from 0.5 to 10 nM.

indicate that the 670DF40 emission filter was far too transmissive, requiring the 655 nm long pass to provide satisfactory performance. While the 670DF40 filter without the long pass filter gave a measurable response at 0.2 nM, the sensitivity divided by the noise was ten times lower than for the best filter combination. This poor sensitivity accounts for the extrapolated LOD being much greater than 0.2 nM.

#### 3-4-2-2-2. Optimization of Excitation Source

The effect of laser power and beam size is also significant, as a balance must be struck between the noise from elastic and inelastic scattering and the emission intensity, which will both increase with increasing power up to some limit <sup>21</sup>. Using an unexpanded laser beam, the optimized filter set and a 200  $\mu\text{m}$  pinhole, the effect of laser power on the signal to noise ratio (S/N) was examined at 10 nM Cy-5. The S/N ratio

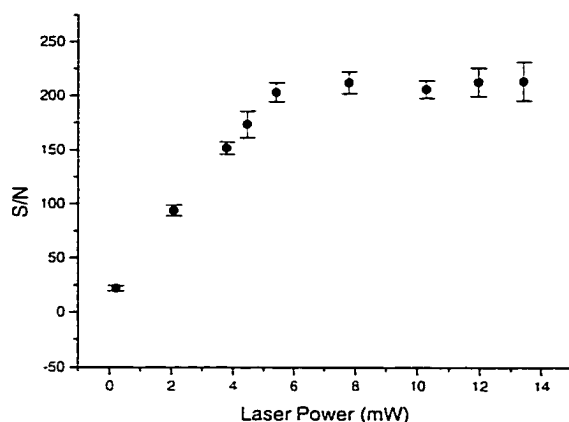


Figure 3-16. The S/N vs. output power of the laser plot

increased linearly up to 6.2 mW of output power, and then remained essentially constant, up to the maximum of 13.0 mW (Figure 3-16). Plots of noise and of signal versus output power also followed the same trend. The results indicate that once the power exceeds a certain level the S/N performance plateaus.

The output of a laser diode is astigmatic, with a different focal distance along the vertical and horizontal axes of the beam. This makes it difficult to focus the laser to a small, intense spot (Figure 3-17). The selected laser included prism-based optics to



collimate the beam, and produce a near-Gaussian beam profile to allow better focusing. For a beam with a TEM 00 Gaussian profile the beam waist,  $w$ , is given by Hecht and Zajac<sup>54</sup>:

$$w = \lambda f / \pi w_0 \quad (3-2)$$

where  $w_0$  is the incident beam radius,  $f$  is the focal length, and  $\lambda$  is wavelength. This equation is valid so long as  $w$  is above the diffraction limit of the lens. For the incident beam diameters used, eq. 3-2 predicts spot sizes smaller than the diffraction limit. The diffraction limited spot diameter,  $d$ , can be determined from<sup>55</sup>:

$$d = 1.22 \lambda / \text{N.A.} = 1.22 \lambda / n \sin \alpha \quad (3-3)$$

where  $n$  is the index in which the lens is immersed,  $\alpha$  is the angular semi-aperture, and

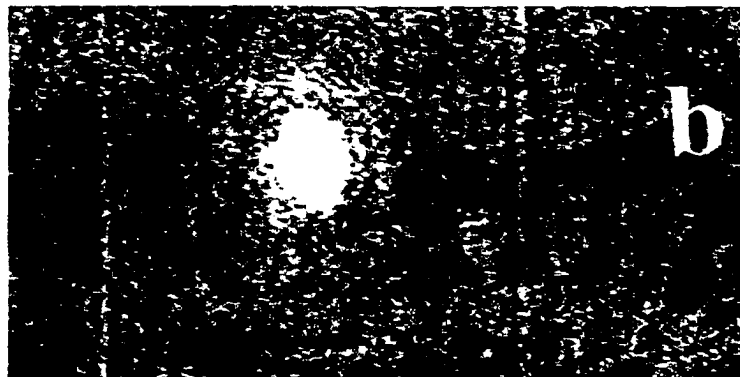
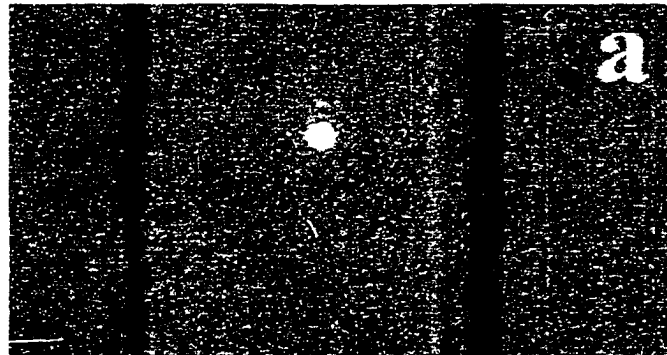


*Figure 3-17. The observed laser spot focused in the channel. a). the laser spot with using the beam expander. The channel width at the top of the trapezoidally shaped channel is 78  $\mu\text{m}$ ; b). the laser spot without using the beam expander. The channel width at the top of the trapezoidally shaped channel is 96  $\mu\text{m}$ .*

N.A. is the numerical aperture. When the beam was expanded to give a collimated source 15 mm in diameter, a 10  $\mu\text{m}$  spot was observed (Figure 3-17, a). The input diameter of the lens was 8.37 mm, so that it was totally filled by the expanded beam. Consequently, we used the stated N.A. of 0.6 to estimate a diffraction limited spot diameter of 1.3  $\mu\text{m}$ . For the unexpanded laser beam, the observed spot size was 18  $\mu\text{m}$  in diameter, while a value of 1.9  $\mu\text{m}$  is calculated from eq. 3-3 using a value of  $\alpha$  of 24.1, estimated from the geometry of the beam diameter and the focal length. The inability to focus to the diffraction limit with and without beam expander must in large part be due to the astigmatic nature of the diode laser source, even with the correction optics. Note that experimentally the expanded beam is much better focused, even though the difference in the calculated diffraction limited spots for the two beams is rather small. Then consider that about 50% of the expanded beam radius is discarded by the lens aperture, so the improved focus probably arises from eliminating non-Gaussian components from the beam profile.

With a laser power of 11.5 mW it was found the laser notch filter reduced the power incident on the dichroic mirror to 6.2 mW. Positioning the beam expander in front of the dichroic mirror further reduced the power incident on it to 3.4 mW. The lens aperture of 8.37 mm resulted in a power reduction to 1.7 mW. This is a greater reduction than the calculated drop to 74% of the incident intensity, as estimated from the irradiance equation for a Gaussian beam<sup>55</sup>. This result is again consistent with a notably non-Gaussian beam profile. A measurement of the power transmitted by the lens indicated it reduces the transmitted intensity to 38.5%. Considering these incident powers and the observed spot sizes, the power density at the focal plane should be about 1100  $\text{W}/\text{cm}^2$  for the unexpanded beam, and 830  $\text{W}/\text{cm}^2$  for the expanded beam.

The depth of field, corresponding to a 5% expansion of the beam beyond the minimum beam waist, can be estimated from eq. 3-4<sup>55</sup> :

$$\Delta z = \pm 0.32 \pi w_0^2 / \lambda \quad (3-4)$$

where  $w_0$  is the focused spot radius, and  $\Delta z$  is the vertical translation. From the observed 18  $\mu\text{m}$  spot diameter (Figure 3-17, b) we estimate a value of  $\pm 130 \mu\text{m}$  for the unexpanded beam. The depth of field estimated for the 10  $\mu\text{m}$  spot (Figure 3-17, a) created by the expanded beam is  $\pm 40 \mu\text{m}$ . Both spots are thus in focus over a much greater distance than the channel depth, so that scattering of the focused laser beam from the glass and the glass/solution interface will occur. Nevertheless, the expanded beam should produce less scatter, because it is focused over a much shorter distance. This was observed experimentally, as the beam expander reduced the noise from  $\pm 9.7$  to  $\pm 4.0$  mV when used with a 13  $\mu\text{m}$  deep COPI device and a 200  $\mu\text{m}$  pinhole.

#### 3-4-2-2-3. Confocal Sectioning Power

The optical sectioning strength of a confocal microscope describes the manner in which fluorescence intensity changes with the axial distance between the objective lens and the object. Wilson<sup>56-57</sup> defined the sectioning power as the full width at half maximum (FWHM) of intensity versus the axial displacement from the focal plane. This section evaluates the sectioning power in 13 and 20  $\mu\text{m}$  deep channels, filled with a continuous flow of 10 nM Cy-5. Background signal was measured with buffer moving in

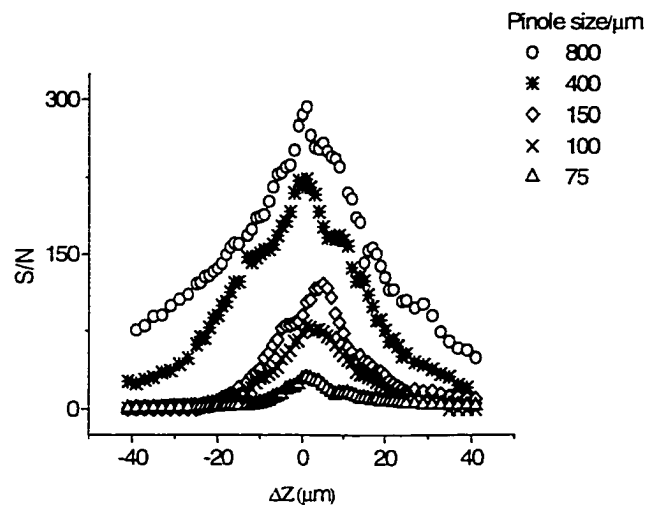


Figure 3-18. Signal-to-noise ratio versus vertical displacement of chip ( $\Delta z$ ) for various pinhole diameters using a 13  $\mu\text{m}$  deep channel. A 10 nM Cy-5 standard solution was continuously flushed through the separation channel of a Pyrex COPI device by vacuum. Confocal microscope was employed as a detector. Beam expander was not used in this study.

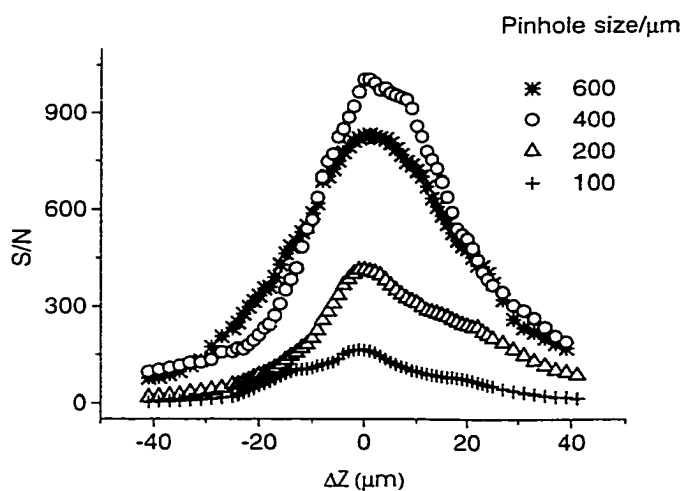


Figure 3-19. Signal-to-noise ratio versus vertical displacement of chip ( $\Delta z$ ) for various pinhole diameters using a 20  $\mu\text{m}$  deep channel. A 10 nM Cy-5 standard solution was continuously flushed through the separation channel of a Pyrex COPI device by vacuum. Confocal microscope was employed as a detector. Beam expander was used in this study.

the flow channel at the same velocity. Figure 3-18 shows a plot of S/N versus axial displacement for a 13  $\mu\text{m}$  deep, Pyrex, COPI device, using an unexpanded beam and several pinhole sizes. Significant distortion from a Gaussian profile is observed, which makes the FWHM values larger than those predicted by a linear extrapolation of Wilson's model<sup>25, 56-57</sup> to the pinhole sizes we used. Figure 3-19 shows the results for a 20  $\mu\text{m}$  deep, Pyrex, COPI device with which the beam expander was also used. The calculated and experimental results for both studies are presented in Table 3-3. The estimated theoretical sectioning power must be convoluted with a slit function model of the channel depth. The result is that the observed sectioning power should be equal to the calculated value when it is larger than the channel depth, and equal to the channel depth when the

Table 3-3. Observed and estimated confocal sectioning power.

Pinhole diam. ( $\mu\text{m}$ )	Calculated sectioning power <sup>(a)</sup> FWHM ( $\mu\text{m}$ )	Observed sectioning power <sup>(b)</sup> FWHM ( $\mu\text{m}$ )	
		13 $\mu\text{m}$ deep	20 $\mu\text{m}$ deep
75	6.5	15.3	
100	8.2	18.4	31.6
150	11.7	19.5	
200	15.1		32.6
400	28.7	34.2	33.5
600	42.4		40.5
800	56.0	36.6	

(a) Estimated by linear extrapolation of Wilson's<sup>56-57</sup> calculations. The value does not include the affect of the slit function introduced by the channel depth (see text).

(b) Determined from Figures 3-18 and 3-19.

calculated value is smaller. Although the agreement with theory is only moderate, the sectioning power afforded by the pinholes does lead to observation of a smaller detection zone than the estimated depth of field of the focused laser spot.

Figure 3-20 shows the trends of S/N versus pinhole size measured by a continuous-flow experiment. The continuous increase in S/N with increasing pinhole size observed for the 13  $\mu\text{m}$  deep channels is not consistent with true confocal performance, while the 20  $\mu\text{m}$  device showed a clear optimum pinhole size of 400  $\mu\text{m}$ . This value is in agreement with our previous study using a 488 nm Ar ion laser, and fluorescein in 30  $\mu\text{m}$  deep channels<sup>25</sup>. The results can be explained by considering the excitation volume created by the laser beam and the probe volume observed by the confocal microscope. The beam waist can be treated as a constant across the channel depth, so that the excitation volume is a cylinder given by the beam waist. The probe volume can also be treated as a cylinder with a height given by the observed sectioning power or channel

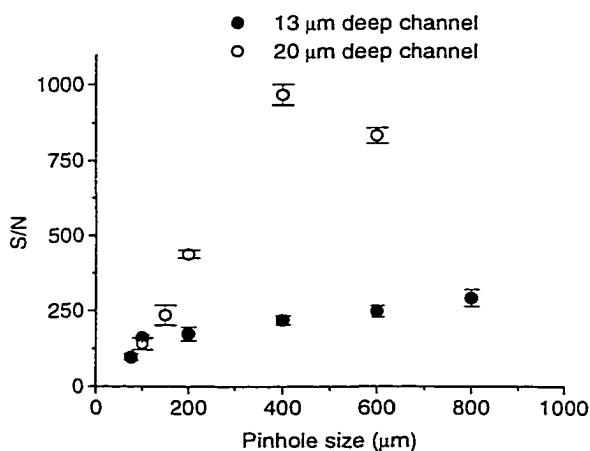
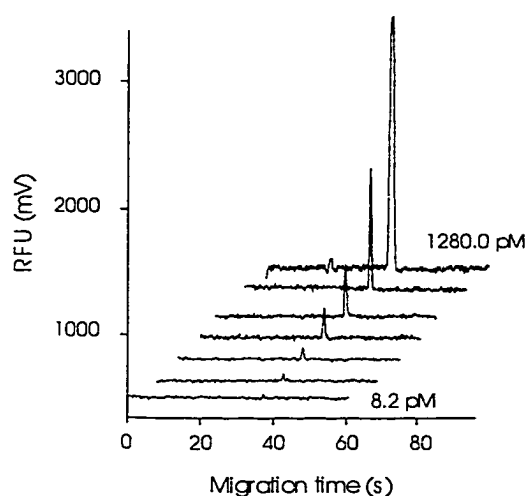


Figure 3-20. Signal-to-noise ratio versus pinhole size for 13  $\mu\text{m}$  and 20  $\mu\text{m}$  deep channels in Pyrex COPI devices. A 10 nM Cy-5 standard solution was continuously flushed through the separation channel by vacuum. Confocal microscope was employed as a detector.

depth, and a diameter given by the pinhole size divided by the magnification (40x). For the unexpanded beam, the 800  $\mu\text{m}$  pinhole gives a probe diameter which most closely matches the excitation volume, optimizing the collection of all intensity generated by the laser. For the expanded beam, the 400  $\mu\text{m}$  pinhole should best match the estimated probe volume of 1.6 pL to the 10  $\mu\text{m}$  diameter excitation volume of 1.6 pL. Since none of the pinholes gave sufficient sectioning power to eliminate scatter from the glass walls, the best match of probe diameter and beam diameter would give the best results, consistent with observations.

#### 3-4-2-2-4. Limit of Detection with Optimized Parameters



*Figure 3-21. Electropherograms of various concentrations of Cy-5 standard solutions in a 20  $\mu\text{m}$  deep, DARPA-NCI device. Injection time: 10 s at -2 kV injection voltage. Separation voltage was -4 kV. Injector-detector distance was 58 mm, PMT voltage: 900 V. Confocal microscope was employed as a detector. See Figure 3-23 for identification of each concentration.*

Once an optimal set of detection parameters was determined, the best detection limits were evaluated for an injected and separated sample plug. Figure 3-21 shows a series of injected sample plugs for a 20  $\mu\text{m}$  deep DARPA-NCI device. A similar data set was obtained with a 13  $\mu\text{m}$  deep DARPA-NCI device. The studies were performed with an expanded beam at 11.2 mW output power, using the optimized filter set and a 400  $\mu\text{m}$  pinhole. For the 13  $\mu\text{m}$  deep device,

the detection limit extrapolated from concentrations above 32.8 pM to a S/N of 3, was 20 pM. A calibration curve (Figure 3-22) forced through the origin gave a slope of  $0.159 \pm 0.013$  and an  $R^2 = 0.9994$  ( $n=18$ ). The lowest concentration we were actually able to determine was 32.8 pM. For a 20  $\mu\text{m}$  deep device the extrapolated LOD was 9 pM, and the lowest concentration we were able to determine was 8.2 pM. A calibration curve (Figure 3-23) forced through the origin gave a slope of  $0.335 \pm 0.012$ , with  $R^2=0.9986$  ( $n=21$ ). This concentration detection limit is somewhat better than the previous best results of 50-100 pM obtained with a red diode laser reported for Cy-5 in a conventional fused silica capillary<sup>21-23</sup>. The confocal, epiluminescent design gave much better performance than the conventional two lens optical detection system, which gives a 110 pM detection limit using a 13  $\mu\text{m}$  deep chip. However, in that study not all of the parameters, such as filter set or the focusing of the laser, had been optimized. The confocal, epiluminescent design is also better than the present commercial 635 nm LIF system on the Beckman instrument, which, in our hands, gives a 100 pM detection limit with a 50  $\mu\text{m}$  diameter capillary and a 3-5 mm long sample plug by using 635 nm notch filter and two 675DF20 emission filters.

About 42,000 theoretical plates were achieved with these devices. For an injector to detector length of 5.8 cm, this plate number corresponds to a peak variance ( $\sigma^2$ ) of  $8.0 \times 10^{-4} \text{ cm}^2$ . If we assign all dispersion to a combination of diffusion and the sample plug length, we can obtain an upper limit of the plug length using eq. 3-5<sup>3</sup>:

$$l^2/12 = \sigma^2 - 2 D t \quad (3-5)$$

where  $l$  is the estimated injected length,  $D$  is the diffusion coefficient (approximated as the value for fluorescein of  $3.3 \times 10^{-6} \text{ cm}^2/\text{s}$ )<sup>3-4</sup>, and  $t$  is the migration time. Equation 3-5



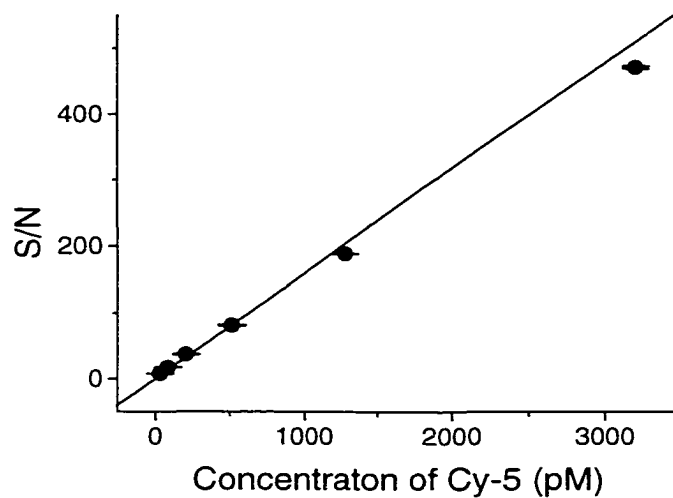


*Figure 3-22. Calibration Curve of Cy5 using 10  $\mu\text{m}$  deep channel. Confocal microscope was employed as a detector.*

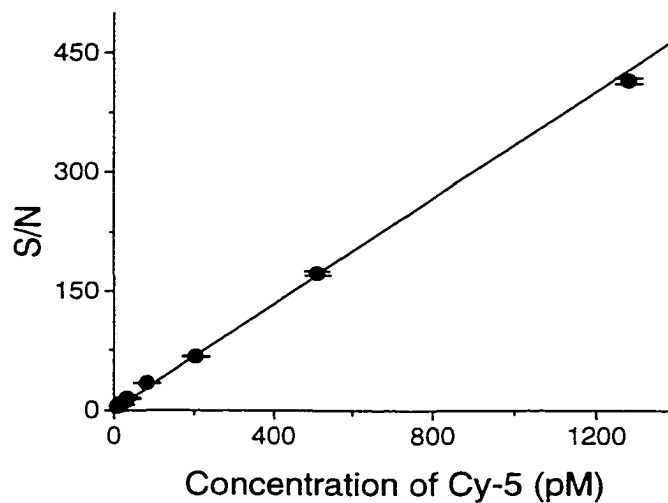


*Figure 3-23. Calibration curve of Cy5 using 20  $\mu\text{m}$  channel depth. Confocal microscope was employed as a detector. Data is from Figure 3-21.*

provides an estimate of 834  $\mu\text{m}$  for the injected plug, suggesting some leakage at the injector. At the extrapolated LOD, the amount of sample volume estimated from this length corresponds to 5900 molecules for the 13  $\mu\text{m}$  deep device and 4560 molecules for the 20  $\mu\text{m}$  deep device. The number of molecules that entered the detection zone was 1300 and 900, for the 13 and the 20  $\mu\text{m}$  deep devices, respectively, given that the probing efficiencies were 22 and 20% for the 13 and 20  $\mu\text{m}$  deep devices, respectively. This mass detection limit is much better than that we achieved with the commercial 635 nm LIF system. It is comparable to the best results reported in CE, which are  $\sim 300$  molecules when using a red diode laser<sup>22</sup>. Importantly, the 900 molecule LOD corresponds to 9 pM in dye concentration, whereas in ref. 22 the 300 molecule LOD corresponded to 50 pM.

### *3-4-3. Conclusion*

Solid state diode lasers provide a convenient, compact and rugged source for instruments that are to be used in the field. This study illustrates that the 635 nm laser is compatible with detection of immunological reaction products on a planar microfluidic device. Optimization of the optics for detection with this laser allows the determination of a few thousand Cy-5 molecules per sample plug in a electrophoretic separation, with a concentration detection limit of approximately 9 pM in a 20  $\mu\text{m}$  deep channel.

The observed concentration LOD is about a factor of 10 poorer than we reported for fluorescein in a 30  $\mu\text{m}$  deep device<sup>25</sup>. A further improvement might be observed if we used 30  $\mu\text{m}$  deep channels with the diode laser, since the sectioning power of a 400  $\mu\text{m}$  pinhole is high enough to eliminate scattering from the walls of a 30  $\mu\text{m}$  deep device. The sectioning power study shows that the correction optics supplied with this laser do not generate a truly Gaussian beam, which limits the ability to focus a tight, high intensity

spot. The background output of the laser required a notch transmittance filter be used, as is often done with gas lasers. It is possible another manufacturer's laser could produce better results in terms of increased focus or lower background emissions. Consequently, detection limits on a chip of  $10^{-12}$  M or less, as obtained with the 488 nm laser/fluorescein system, may yet be achievable with Cy-5 and a diode laser.

**References:**

1. A. Manz, D. J. Harrison, E. M. J. Verpoorte, J. C. Fettinger, A. Paulus, H. Lüdi, H. M. Widmer, *J. Chromatogr.* **1992**, *593*, 253-258.
2. D. J. Harrison, K. Fluri, K. Seiler, Z. Fan, C. S. Effenhauser, A. Manz, *Science* **1993**, *261*, 895-897.
3. K. Seiler, D. J. Harrison, A. Manz, *Anal. Chem.* **1993**, *65*, 1481-1488.
4. Z. H. Fan, D. J. Harrison, *Anal. Chem.* **1994**, *66*, 177-184.
5. S. C. Jacobson, R. Hergenröder, L. B. Koutney, R. J. Warmack, J. M. Ramsey, *Anal. Chem.* **1994**, *66*, 1107-1113.
6. C. L. Colyer, T. Tang, N. Chiem, D. J. Harrison, *Electrophoresis* **1997**, *18*, 1733-1741.
7. C. S. Effenhauser, G. J. M. Bruin, A. Paulus, *Electrophoresis* **1997**, *18*, 2203-2213.
8. A. G. Hadd, D. E. Raymond, J. W. Halliwell, S. Jacobson, J.M. Ramsey, *Anal. Chem.* **1997**, *69*, 3407.
9. N. H. Chiem, D. J. Harrison, *Clin. Chem.* **1998**, *44*, 591-598.
10. N. H. Chiem, D. J. Harrison, *Electrophoresis* **1998**, *19*, 3040-3044.
11. W. E. Lee, A. B. Jemere, S. Attiya, N. H. Chiem, M. Paulson, J. Ahrend, G. Burcheff, D. E. Bader, Y. B. Ning, D. J. Harrison, *J. Cap. Elec. And Microchip Tech* **1999**, *6*, 51-59.
12. T. Imasaka, *Fresenius Journal of Anal. Chem.* **1996**, *355*, 216-221.
13. L. C. Shriver-Lake, K.A. Breslin, P. T. Charles, D.W. Conrad, J. P. Golden, F. S. Ligler, *Anal. Chem.* **1995**, *67*, 2431-2435.
14. U. Narang, P. R. Gauger, F. S. Ligler, *Anal. Chem.* **1997**, *69*, 2779-2785.
15. T. McDonnell, J. Pawliszyn, *Anal. Chem.* **1991**, *63*, 1884-1889.
16. T. Imasaka, K. Nishitani, N. Ishibashi, *Analyst* **1991**, *116*, 1407-1409.
17. J. Wu, P. Frank, J. Pawliszyn, *App. Spec.* **1992**, *46*, 1837-1840.
18. T. Higashijima, T. Fuchigami, T. Imasaka, N. Ishibashi, *Anal. Chem.* **1992**, *64*, 711-714.
19. M. Jansson, J. Roeraade, *Anal. Chem.* **1993**, *65*, 2766-2769.

20. B. Krattiger, G. J. M. Bruin, A. E. Bruno, *Anal. Chem.* **1994**, *66*, 1-8.
21. F. T. A. Chen, A. Tusak, J. S. Pentoney, K. Konrad, C. Lew, E. Koh, J. Sternberg, *J. Chromatogr. A* **1993**, *652*, 355-360.
22. A. J. G. Mank, E. S. Yeung, *J. Chromatogr. A* **1995**, *708*, 309-321.
23. F. T. A. Chen, *Anal. Biochem.* **1995**, *225*, 341-345.
24. J. H. Flanagan, B. L. Legendre, R. P. Hammer, S. A. Soper, *Anal. Chem.* **1995**, *67*, 341-347.
25. G. Ocvirk, T. Tang, D. J. Harrison, *Analyst* **1998**, *123*, 1429-1434.
26. P. Vasil'ev, *Ultrafast Diode Lasers, Fundamentals and Applications*, Artech House. Boston, MA, **1995**.
27. K. Petermann, *Laser Diode Modulation and Noise*, Kluwer Academic Publishers, Dordrecht, The Netherlands, **1988**.
28. H. Nelson, H. Kressel, *Appl. Phys. Letters* **1969**, *15*, 7-9.
29. H. Kressel, H. F. Lockwood, H. Nelson, *Journal of Quantum Electronics* **1970**, *6*, 278-284.
30. J. J. Coleman, N. J. Holonyak, M. J. Ludowise, P. D. Wright, R. Chin, W. O. Groves. D. L. Keune, *Appl. Phys. Letters* **1976**, *29*, 167-169.
31. A. Usui, T. Matsumoto, M. Inai, I. Mito, K. Kobayashi, H. Watanabe, *Jpn. J. Appl. Phys* **1985**, *24*, 163.
32. A. Usui, T. Matsumoto, M. Inai, I. Mito, K. Kobayashi, H. Watanabe, *Electron. Lett.* **1985**, *21*, 54.
33. M. Ikoda, Y. Mori, H. Sato, K. Kaneko, N. Watanabe, *Appl. Phys. Letters* **1985**, *47*, 1027-1028.
34. K. Kobayashi, S. Kawata, A. Gomyo, I. Hino, T. Suzuki, *Electronics Letters* **1985**, *21*, 931-932.
35. G. P. Agrawal, N. K. Dutta, *Semiconductor Lasers*, second ed., Van Nostrand Reinhold, New York, **1993**.
36. S. M. Sze, *Physics of Semiconductor Devices*, Second Ed. New York: John Wiley & Sons, **1981**.
37. <http://www.powertechnology.com/TECHLIB/BEAMCHAR/BEAMCHAR.HTM>, Tech. Library, Power Technologies, AR, USA.

38. C. C. Cain, R. B. Wilson, R. F. Murphy, *J. Biol. Chem.* **1991**, *266*, 11746-11752.
39. F. A. Chen, R. A. Evangelista, *Clinical Chemistry* **1994**, *40*, 1819-1822.
40. R. A. Evangelista, J. M. Michael, F-T. A. Chen, *American Clinical Laboratories* **1995**, 27-28.
41. M. Z. Hossain, L. A. Ernst, J. I. Nagy, *Neuroscience Letters* **1995**, *194*, 71-74.
42. P. M. Landsdorp, W. J. Dragowska, *Exp. Medicine* **1992**, *175*, 1501-1509.
43. C. N. Levelt, K. Eichmann, *Cytometry* **1994**, *15*, 84-86.
44. R. Oberfelder, W. Russ, *Annals of the New York Academy of Science* **1993**, 444-446.
45. D. M. Sipe, A. Jesurum, R. F. Murphy, *J. Biol. Chem* **1991**, *266*, 3469-3474.
46. C. C. Stewart, S. J. Stewart, *Annals of the New York Academy of Sciences* **1993**, 94-112,
47. R. Y. Tsien, A. S. Waggoner, Chapter 16: Fluorophores for Confocal Microscopy: Photophysics and Photochemistry, *Handbook of Biological Confocal Microscopy*, Plenum Publishing Corporation, edited by James B. Pauley, **1990**.
48. A. S. Waggoner, L. A. Ernst, *Fluorescent Reagents for Flow Cytometry*, Part 1: Principles of Clinical Flow Cytometry, 111-116.
49. N. H. Chiem, D. J. Harrison, *Anal. Chem.* **1997**, *69*, 373-378.
50. S. Attiya, Ph.D. Dissertation, University of Alberta, **2000**.
51. P. D. Grossman, J. C. Colburn, H. H. Laurer, R. G. Neilsen, R. M. Riggin, G. S. Sittampalam, E. C. Rickard, *Anal. Chem.* **1989**, *61*, 1186-1194.
52. Y. H. Chu, W. J. Lees, A. Stassinopoulos, C. Walsh, *Biochem.* **1994**, *33*, 10616-10621.
53. L. Tao, R. T. Kennedy, *Anal. Chem.* **1996**, *69*, 3899-3906.
54. D. Schmalzing, W. Nashabeh, *Electrophoresis* **1997**, *18*, 2184-2193.
55. E. Hecht, A. Zajac, *Optics*, Addison-Wesley Pub. Co., Reading, Mass. **1974**.
56. T.J. Wilson, *J. Microscopy* **1989**, *154*, 143-156.
57. T. Wilson, In: J. B. Pawley, (Ed.), *Handbook of biological confocal microscopy*, Plenum Press, New York, **1990**, 113-126.
58. G. Jiang, S. Attiya, G. Ocvirk, W. E. Lee, D. J. Harrison, *Biosensors & Bioelectronics* **2000**, *14*, 861-869.

## **Chapter 4. Summary and Future Outlook**

In Chapter 2, the first two steps in cDNA library construction, mRNA isolation and cDNA synthesis, were integrated on a microfluidic device using magnetic bead based technology. The quality of mRNA isolated on chip was evaluated, and was determined to be suitable for cDNA library construction. The device is sufficiently robust to be used with realistic mRNA samples. A capture efficiency of about 26% mRNA was obtained using the magnetic bead bed compared with off chip mRNA isolation. This is likely caused by the inefficient mixing of mRNA with the oligodT beads resulting from the loose magnetic bead bed structure which causes of channeling in the bed. Some modifications are needed to improve the capture efficiency. A rotating motor could be built on the magnets and employed to stir the bed to enhance the mixing. This problem could also be solved by using a better microfluidics design for the chip. A dam built in the channel might be suitable for this purpose. The beads could be blocked by the dam to form a more compact bed structure (Figure 4-1). Another design might improve the mixing, too. A channel-array could be fabricated inside the reaction chamber in the channel, such as shown in Figure 4-2. When the beads and solution are introduced into the reaction chamber, the main flow will be split into several flows, causing better mixing. In addition, the bead bed in a narrow channel might reduce the channeling, making a better quality magnetically trapped bead bed.

The heating system used in first strand cDNA synthesis needs to be improved because the heat was not confined to one location. In the second strand cDNA synthesis, three temperatures would be required. For example, the polyT primer would be



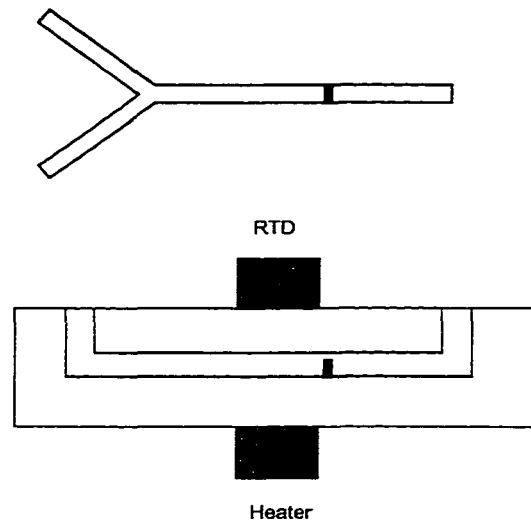


Figure 4-1. The schematic layout for the device. A dam is fabricated inside the channel. The gap over the top of the dam is  $2\ \mu\text{m}$ , which should be less than the diameter of the bead.

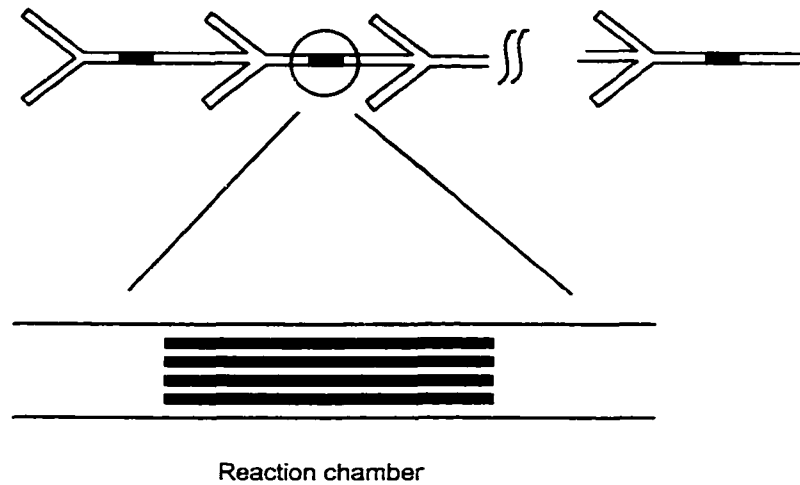


Figure 4-2. The schematic layout for integrating cDNA library construction on a microfluidic device.

extended at 30 °C first, then the annealing of the primer to the first strand cDNA template would take place at 60 °C followed by extension of second strand of cDNA at 72 °C. The isolation of the heated area from the rest of the chip with a water-cooling system around the heater would improve the ability to quickly adjust temperature. Such a heating element added to the cDNA synthesis device might be beneficial for the temperature control required in second strand cDNA synthesis.

There are several steps involved in cDNA library construction: mRNA isolation from TRNA, first strand synthesis of cDNA, second strand synthesis of cDNA, molecular cloning of the second strand of cDNA and screening cDNA library. Figure 4-3 illustrates the protocol for cDNA library construction from small amounts of mRNA<sup>2-3</sup>. A PCR amplification of second strand of cDNA will be necessary with microfluidic devices since the input of TRNA is small.

After the integration of the first two steps involved in cDNA library construction, the second strand of cDNA will need to be synthesized on the chip device. The temperature in the reaction chamber will be heated up to 65 °C for 5 min to inactivate the reverse transcriptase, which was used in the first strand cDNA synthesis. Then T4 polymerase will be added into the reaction chamber to destroy any single strand poly T present either on the surface of the Dynal beads or in the reaction mixture used for first stand cDNA synthesis. The reaction chamber will be incubated at 16 °C for 1 hour, then heated to 74 °C for 5 min. After the washing step, RNase H will be introduced into the reaction chamber to destroy the mRNA. The reaction chamber will be incubated at 37 °C for 1 hour, then washed with EDTA solution and heated up to 75 °C for 5 min. Then terminal tranferase and dATP will be added into the chamber to synthesize an A tail to the first

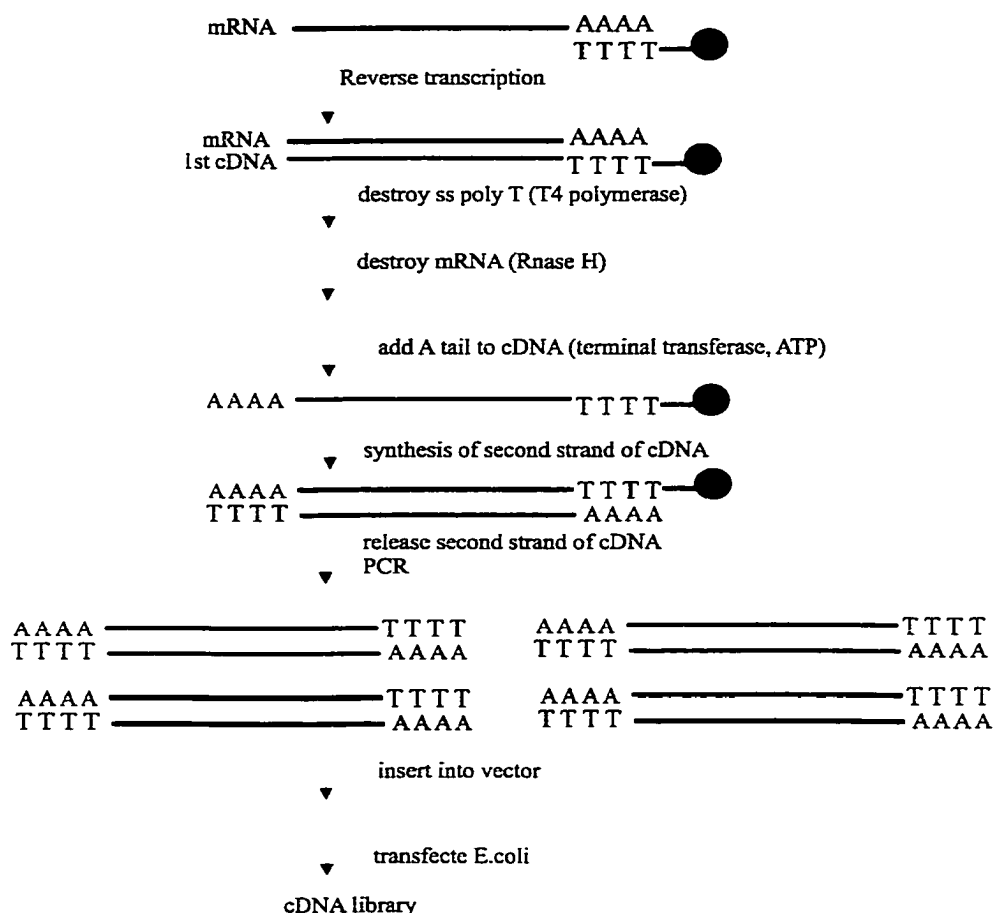


Figure 4-3. Schematic illustration for construction of cDNA library

strand of cDNA. Only one primer is required for synthesis of a second strand of cDNA, which will be carried out using T<sub>15</sub> as a primer, which will be bound on the synthetic A tail of first strand of cDNA. The reaction mixture contains DNA polymerase, dNTP's, Mg<sup>2+</sup> and the buffers. The temperature in the reaction chamber will be held at 30 °C for 15 min for extension of the T<sub>15</sub> primer. Then the temperature will be held at 60 °C for 15 min for the annealing of the primer to the template cDNA, and 72 °C for 15 min for the extension of the second strand of cDNA. After second strand cDNA synthesis, the second strand of cDNA will be released by raising the temperature in the reaction chamber to 94

°C. PCR amplification will then be carried out to amplify all of the second strands of cDNA. The PCR amplification of the cDNA products will be separated from the free primers using an HPLC column, then ligated with vector. Then *E. Coli* cells will be transfected with the vectors.

The synthesis of second strand of cDNA could be done on the same microfluidic device as illustrated in Figure 4-2. During the synthesis of second strand of cDNA, numerous washing steps will be involved. A device layout is illustrated in Figure 4-2 showing the sequential mixing, washing and reaction stages within a single device. After one stage of the washing during second strand cDNA synthesis, the beads will be released from the first reaction chamber by removing the magnets and captured in the second reaction chamber with magnets. Then the next stage will be carried out in the second reaction chamber. The advantage of reconstructing a new bed is improved reagent mixing. However, this device needs to interface to a PCR reaction device down stream after the second strand synthesis of cDNA. There are numerous research groups that have demonstrated PCR on microfluidic devices<sup>4-7</sup>. It is feasible to integrate the cDNA synthesis device with such a PCR reaction device. For example, the cDNA device could interface nicely to the continuous flow PCR design of Manz and coworkers<sup>5</sup>.

The purification of the cDNA PCR product will require something like a microfabricated liquid chromatography (LC)<sup>8</sup>. Then, after some modification of the cDNA PCR product, it is ligated to a vector, which could be done using the same device layout as first strand cDNA synthesis device. Then the *E. Coli* cell will be transfected by the vector. This process was recently demonstrated on a microfluidic device by Harrison's group<sup>9</sup>. As a result, we can see that all the required components are either

possible or available. Thus, it should eventually be possible to integrate all of the steps involved in cDNA library construction onto one microfluidic device.

In Chapter 3, a confocal microscope was employed as a detector, which gave high sensitivity LIF detection of Cy-5 on microfluidic devices using a diode laser. The concentration limit of detection (LOD) was 5 times better than achieved by other groups using capillary electrophoresis<sup>10-12</sup>. However, there is still room for optimization. A further improvement might be observed if we were to use 30  $\mu\text{m}$  deep channels, since the sectioning power of a 400  $\mu\text{m}$  pinhole is high enough to eliminate scattering from the walls of a 30  $\mu\text{m}$  deep device. Also, the fluorescence signal might be enhanced by increasing the number of fluorescence molecules using a deeper channel, in which the probe volume will be increased. A more focused spot and higher fluorescence signal collection efficiency will be obtained by using a high N.A. number of microscope objective. As a result, the fluorescence signal will be increased and the background scattering might be reduced. The use of a smaller pinhole will increase the sectioning power of the confocal microscope. The scattering light from the walls of the channel might be reduced in this case. Therefore, S/N is improved. The sectioning power study shows that the correction optics supplied with this laser do not generate a truly Gaussian beam, which limits the ability to focus a tight, high intensity spot. The background output of the laser required a notch transmittance filter be used, as is often done with gas lasers. It is possible that another manufacturer's laser could produce better results in terms of increased focus or lower background emissions.

**References:**

1. Y. Badal, *Ph.D dissertation* **2001**, Department of Chemistry, University of Alberta.
2. K. N. Lambert and V. M. Williamson, *Nucleic Acids Res.* **1993**, *21(3)*, 775-776.
3. I. Raineri, C. Moroni and H. P. Senn, *Nucleic Acids Res.* **1991**, *19(14)*, 4010.
4. M. U. Kopp, M. B. Luechinger, A. Manz, in: D. J. Harrison, A. Van den Berg (Editors), *Micro Total Analysis Systems '98*, **1998**, Kluwer, Dordrecht, , p. 271
5. M. U. Kopp, A. J. deMello, A. Manz, *Science* **1998**, *280*, 1046.
6. A. T. Woolley, D. Hadley, P. Landre, A. J. deMello, R. A. Mathies, M. A. Northrup. *Anal. Chem.* **1996**, *68*, 4081.
7. L. C. Waters, S. C. Jacobson, N. Kroutchinina, J. Khandurina, R. S. Foote, J. M. Ramsey, *Anal. Chem.* **1998**, *70*, 158.
8. G. Ocvirk, E. Verpoorte, A. Manz, M. Grasserbauer, H. M. Widmer, *Anal. Methods Instrum.* **1995**, *2*, 74.
9. S. Attiya, E. Majid, D. J. Harrison, *Proceedings of HPCE 2001*, pp.263, Boston, Jan.13-19, 2001.
10. F. T. A. Chen, A. Tusak, J. S. Pentoney, K. Konrad, C. Lew, E. Koh, J. Sternberg, *J. Chromatogr. A* **1993**, *652*, 355-360.
11. A. J. G. Mank, E. S. Yeung, *J. Chromatogr. A* **1995**, *708*, 309-321.
12. F. T. A. Chen, *Anal. Biochem.* **1995**, *225*, 341-345.

## Appendix I

*Drosophila* (bicoid) mRNA (major 2.6 kb transcript):

1 atgcgaagca gtggatcgca aaaacgcaaa atgtgggcga aataagttcg cgagcgtctc  
 61 gaaagtaacc ggtfactgaa aatacaagaa agttccaca ctctttgcc attttccgc  
 121 gcggcgcttg gaaattcgta aagataacgc ggcggagtgt ttggggaaaa tggcgcaacc  
 181 gccgccagat caaaactttt accatcatcc gctgccccac acgcacacac atccgcaccc  
 241 gcactcccat ccgcatccgc actcgcaccc gcacccacat caccaacatc cgcagcttca  
 301 gttgccgcca caattccgaa atcccctcga tttgctttc gatgagcga cgggagcga  
 361 aaactacaac tacatacgtc cgtatctgcc caaccagatg cccaagccag aggagctgcc  
 421 cgactctctg gtgatgcggc gaccacgtcg caccgcacc acttttacca gctctcaat  
 481 agcagagctg gagcagcact ttctgcaggg acgatacctc acagcccccc gacttgcgga  
 541 tctgtcagcg aaactagccc tgggcacagc ccaggtgaag atatggttta agaaccgtcg  
 601 gcgtcgtcac aagatccaat cggatcagca caaggaccag tcttacgagg ggatgcctct  
 661 ctgcccggt atgaaacaga gcgatggcga tccccccagc ttgcagactc ttagcttggg  
 721 tggaggagcc acgccaacg cttgactcc gtcaccacg ccctcaacgc cactgcaca  
 781 catgacggag cactacagcg agtcattcaa cgcctactac aactacaatg gaggccacaa  
 841 tcacgccag gccaatcgt\c acatgcacat gcagtatcct t\ccggagggg gggcaggacc  
           primer 1       g tgtacgtgta cgtcatagga a  
 901 tgggtcgacc aatgtcaatg gcggccagtt cttccagcag cagcaggtcc ataatcacca  
 961 gcagcaactg caccaccagg gcaaccacgt gccgcaccag atgcagcagc agcaacagca  
 1021 ggctcagcag cagcaatacc atcacttga ctccagcaa aagcaagcca gcgcctgtcg  
 1081 cgtcctggtc aaggacgaac cggaggccga ctacaacttc aacagctcgt actacatgag  
 1141 atcgggaatg tctggcgcca ctgcatcggc atccgctgtg gcccaggcg ctgcctcgcc

1201 gggctccgag gtctacgagc cattaacacc caagaatgac gaaagtccga gtctgtgtgg  
1261 catcggcatc ggcggacctt gcgccatcgc cggtggcgag acggaggcgg ccgacgacat  
1321 ggacgacgga acgagcaaga agacgacgct acagatcttg gagccttga agggctctgga  
1381 caagagctgc gacgatggca gtagcgacga catgagcacc ggaataagag ccttagcagg  
1441 aaccggaat cgtggagcgg catttgccaa attggcaag ccttcgcccc cacaaggccc  
1501 tcagccgcc ctcgggatgg ggggcgtggc catgggc\gaa tcgaaccaat atcaatgca\c  
                  primer 2  ctt agcttggtta tagttacgt  
  
1561 gatggatacg ataatgcaag cgtataatcc ccatcggaac gccgcgggca actcgcagtt  
1621 tgcctactgc ttcaattagc ctggacgaga ggcgtgttag agagtttcat tagctttagg  
1681 ttaaccactg ttgttctga ttgtacaaat accaagtgat ttagatatac tacgcgtaga  
1741 aagttaggtc tagtcctaag atccgtgtaa atggttccca gggaagtttt atgtactagc  
1801 ctagtcagca ggccgcacgg attccagtgc atatcttagt gatactccag ttaactctat  
1861 actttccctg caatacgtca ttgccttag atgtatctgg gtggctgctc cactaaagcc  
1921 cggaatatg caaccagtta catttgaggc catttgggct taagcgtatt ccatgaaaag  
1981 ttatcgtccc acatttcgga aattatattc cgagccagca agaaaatctt ctctgttaca  
2041 atttgacata gctaaaaact gtactaatca aatgaaaaa tgtttctctt gggcgtaatc  
2101 tcatacaatg attacctta aagatcgaac atttaaacia taatatttga tatgatattt  
2161 tcaattteta tgctatgcca aagtgtctga cataatcaa catttgcgca ttcttgacc  
2221 aagaatagtc agcaaattgt atttcaatc aatgcagacc atttgttca gattctgaga  
2281 tttttgctg ccaaacggaa taactatcat agctcacatt ctattacat cactaagaag  
2341 agcattgcaa tctgttaggc ctcaagtta atttaaaat gctgcacctt tgatgttgc  
2401 tctttaagct ttgtattttt aattacgaaa atatataaga actactctac tcgggt



*Drosophila melanogaster* bicoid gene bcd (5130 bp)

1 gtcgactgga gtgtctgtga attgactttt gttgccagtt ggcagcggca gaagcagcaa  
 61 agcccgcca acagcaaca gctcctgcca gatcccaaaa gcaaacacga caattattg  
 121 gcaaatgtca ttaaaaaata ttcacttaa ggccttgcca cacttgctta aaggtaact  
 181 ggctcgttg gtgtgttta aatgttaaa gcttgggcca atgcactgag caacttaatg  
 241 cttgtagata ttacacaat attctcaac gctaaacata tcgaatttc caaatatgga  
 301 gcctgaaaat aataattgcc aatcctagct taaaatcaga aatgagtaga acaacttaa  
 361 aaaattaaca aaagaatcga acgctacagc taattaactc gacaactggt tacctttat  
 421 tcttctaata cattttataa tgcactgct aacaggtaca gatagcaagc actatatgct  
 481 gtcttaaaa acgattatat gatatttct ttcgtacgta gccgttgag atcatttga  
 541 aaaacaaact cgatctccac catccttatt ctttgccta agtccttata tatctcga  
 601 tactaagatt gaataatga gttattaata gcggaagtat gtaacagaat aactacaaa  
 661 gtgcacattt tgtcaattc aggctggact ggactggagc atattaatat tataatatta  
 721 acaaaaattc aaattaaaca ttcgacactt gtctaattga ttcctaaatt tggggtgct  
 781 gtttgttaat taaatgttaa tattatgaag ttccaacag agcaaagagt ttaagttta  
 841 ttggttctac ttattgtta caatattca gctttttta ttattattct caaatgcaa  
 901 tctctacaaa taaataaacc tccgacgtt tagaacattc acctttgtc agtgagcaca  
 961 accttcaat acagcccgac agggggctct ctactgctgt ctcttcacgc ccctggtga  
 1021 aaacgctgtg cactcaatcg gttgcagct ttgccgtact gttcgattaa aaactttta  
 1081 attagaggca aacatttaa aataaaatgt ccaaatatt gtctaaatg tattgtagac  
 1141 gcttattgat ttttaatta ctcaaagaa tgttcatcga gggagggccg ccaattgtg  
 1201 catctctaca tctctcgt catcctaaa taacggcact ctgcagatgc gaagcagtgg  
 1261 atcgcaaaaa cgcaaatgt gggcgaata agttcgcgag cgtctcga gtaaccggtt

1321 actgaaaata caagaaagtt tccacactcc ttgccattt ttccgcgcgg cgcttgaaa  
1381 ttcgtaaaga taacgcggcg gagtgtttg ggaaaatggc gcaaccgccg ccagatcaaa  
1441 actttacca tcacccgctg cccacacgc acacacatcc gcatccgcac tccatccgc  
1501 atccgcactc gcatccgcac ccacatcacc aacatccgca gcttcagttg ccgccacaat  
1561 tccgaaatcc cttegatttg gtgagttccc atcgcagcag agaagggctc ttgtcccagg  
1621 aaagctacag tacagattcc ctatggtgaa caaacaacca gtgcgatcac tgatgacct  
1681 aaacatttat tgagccgcag caaatgtgtt tctagaacat agggcgaaat cttctattat  
1741 cttgtttgtg acttttaaag tctcgtagca gaatctaat aacaattgat attattaatc  
1801 gttacagtta gtatagtata taattgtata tgaattgtgg ggcaacatgt tattagtgat  
1861 ttgccgaaat gtctaaaag atgtttcatt gaaatggacg aatgttaac ctgttgact  
1921 cacaccgaat atcagtaatg tctattttc aaaagccaca tctatggcca ctgggtatac  
1981 attattgact taatacactt catacaacat atttcaaaa acaagcattg ttgtcctgca  
2041 tgatgattag tgaaagtaat attgcaagat teggtccccg aagcgaatcg tctttcacg  
2101 ttttatata aagacagtgt accccttgat tctttgaagc tttcgatga gcgaacggga  
2161 gcgataaact acaactacat acgtccgtat ctgcccaacc agatgcccac gccaggtgag  
2221 ctcaaagcca acaaagtcag ccacgtctt atcagatgtc tttccctcag aggagctgcc  
2281 cgactctctg gtgatgcggc gaccacgtcg caccgcacc actttacca gctctcaat  
2341 agcagagctg gagcagcact ttctgcaggg acgatacctc acagccccc gacttgcgga  
2401 tctgtcagcg aaactagccc tgggcacagc ccaggtgaag atatggtta agaaccgtcg  
2461 gcgtcgtcac aagatccaat cggatcagca caaggaccag tctacgagg ggatgcctct  
2521 ctgccgggt atgaaacaga gcgatggcga tccccccagc ttgcagactc ttagcttggg  
2581 tggaggagcc acgccaacg ctttgactcc gtcaccacg ccctcaacgc cactgcaca  
2641 catgacggag cactacagcg agtcattcaa cgcctactac aactacaatg gaggccaaa

2701 tcacgccag gccaatgtc acatgcacat gcagtatcct tccggagggg ggccaggacc  
 primer 1 g tgtacgtgta cgtcatagga a

2761 tgggtcgacc aatgtcaatg gcggccagtt cttccagcag cagcaggtcc ataatacca

2821 gcagcaactg caccaccagg gcaaccacgt gccgcaccag atgcagcagc agcaacagca

2881 ggctcagcag cagcaatacc atactttga cttccagcaa aagcaagcca gcgcctgtcg

2941 cgtcctggtc aaggacgaac cggaggccga ctacaacttc aacagctcgt actacatgcg

3001 atcgggaatg tctggcgcca ctgcatcggc atccgctgtg gcccgaggcg ctgcctcgcc

intron starts

3061 gggctccgag gtctacgagc cattaacacc caagaatgac gaaagtccga gtctg tgtgg

3121 catcggcatc ggccggacct gcgccatcgc cgttggcgag acggaggcgg ccgacgacat

3181 ggacgacgga acgagcaaga agacgacgct acaggtcagg catgagtcca caacctttt

3241 tgatctctg attctgagtg tggcgttat aaattgaagc ttaagcttt gtaactttca

3301 aactgtctgg ttgagatgt tattctgaaa gtacttctat tccgatcga tgagattgg

3361 gagtcttca atatttaaca ttaacttat taagttttg ttttctaat tagacatggc

3421 atttctgaaa gggaagtaca agtgtaaag atgtatttta atatagaatt tgtatcaaag

3481 gttaagatt caaccgttg aaagccctta gtttcaggg tttttactt ttttattcat

3541 gtaatcactc ttaatacact gcaagtaaa atagcatttc tttgaccaga aaaataagaa

3601 tctatgcatt ttaaagtga aacagactc atatgctgat gaacatttt agctataaat

3661 tgtaacaata atttagcaat ttaattgaa tttattatg ttctaatgc gttcgctctc

3721 tcctag atc ttggagcctt tgaagggtct ggacaagagc tgcgacgatg gcagtagcga

intron stops

3781 cgacatgagc accggaataa gagccttagc aggaaccgga aatcgtggag cggcatttgc

3841 caaatttggc aagccttcgc cccacaagc ccctcagccg ccctcggga tggggggcgt

3901 ggccctgggc \gaatgaacc aatatcaatg ca\c gatggat acgataatgc aagcgataa  
primer 2 cttagcttgg ttatagttac gt

3961 tccccatcgg aacgccgcgg gcaactcgca gttgcctac tgcttcaatt agcctggacg

4021 agaggcgtgt tagagagttt cattagcttt aggttaacca ctgttgttcc tgattgtaca

4081 aataccaagt gattgtagat atctacgcgt agaaagttag gtctagtcct aagatccgtg

4141 taaatggttc ccagggaagt tttatgtact agcctagtca gcaggccgca cggattccag

4201 tgcatatctt agtgatactc cagttaactc tatactttcc ctgcaatacg ctattcgct

4261 tagatgtatc tgggtggctg ctccactaaa gcccgggaat atgcaaccag ttacatttga

4321 ggccatttgg gcttaagcgt attccatgga aagttatcgt cccacattc ggaaattata

4381 ttccgagcca gcaagaaaat cttctctgtt acaatttgac atagctaaaa actgtactaa

4441 tcaaatgaa aatgtttct cttgggcgta atctcataca atgattacc ttaaagatcg

4501 aacatttaaa caataatatt tgatatgata ttttcaattt ctatgctatg ccaaagtgc

4561 tgacataatc aaacatttgc gcattctttg accaagaata gtcagcaaat tgtatttca

4621 atcaatgcag accatttgtt tcagattctg agattttttg ctgccaaacg gaataactat

4681 catagctcac attctattta catcactaag aagagcattg caatctgta ggcctcaagt

4741 ttaattttaa aatgctgcac ctttgatgtt gtctctttaa gctttgtatt ttaattacg

4801 aaaatatata agaactactc tactcgggta aattgtgact aactacacat aactacatac

4861 ttagcccata ttccgtccc ttctagaat gaacgaaaac agtatctggg ttcccgaaa

4921 atcttatgaa tttaaaatg cactttattg cacatactca cacatgcctg ccataaata

4981 tgattcgga ttttccgcg aacaccgcg gatcataaaa catttgcacc agctgcctgt

5041 gtttattcac ctacctgaaa cccatactct tategcctga tcctcgcgcg gtcgcactat

5101 ttaggtagac actgtacagg cagcactagc